ÉCOLE DE TECHNOLOGIE SUPÉRIEURE
UNIVERSITÉ DU QUÉBEC

THESIS PRESENTED TO
ÉCOLE DE TECHNOLOGIE SUPÉRIEURE

IN PARTIAL FULFILLMENT OF THE REQUIREMENTS FOR
DEGREE IN ELECTRICAL ENGINEERING
M. Eng.

BY
Parisa MOSLEMI

DESIGN, FABRICATION, AND TEST OF A RADIATING ELEMENT FOR A
KU-BAND SMART ANTENNA

MONTREAL, 17TH DECEMBER, 2012

BOARD OF EXAMINERS (THESIS M. ENG.)

THIS THESIS HAS BEEN EVALUATED

BY THE FOLLOWING BOARD OF EXAMINERS

Mr. Ammar Kouki, Thesis Supervisor
Département de génie électrique à l'École de technologie supérieure

Mr. Naïm Batani, President of the Board of Examiners
Département de génie électrique à l'École de technologie supérieure

Mrs. Véronique François, Member of the jury
Département de génie électrique à l'École de technologie supérieure

THIS THESIS WAS PRENSENTED AND DEFENDED

IN THE PRESENCE OF A BOARD OF EXAMINERS AND PUBLIC

13$^{\text{TH}}$ DECEMBER, 2012

AT ÉCOLE DE TECHNOLOGIE SUPÉRIEURE

ACKNOWLEDGMENT

DESIGN, FABRICATION, AND TEST OF A RADIATING ELEMENT FOR A KU-BAND SMART ANTENNA

Parisa MOSLEMI

RESUME

Les antennes planaires multiéléments ont fait l'objet de nombreuses recherches ces dernières années en tant que candidates pour diverses applications telles que les communications par satellite. Parmi les nombreux avantages de ce type d'antenne on compte la capacité de diriger le faisceau de façon électrique, sa haute fiabilité, ainsi que son moindre coût à long terme; cela motive de pousser encore plus loin la recherche dans ce domaine.

Les antennes microrubans sont largement utilisées dans les réseaux d'antennes en raison de leur faible coût et de leur légèreté. De plus, elles peuvent facilement être imprimées sur un substrat diélectrique avec des techniques de photolithographie.

L'objectif de ce mémoire est la conception et la fabrication d'une antenne patch large bande, afin qu'elle soit utilisée dans un réseau d'antennes dans le contexte d'application de la communication par satellite. Ce patch est conçu pour fonctionner dans le domaine fréquentiel entre 10.7 GHz et 12.7 GHz. Dans ce projet, nous avons utilisé la technologie de la céramique cocuite à basse température à côté du circuit imprimé, ce qui n'a jamais encore été appliqué auparavant. En outre, nous proposons une nouvelle structure de l'antenne patch qui augmente la bande passante jusqu'à 19%. Les correctifs proposés sont fabriqués avec les matériaux 591 et 9K7 Green Tape et Rogers RT5870. Les dessins ont été effectuées en utilisant le simulateur de champ électromagnétique planaire Momentum, faisant partie de Advanced Design System (ADS) de Agilent technologies.

Mots-clés: Bande passante, Low Temperature Co-Fired Ceramic Technology, patch, antenne à balayage électronique, satellite.

DESIGN, FABRICATION, AND TEST OF A RADIATING ELEMENT FOR A KU-BAND SMART ANTENNA

Parisa MOSLEMI

ABSTRACT

Planar phased array antennas have been the focus of much research in recent years as candidates for applications such as satellite communication. Many advantages of this kind of antenna like the ability to steer electrically, its high reliability, and its long-term reduced cost motivate further research in this area.

Microstrip antennas are extensively used in array antenna because of their low cost and weight. They also can be easily printed over a dielectric substrate with photolithography techniques.

The objective of this thesis is the design and fabrication of a wideband dual polarized patch antenna to be used in an antenna array for the application of satellite communications. This patch is designed to work in the frequency domain from 10.7 GHz to 12.7 GHz. In this project we used Low Temperature Co-Fired Ceramic Technology beside printed circuit board which was never applied before. In addition we proposed a new structure for the patch antenna which increases the bandwidth up to 19%. The proposed patches are fabricated with the material 591 and 9K7 Green Tape and Rogers RT5870. The designs were carried out using the planar electromagnetic field simulator Momentum, part of the Advanced Design System (ADS) of Agilent technologies.

Keywords: Bandwidth, Low Temperature Co-Fired Ceramic Technology, patch, phased array Antenna, satellite.

TABLE OF CONTENTS

LIST OF TABLES

LIST OF FIGURES

Page

LIST OF ABREVIATIONS

ADS	Advanced Design System
BW	Band Width
HPBW	Half Power Band Width
BWFN	Beam Width between the First Nulls
GPS	Global Positioning System
LNA	Low Noise Amplifier
LNB	Low Noise Block Converter
LNF	Low Noise Feed Horn
LTCC	Low Temperature Co-Fired Ceramic Technology
LO	Local Oscillator
PCB	Printed Circuit Board

LIST OF SYMBOLS

BASIC UNITS		$D_{iameter}$	diameter	
m	mètre (unité de longueur)	e_r	Reflection Efficiency	
s	seconde (unité de temps)	e_c	Conduction Efficiency	
K	kelvin (unité de température)	e_d	Dielectric Efficiency	
		f	focal length	
LENGTH UNITS		G	gain	
m	meter	h	hiegth	
dm	decimeter	K	Kelvin	
cm	centimeter	k_0	free space wave number	
mm	milimeter	L	length	
μm	micrometer	l_f	feed loss	
		l_t	the radiation losses of a T-junction	
AREA UNITS				
m^2	square meter	l_b	the radiation losses of a bend	
dm^2	square decimeter	l_c	the radiation losses of a coax	
cm^2	square centimeter	N	number of element	
mm^2	square milimeter	n_r	the number of a T-junction	
$μm^2$	square micrometer	n_s	the number of bends	
mils	mils(0.0254mm)	R_0	voltage ratio	
		S	area	
TIME UNITS		W	width	
h	hours	Y	input impedance	
min	minute	z_0	input impedance	
s	second	ε_r	Dielectric Constant	
ms	millisecond	λ	Wave Length	
μs	microsecond			
		GREEK LETTERS		
FREQUENCY UNITS		α	alpha	
Hz	hertz	β	beta	
KHz	hilohertz	δ	delta	
MHz	hegahertz	ε	epsilon	
GHz	gigahertz	η	eta	
		γ	gamma	
LOGARITHM UNITS		κ	kappa	
dB	decibel	λ	lambda	
dBi	decibel (Isotropic)	μ	mu	
		ν	nu	
REGULAR SYMBOLS		ω	omega	
A	Area	φ	phi	
p	Power	π	pi	
c	speed of light in vacuum	θ	theta	
d	element spacing	υ	upsilon	
D	directivity	ζ	zeta	

INTRODUCTION

The main characteristic of satellite communications that makes them distinguished is their ability of broadcasting and multicasting. There are three types of orbits employed by satellites: Geostationary Orbits, Low-Earth Orbits and Molniya types. For telecommunication, Geostationary Orbits are useful. A geosynchronous satellite is a satellite in a geostationary orbit, a circular orbit above the Earth's equator, which returns to the same place after each day. In satellite communication, the satellite can be used as a receiver or a transmitter. To receive and transmit signal properly to the satellite, the ground station antenna should be pointed directly to the satellite. For this reason the movement of satellite should be tracked. In other words the direction of the main beam of the antenna should be adjusted toward the satellite in spite of its movement. This tracking operation can be done mechanically or electrically.

The beam direction can be varied mechanically which is not as fast as satellite moving. For this reason it is preferred to use electrical methods which are cheaper and faster. The signal processing technique which is used to adjust the beam shape electrically is called beam forming. Beam forming is done by using an array of radiating elements and combining their radiation of patterns with proper weight. The elements of the array can be reflector types or lens types. An example of an antenna array with beamforming capacity is shown in Figure 0.1.

In space communications large parabolic reflector antennas are usually used. Despite their many advantages, there are some important impairments regarding their mechanical complexity, low flexibility, and high operation maintenance costs. To overcome these limitations, planar array technology may be used.

Using planar array antennas can help to do beam forming electrically which is faster and more reliable than one doing mechanically. The most important advantages of antenna arrays is that the beam steering can be controlled electrically or/and mechanically; however there are other disadvantages like less scan angle. In general some of the advantages of planar
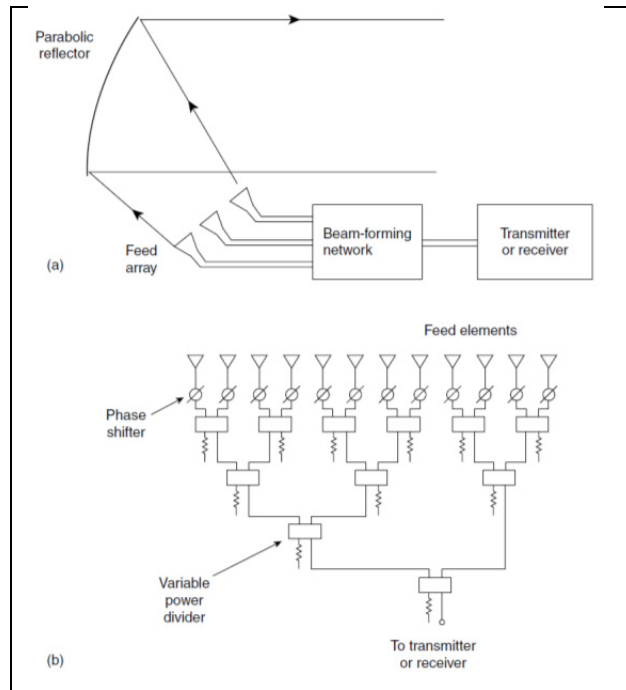
Figure 0.1 Shaped beam antenna being an array of radiating elements
Drawn from Maral et al.(1998, p. 509)

phased array antenna are:

- the antenna beam can be moved almost instantaneously to any desired direction;
- a phased array consists of many radiating elements. If one element fails the system can continue to work;
- failed elements can be identified and repaired without disturbing the operation of the system;
- mechanical motion is not needed;
- it has the ability of creating multiple beams;
- long term maintenance is less expensive.

Some of the disadvantages of the phased array antenna are:

- the beamforming network is complex;
- it has limited ability of multi-frequency operation;
- it is not flexible to work in many frequencies;

- its operation at low elevation angles is not strong;
- it is expensive.

The most commonly used technology for a planar antenna array is microstrip technology. This is because microstrip has low cost, low weight, and can be printed easily over a dielectric substrate with photolithography techniques.

The objective of this thesis is the design and fabrication of a wideband patch antenna to be used as the building block of an array antenna for the satellite signal reception. This patch must work in the band between 10.7GHz and 12.7GHz which covers the downlink frequencies for satellite TV broadcast.

Chapter one presents some basic satellite communications concepts and discuss in some details, dish antennas, which are the most commonly used antennas. Satellite tracking by ground board antennas is also discussed.

Chapter two presents a general literature review of the previous works on planar array antennas used in satellite communications.

In chapter three, the characteristics of array antennas and antenna parameters are studied. Then the specifications of a planar array antenna that would provide the same performance as a dish antenna for satellite TV reception are presented.
In chapter four, the patch element array is studied and its characteristics as an array antenna element are presented. Then the effect of using stacked elements and different aperture feed lines on bandwidth are investigated and the simulation results in Momentum software are pretested.

In chapter five, a new efficient structure for patch antenna is proposed and its parameters are investigated totally. The simulation results in Momentum software are also presented.

In chapter six, the process of prototyping in LTCC technology and the results of testing the circuit are presented.

CHAPITRE 1

SATELLITE COMMUNICATIONS

1.1   Satellite Communications

A satellite is an object which revolves around another object. Artificial satellites that are used as wireless receiver/transmitter are placed in a determined orbit around the Earth. Satellite communications are a special example of wireless communications which are popular these days.

The first human-made satellite, called Sputnik, was launched by the Soviet Union in 1957. It was made to transmit a Morse code signal repeatedly. Nowadays, satellites can receive and transmit many complex signals at the same time. They are used for Internet communications, television broadcasting, amateur radio communications, weather forecasting and Global Positioning Systems (GPS).

One of the important applications of satellite communication is Remote-sensing. Remote-sensing satellites use powerful cameras to study the surface of the Earth. They are also used to study the changes of the surface of the Earth, weather forecasting and many other applications. The obtained data can be useful for researchers, government, and many industries like mining.

1.1.1   Frequencies Used in Satellite Communication and TV Broadcasting

There are some parameters that determine the frequency in satellite communication:

1. Atmosphere absorption: figure 1.1 and 1.2 show the average atmospheric absorption as a function of frequency. Figure 1.1 shows resonant absorption peaks which are due to different molecules in the atmosphere. These frequencies may be used in a few special cases so that the signal does not propagate beyond a certain range. Figure 1.2 shows that rain and fog increase the attenuation of microwave signals. It also shows that rain and fog

have less effect on the lower frequency (up to 15GHz). It means that these frequencies are proper for communication;
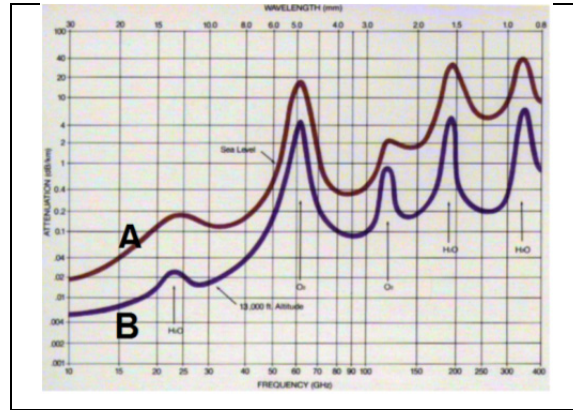
Figure 1.1 Average atmospheric absorption of millimeter waves. A: Sea level; T = 20°C; P = 760mm; PH2O = 7.5g/m3. B: 4 km; T = 0°C; PH2O = 1g/m3. Drawn from Silver (2004, p. 1)
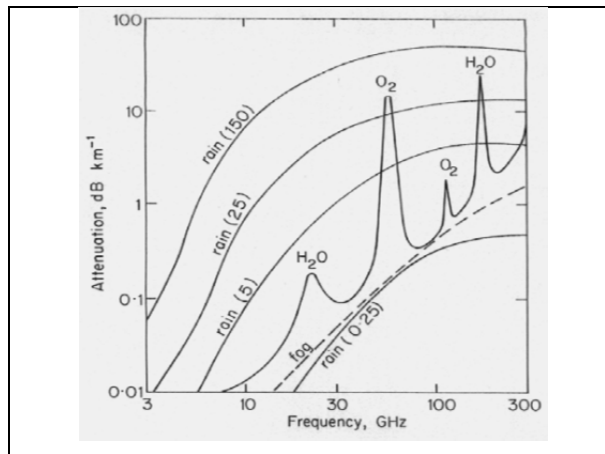
Figure 1.2 Atmospheric absorption of millimeter waves due to fog and rain Drawn from Silver (2004, p. 2)

2. The antenna size: the size of the antenna depends on the wave length (λ). If D is the maximum dimension of the antenna aperture and θ is the angular breadth of the main beam between 3dB points then $\theta = \lambda/D$. The more frequency, the smaller is the antenna but the attenuation of the atmosphere is also more;

3. International regulations: there is an agreement among various international agencies about using the frequency spectrum. Table 1.1 shows the allocation from 4990 to 7075MHz;

4. For TV broadcasting, the downlink frequencies are in the band of 10.7GHz to 12.7GHz; for the central frequency of 11.7GHz, this is expressed as a frequency bandwidth of 17%. The uplink frequencies are also in the ku-band, between 12.7GHz to16.7GHz.

Table 1.1 Region 1: Europe, Africa, N Asia; Region 2: N & S America;
Region 3: rest of Asia
Drawn from Silver (2004, p. 2)

Allocation to Services		
Region 1	Region 2	Region 3
4990 – 5000 FIXED MOBILE except aeronautical mobile RADIO ASTRONOMY Space Research (passive) 795		
5350 – 5255 RADIOLOCATION Space Research 713 798		
5650 – 5725 RADIOLOCATION Amateur Space Research (deep space) 664 801 803 804 805		
5725 – 5850 FIXED SATELLITE (Earth-to-space) RADIOLOCATION Amateur 801 803 805 806 807 808		
5850 – 5925 FIXED FIXED-SATELLITE (Earth-to-space) MOBILE 806	5850 – 5925 FIXED FIXED- SATELLITE (Earth-to-space) MOBILE Amateur Radiolocation 806	5850 – 5925 FIXED FIXED- SATELLITE (Earth-to-space) MOBILE Radiolocation 806
5850 – 5925 FIXED FIXED-SATELLITE (Earth-to-space) MOBILE 791 809		

To understand the satellite behaviour we should know about the satellite and the Earth station which are two certain parts of the satellite system.

1.1.2   Orbiting and Geostationary Satellites

There are two kinds of satellites:

1. Orbiting satellites: these satellites, which are cheap to launch, have low orbits with altitude around 800 km. They are not available all the time for communication. They are used for collecting and transmitting data to fixed earth stations. Rotation of the Earth helps the satellite to cover the Earth and the antenna receivers must track the satellite.
2. Geostationary satellites: these satellites have a fixed position in relation to the earth. Generally, three satellites are needed to cover most of the Earth. Their orbit altitude is around 3600km.

1.1.3   The Earth Station

Every reception or transmission installation on the Earth surface is called Earth station. Examples are briefcase satellite phones, handheld devices for mobile satellite telephony, and satellite TV reception.

Generally the Earth station refers to the antenna (often a dish antenna) and all the other equipment (transmitter, decoder, and receiver) needed to communicate with the satellites.

Figure 1.3 Handheld satellite telephone, antenna for satellite TV reception, satellite transmitting Earth station
Drawn from JISC

The other part of the Earth station is the application device. The application device, as a receiver, translates the signal to the information that can be shown on TV or processed by a computer. As a transmitter, they convert the information to the signal suitable for transmitting with antenna, modulating, amplifying and other necessary processing.

The antenna size can be changed according to the application. For instant a 70cm antenna is good for receiving satellite TV programs at home; but it is not suitable enough to transmit the TV programs.

1.1.4   Payload: antennas, transponders

Payload is all the equipment that a satellite needs to communicate such as antenna, camera, radar and electronics. For instant the payload of the communication satellite contains large antennas for transmitting signals.

Transponder is a part of the payload which involves the connected units to form a communication channel between the receiver antenna and the transmitter antenna. It takes the signal from the earth station, then filters and translates them and redirects them to the transmitting antenna. The transponders enable the communication satellite to deliver multiple channels of communication at the same time (carriers).

Figure 1.4 shows the channelling scheme for 12 transponders in c band. In this channel, the carrier at frequency 5.925-6.425 GHz is received at the antennas and in width band receiver, the carrier frequency shifts to 3.7-4.2 GHz.

There are two kinds of transponders:
- the bent pipe repeater: this transponder does not process the signal;
- the onboard processor: this transponder can do digital detection for the uplink signal and do digital switching and modulation for the down link.
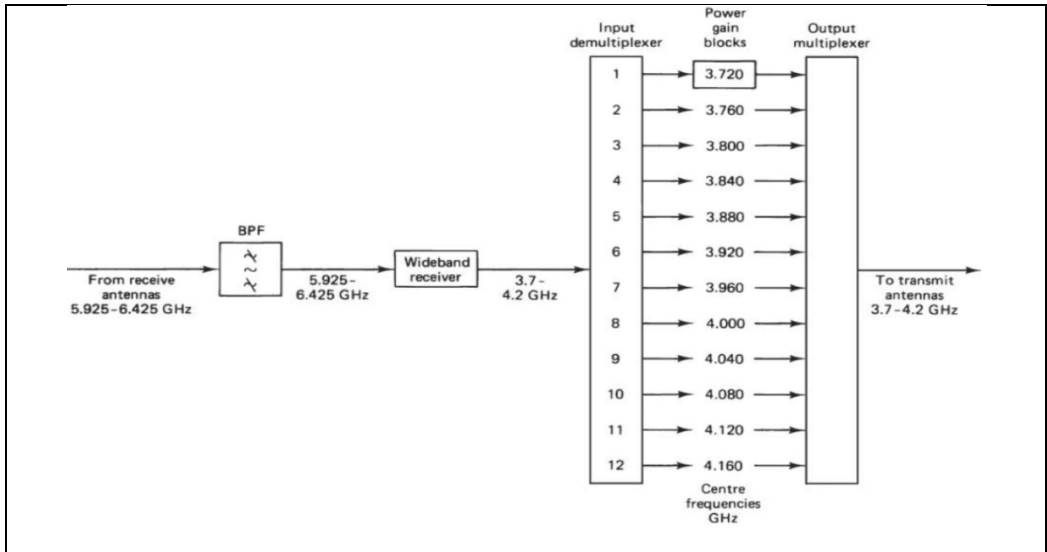
Figure 1.4 Satellite transponder channels
Drawn from Roddy et al. (2001, p. 236)

1.2　　　Satellite Receiver Antenna

In general antennas can be classified as transmitter or receiver. Although the requirement for each function is different, the antenna can be used as transmitter or receiver simultaneously. In fact, antennas form a link between space propagation path, and transmitting and receiving equipments. Figure 1.5 shows the antenna in transmitter and receiver mode.
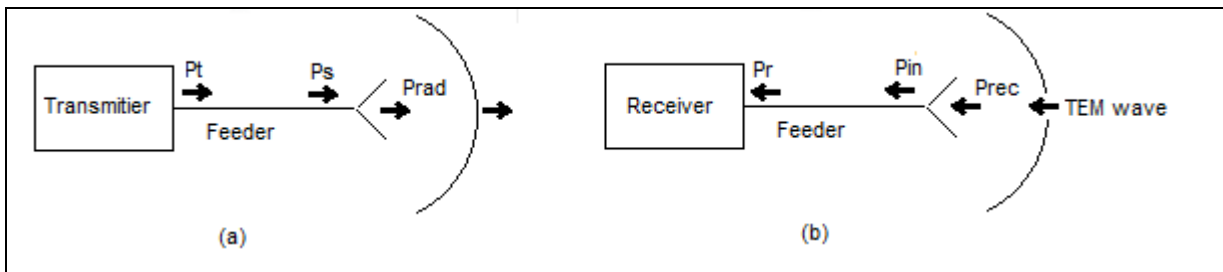
Figure 1.5 (a) Transmitting antenna (b) Receiving antenna
Adapted from Roddy et al. (2001, p. 138)

In the both cases feeder connect the power amplifier to the antenna. In the transmitter mode the power P_T will be reduced by passing through the feeder and antenna because of ohmic losses and mismatch losses. So P_{RAD} is less that the power generated in transmitter. This is

the same about receiver mode; P_R is less than P_{REC} because of ohmic losses and mismatch losses.

Reciprocity Theorem for Antennas: This theory shows that if an Electro-Magnetic Field applied at the terminals of transmitter antenna A generates current I in receiver antenna B, then the same current will appear in the terminal of receiver A if the same Electro-Magnetic Field applied at B. (figure 1.6)
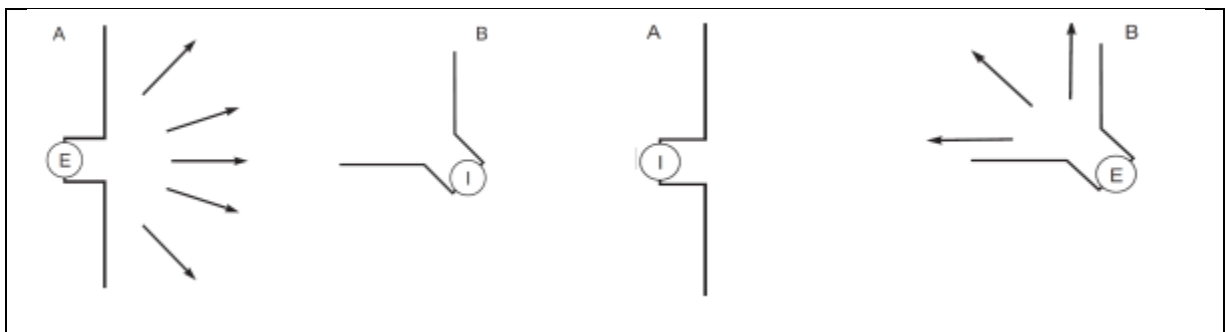
Figure 1.6 The reciprocity theorem
Adapted from Roddy et al. (2001, p. 139)

One of the important results from the reciprocity theorem is that the directional pattern of a transmitter antenna is the same as that as a receiver antenna. Another result is that the antenna impedance which is the same for both receiver and transmitter modes.

1.2.1   Receiver Antenna

There are three main components for satellite receiver antenna: reflective surface, the feed horn and amplifier section such as low noise amplifier (LNA), low noise block converter (LNB), low noise converter (LNC), low noise feed horn (LNF).
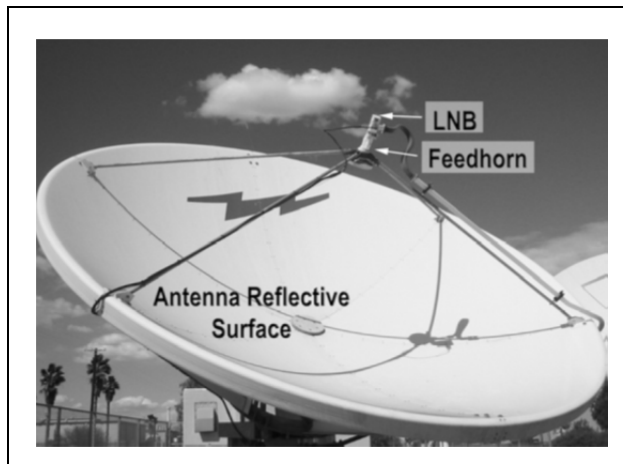
Figure 1.7 Components of antenna receiver
Drawn from AFRTS (2010, V.3.26)

1.2.1.1 Reflective Surface

Reflective surface reflects the satellite signal to a very sharp focal point. Reflective surfaces are in different shapes and size. The parabolic or offset shape, which is small section of parabolic antenna, is the most common receiver antenna. It reflects the satellite signals to the focal point of the parabolic. This point is in front and to the center of the surface. A larger reflective surface results in more gain.

In general there are different kinds of antenna used as receiver in satellite communication:

- The horn antenna;

  The horn antenna: this kind of antenna was used at the beginning of space communication with the Telstar satellite (Pleumeur Bodou in France). The horn antenna has a lot of advantages but it is not used more because of being expensive and heavy.

- The parabolic antenna.

  This kind of antenna is the most popular one. Parabolic antenna is discussed in chapter 1.4 in details.

- The phased array antenna;

Phased array antennas are useful when the beam is in constant movement, however it is expensive and the technology is complicated.

1.2.1.2   Feed Horn

This element is particularly used in parabolic antenna. It is a small horn antenna uses to convey signals from the transmitter to the receiver. In receiving antennas, incoming signals are focussed by the reflector on the feed horn. The feed horn converts the waves to a tiny radio frequency voltage which are amplified by the receiver.

1.2.1.3   Amplifier (LNA/B/C/F)

Figure 1.8 shows the wideband receiver. It contains two similar parts. One of them which is called redundant receiver is provided for when the other part is failed.
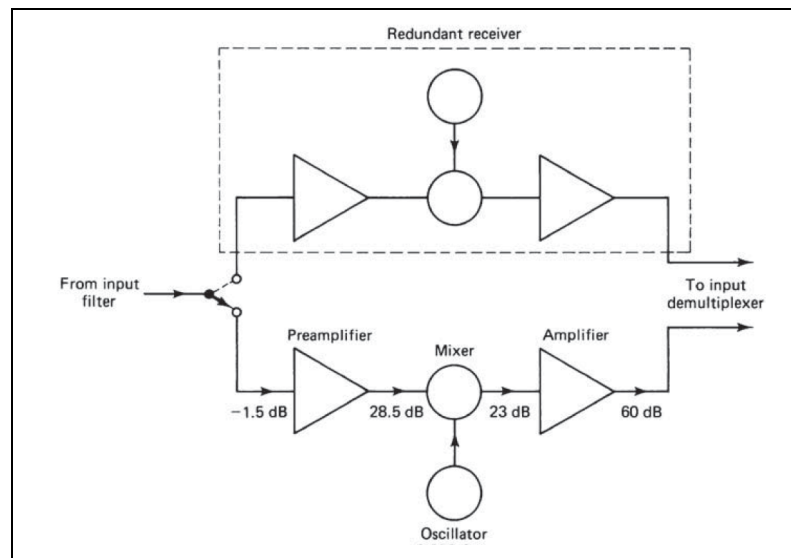
Figure 1.8 Satellite wideband receiver
Drawn from Roddy et al. (2001, p. 207)

The first unit of the receiver is a low noise amplifier (LNA) that has a low noise floor. This amplifier adds little noise to the amplified carrier and adds enough amplification to the carrier to override the higher noise level which is present in mixing step. The most

commonly used LNAs use gallium arsenide field effect transistors (GaAsFETs). Typical noise temperatures of amplifiers produced today range from 15° K to 60°K (LNB\C\F). (AFRTS, 2010)

LNA provides sufficient gain for the signal to transport from the antenna to the receiver. This signal is in several gigahertz frequency and need an expensive transmission line to reach the receiver. For avoiding this problem we can down-convert the signal and then transport it to the receiver. This is done by LNB/C/F. It changes the frequency to the L-band (940-1450GHz).

Referring total noise levels to the LNA input is very easy when the noise be expressed in noise temperature. The system noise temperature is a function of antenna noise temperature, the feeder losses between the antenna and receiver input, the thermodynamic temperature of the feeder and the effective noise of the receiver.(Maral et al., 1998) Total noise is in the order of a few hundred kelvins. (Roddy et al., 2001)

There is a trade off between the antenna size and LNB noise temperature (G/T). Smaller antenna needs the LNB with lower noise temperature and a bigger one needs the LNB with higher noise temperature. The job for the LNB is to overcome this noise figure with a carrier to noise C/N separation of greater than 8dB. (AFRTS, 2010)

The next step is mixing the output of the LNA by a local oscillator (LO) signal, with a power around 10 dBi, to shift the frequency.

The third step is providing a gain of 60 dB by the second amplifier.

1.3   Satellite Antenna Parameters

1.3.1   Directivity, Gain and Efficiency

One of the important characteristics of an antenna is the ratio of the field and power radiated by the antenna in a given direction to the maximally field and power radiated by the same

antenna. To compare different antennas with each other we need a reference. This reference is the isotropic radiator. The isotropic antenna is an antenna which radiates equally in all directions'. (Figure 1.9)
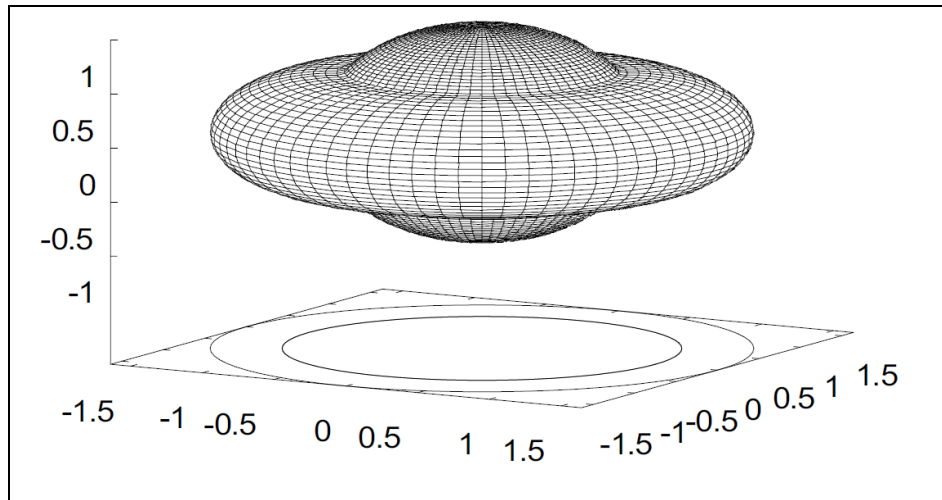
Figure 1.9 Three-dimensional, normalised electric field or power radiation pattern of a
(hypothetical) isotropic radiator
Drawn from Visser et al. (2005, p. 100)

Directivity of an antenna D(υ,φ) is the ratio of the power radiated in a direction (υ,φ) to the power radiated from an isotropic antenna in the same direction. In other words it is normalized by the corresponding isotropic intensity.

$$D(v, \varphi) = P(v, \varphi)/P_t/4\pi \tag{1.1}$$

$$D = Max(D(v, \varphi)) \tag{1.2}$$

In fact the total power radiated from an antenna is not known or difficult to be known. For this reason, the Gain function is defined. Gain is similar to the directivity with the difference that instead of total power it uses input power (P_{in}). P_{in} is the power accepted by the antenna at its input power rather than radiated power P.

$$G(v, \varphi) = P(v, \varphi)/P_{in}/4\pi$$

$$G = Max(G(v, \varphi)) \tag{1.4}$$

P_{in} does not account for the impedance mismatch which is around 99% of the total power. In fact, the gain tells us how the remaining 1% power is propagated in space.

We can also define the gain as:

$$G = (4\pi/\lambda^2)A_{eff} \tag{1.5}$$

Where λ is c/f; c or velocity of light is $3*10^8$m/s and f is frequency. A_{eff} is the effective aperture area of the antenna. A_{eff} is equal to eA, where e is the antenna efficiency. So the gain for a circular aperture or reflector of diameter $D_{iameter}$ and surface of A= $\pi D_{iameter}^2/4$ is:

$$G = e(\pi D_{iameter}/\lambda)^2 = e(\pi D_{iameter}f/c)^2 \tag{1.6}$$

There is another antenna parameter which is called efficiency. The antenna efficiency is a critical component which shows the antenna ability to transmit the input power to the radiation.

In general the overall efficiency can be written as:

$$e = e_r e_c e_d \tag{1.7}$$

e_r = reflection(mismatch) efficiency = $1-\Gamma^2$
e_c = conduction efficiency
e_d = dielectric efficiency

$$e_{cd} = e_c e_d \tag{1.8}$$

The total radiation power (P_t) is related to the input power (P_{in}) by radiation efficiency (e_{cd}):

$$e_{cd} = P_t/P_{in} = G/D \tag{1.9}$$

1.3.2   The Radiation Pattern

The radiation pattern shows the variations of the antenna gain with the direction (figure 1.10). The main lobe is the biggest lobe of the pattern. It contains the direction of the maximum radiation. Other lobes are called minor lobes or side lobes. They contain the radiation in the direction other than the direction of the main lobe. Side lopes should be kept to minimum.
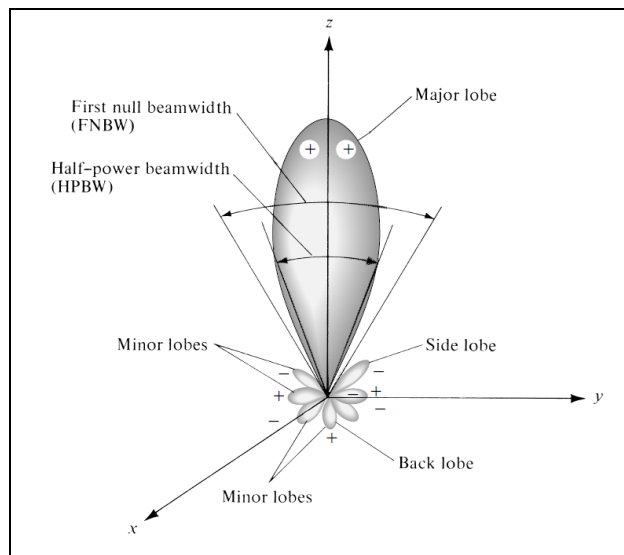
Figure 1.10 Antenna radiation pattern
Drawn from Balanis et al. (1982, p. 30)

1.3.3   The Beamwidth

One of the most important parameters of an antenna is the beamwidth. The beam width of a radiation pattern is the angular distance between two identical points on opposite side of the main beam. One of the most widely used beamwidths is the 3dB or Half-Power Beamwidth (HPBW) which is the angle between the two directions in which the radiation intensity is one-half value of the beam. (Balanis et al., 1982)
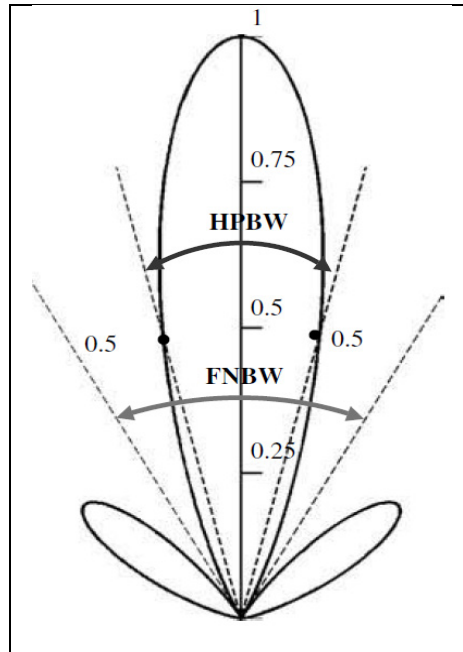
Figure 1.11 Antenna beamwidth
Drawn from Balanis et al. (1982, p. 42)

The HPBW is related to the ratio $\lambda/D_{iameter}$ by a coefficient α. α is depends on the illumination law. For uniform illumination, α is 58.5˚. Nun-uniform illumination laws lead to attenuation at the reflector boundaries, so the HPBW increases. In this case the value of α commonly is used 70˚. Hence: (Maral et al., 1998)

$$\theta°_{3dB} = 70(\lambda/ D_{iameter}) = 70(c/f D_{iameter}) \qquad (1.20)$$

Base on equation 6 and 10, the value of the gain is given by:

$$G = e(\pi 70/ \theta°_{3dB})^2 \qquad (1.31)$$

The area of the earth which should be illuminated has a direct relation with the satellite antenna beamwidth. The beamwidth also determines the antenna gain. In the crowded Geostationary orbit 2˚ is needed to recognize a satellite, so the receiver antenna needs the beamwidth of 2˚. This amount of beamwidth can determine the gain and the size of the antenna.

1.3.4   Polarization

The polarized wave is a wave which oscillates in one direction or plane. The direction of oscillation to the direction of the travel is described as polarization. In far field region, the electric field of an antenna has two spherical coordinate components, E_ϑ and E_ϕ (figure 1.12)
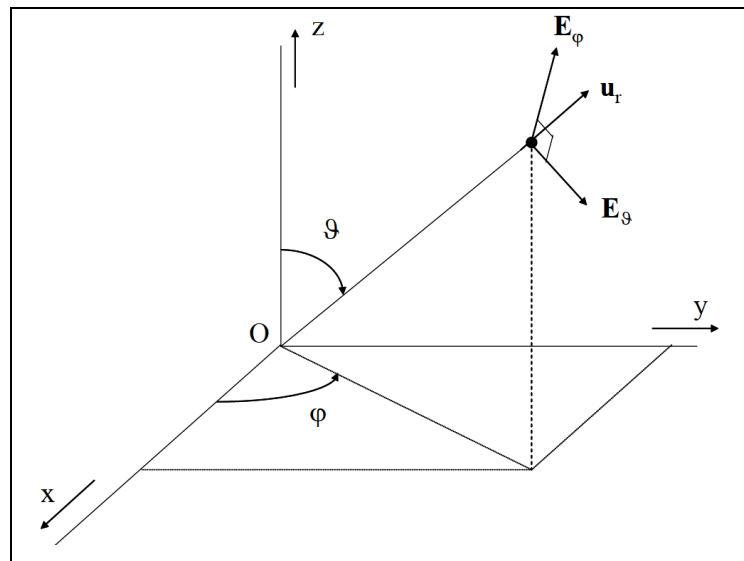
Figure 1.12 Electric field components E_ϑ and E_ϕ in the far-field region of an antenna placed in the origin O. u_r is the unit vector in the direction of wave propagation.
Drawn from Visser et al. (2005, p. 107)

The phase difference between the two components $E\vartheta$ and $E\phi$ causes the electric field vector as a function of time to describe an ellipse in the ϑ-ϕ plan. This kind of propagating electric field is called **elliptical polarization**.

When the phase difference is plus or minus 90 degrees and the amplitude of the components is equal to each other, the ellipse changes to a circle and the polarization is called **circular polarization**. If the signal rotates in a right-hand direction it is called right-hand circular polarization (RHCP) and if the signal rotates in the left-hand direction it is called left-hand circular polarization (LHCP).

When the phase difference is 0° or 180˚, the ellipse changes to a line and the polarization is called the **linear polarization**.
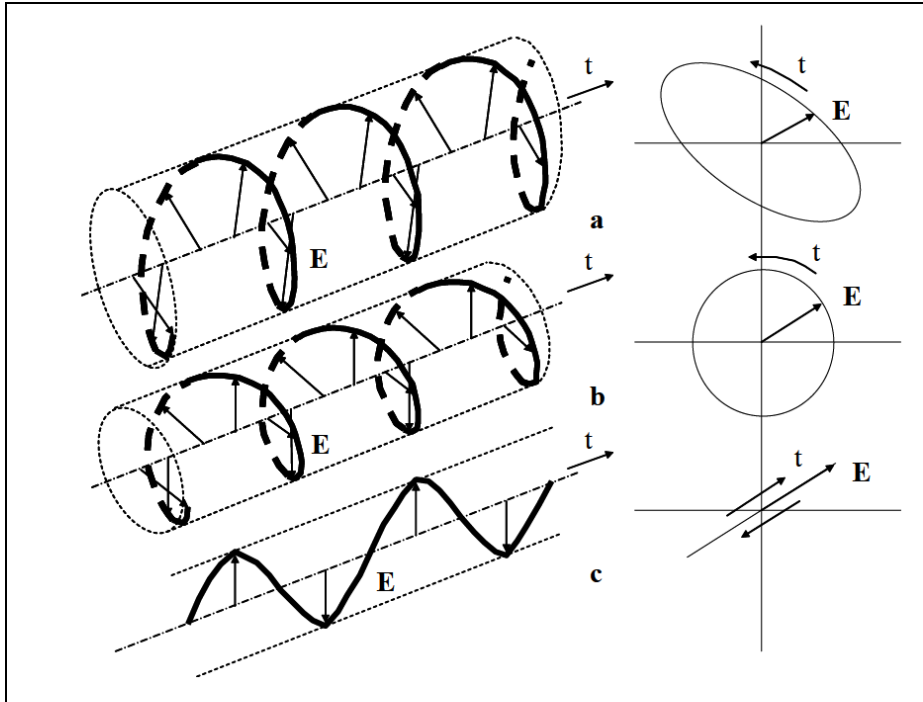
Figure 1.13 Polarization states. a. Elliptical polarization. b. Circular polarization
c. Linear polarization
Drawn from Visser et al. (2005, p. 108)

Linear and circular polarizations are two common polarizations which are used in C and Ku-band satellite communication links. The main advantage of using circular one is elimination of the need for skew adjustment; so the feed that receives RHCP or LHCP signal can be installed in any orientation. But for receiving linear polarization the feed must be lined up with the plane of polarization to receive highest possible power.

1.3.4.1 Orthogonal polarization

If the electric fields of two waves describe ellipses in opposite directions, the waves are in orthogonal polarization. In this case the following can be obtained:

- two orthogonal circular polarization described as right-hand and left hand circular polarization(the direction of rotation is for an observer looking in the direction of propagation) (Maral et al., 1998);
- two orthogonal linear polarization described as horizontal and vertical(relative to a local reference) (Maral et al., 1998).

A dual polarization is a wave which polarized both horizontally and vertically. It excited two vertically electric field and horizontally electric field. Many applications, especially wireless communication demand dual polarized operations. These antennas reduce side effects of multi-path fading and increase channel capacity per frequency in many applications. In other words overall system performance can be improved by polarization diversity. In addition using the same frequency simultaneously for the receiving and transmitting waves provide double transmission channels in a frequency-reuse communication system.

The receiver and transmitter antenna can neither transmit nor receive in the orthogonal polarization. For that we can use the same frequency simultaneously for the receiving and transmitting waves. It means two polarized antennas must be provided at each end of the link or one antenna which operates with two special polarizations can be used.

1.4 The Parabolic Reflector

Parabolic antennas are used widely in satellite communication. These reflectors can concentrate energy in a special direction. The most commonly used parabolic reflector has a circular aperture. The main characteristic of parabolic reflector is focusing. It can cover parallel radiated rays to a point known as the focus.
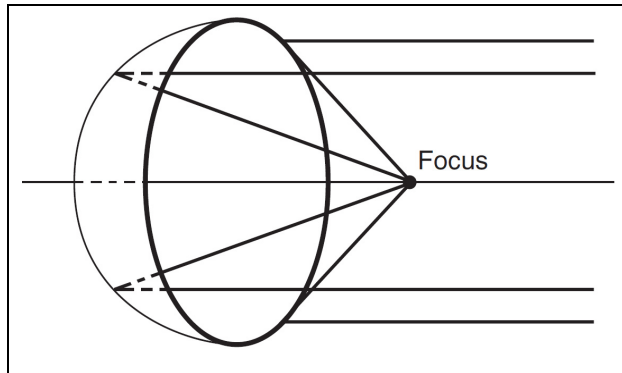
Figure 1.14 The focusing property of a paraboloidal reflector
Drawn from Roddy et al. (2001, p. 160)

Parabolic antennas are the most common antennas. There are three types of mounting for that:

- symmetric or axisymmetric mounting;
- offset mounting;
- Cassegrain mounting.

1.4.1 Types of parabolic antennas mounting

1.4.1.1 Symmetrical or axisymmetric mounting

Figure 1.15 shows a parabolic antenna which is symmetrical with respect to the main axis. In this antenna the feed is placed in the focal point. The main defect of this mounting is that the feed is placed in front of the radiation. This blocking decreases the antenna efficiency and increase the side lobes level. In addition a part of the feed radiation which is not reflected by the reflector will be emitted by the ground and makes a huge amount of antenna noise temperature. To avoid this phenomenon we should use a directional feed and a long focal length. Another weakness of this kind of mounting is that the installation of the microwave circuits behind the feed of this heavy antenna is not only difficult but also makes the same masking problem.
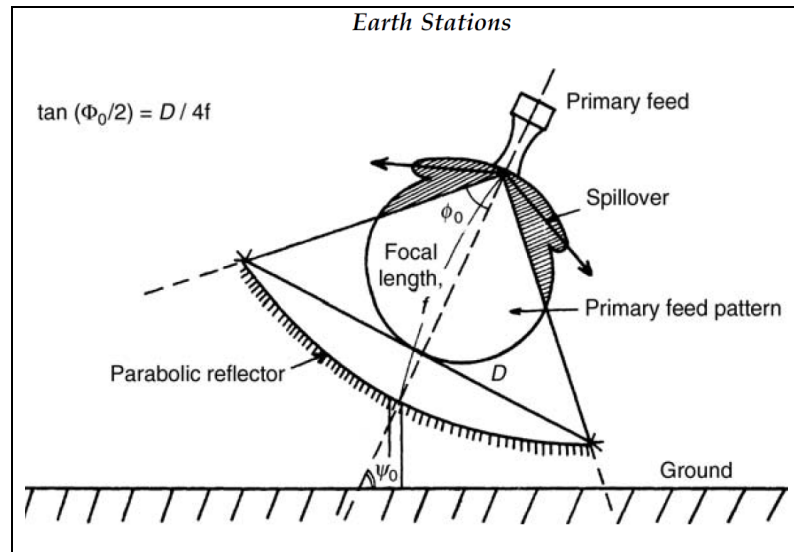
Figure 1.15 Axisymmetric parabolic reflector antenna
Drawn from Maral et al. (1998, p. 386)

1.4.1.2   Offset Mounting

Figure 1.16 shows offset mounting. In this mounting the feed is located in the focal point and uses the part of parabolic which is located on one side of the vertex .In this mounting the microwave circuit can be placed easily behind the feed without masking effect.
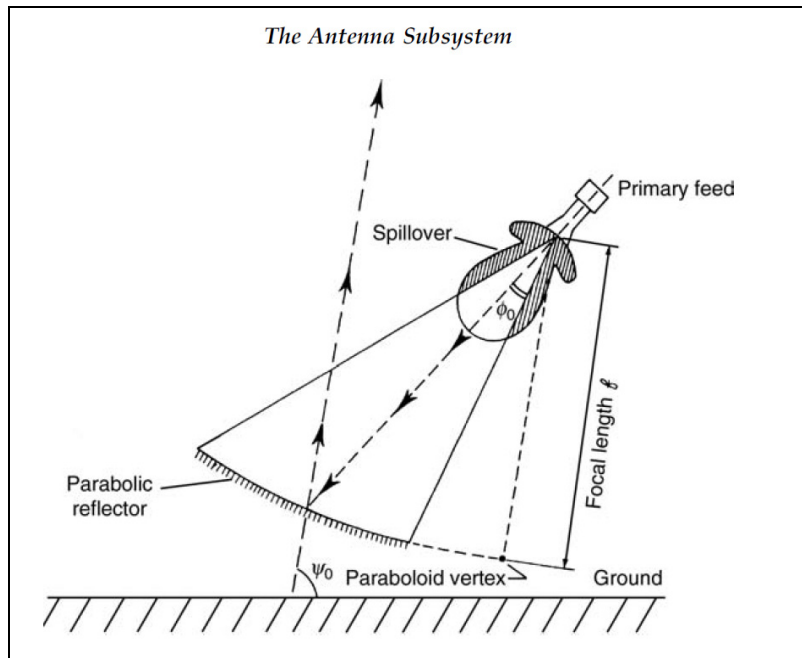
Figure 1.16 Offset-fed parabolic reflector antenna
Drawn from Maral et al. (1998, p. 387)

1.4.1.3   Cassegrain Mounting

Figure 1.17 shows Cassegrain mounting. In this mounting the phase center of the feed is located in the first focus S of the hyperbolic reflector and the other focus of the hyperbolic reflector (R) is placed on the focus of the main parabolic reflector.

One of the advantages of Cassegrain antenna is that it is less cumbersome and has lower antenna noise temperature. Another advantage is that the microwave circuit can be easily located behind the feed which is located behind the parabolic reflector.

The disadvantage of Cassegrain antenna is that the auxiliary reflector makes masking effect which is negligible for small auxiliary reflector with respect to the main reflector.
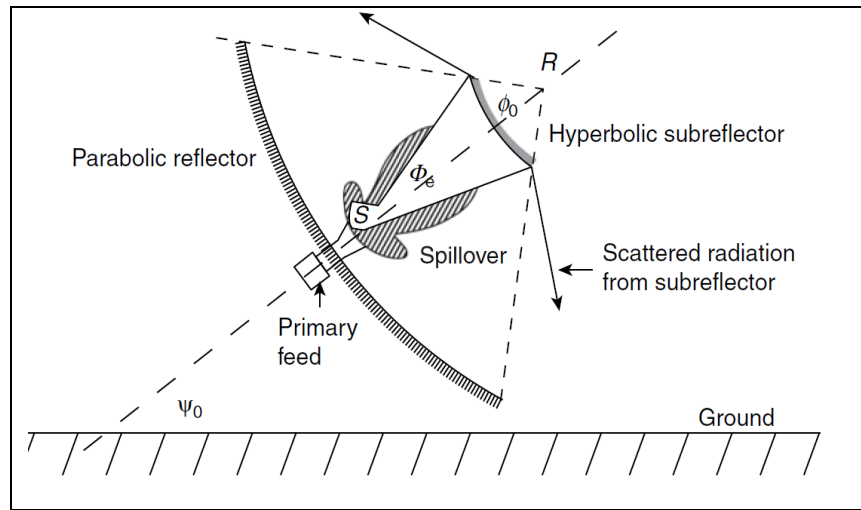
Figure 1.17 Dual-reflector Cassegrain antenna
Drawn from Maral et al. (1998, p. 387)

1.4.2 Properties of the Parabolic Reflector (Geometry properties, Radiation, pattern, HPBW, BWFN, Gain)

Geometry properties: The geometry properties of the parabolic reflector can be shown by the parabola (Figure 1.18). S is the focus or the focal point and A is the vertex. The line passing through A and S is the axis. P is on the curve and Q is in the aperture plane. PQ is parallel to the axis. For all P points, the path lengths of SQP are equal to each other. It means all the parallel rays concentrate in focus.
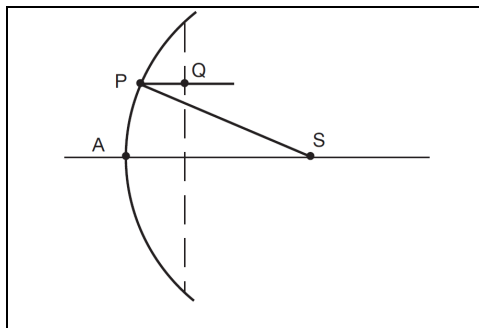
Figure 1.18 Parabolic geometry
Drawn from Roddy et al. (2001, p. 161)

One important factor in parabolic reflector is the ratio of aperture diameter ($D_{iameter}$) to focal length (f). Figure 1.19 demonstrates three parabolic ones with the different ratios.

$$\frac{f}{D} < 0.25 \qquad\qquad \frac{f}{D} = 0.25 \qquad\qquad \frac{f}{D} > 0.25$$
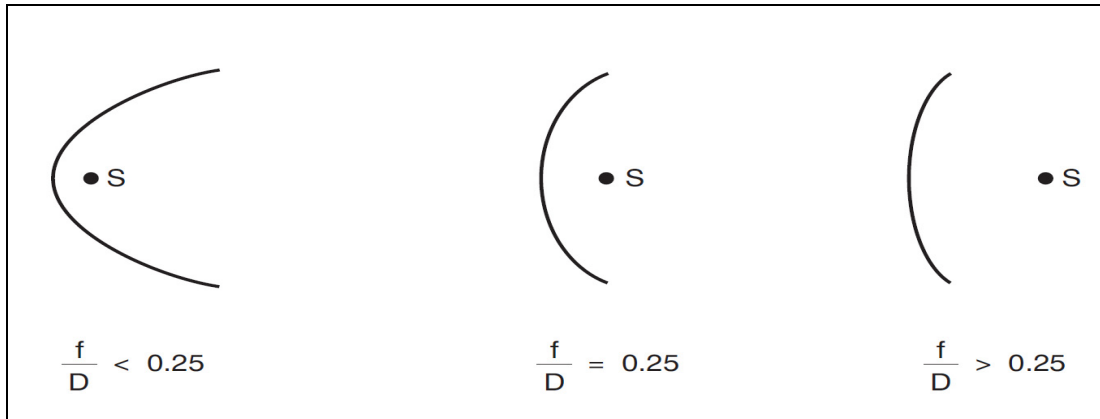
Figure 1.19 Position of the focus for various f/ $D_{iameter}$ values
Drawn from Roddy et al. (2001, p. 163)

The focal length can be defined with the depth of the reflector, perpendicular distance from the aperture plane to the vertex, and its diameter: (Roddy et al., 2001)

$$F = D^2/16 D_{iameter} \tag{1.12}$$

The aperture area is:

$$Area = \pi D_{iameter}^2/4 \tag{1.13}$$

Radiation pattern: Radiation pattern for the parabolic reflector is similar to the figure 1.20.
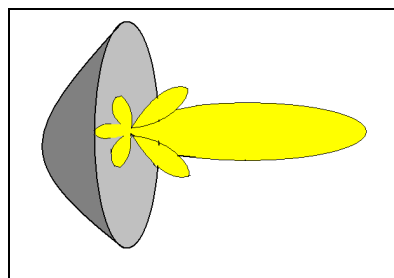
Figure 1.20 The radiation pattern for the parabolic reflector

HPBW & BWFN: Approximately half-power beamwidth and the beamwidth between the first nulls (BWFN) are obtained from: (Roddy et al., 2001)

$$HPBW° \approx 70\lambda/D_{iameter} \tag{1.44}$$

$$BWFN° \approx 2HPBW \tag{1.55}$$

Gain: There are some factors that affect on the parabolic antenna gain. These factors include the following: (Visser et al., 2005)

1. Diameter of the parabolic reflector antenna (reflecting surface);
2. Surface accuracy;
3. Quality of illumination of the reflecting surface;
4. Frequency or wavelength of the signal being received or transmitted.

In parabolic antenna Gain can be obtain by:

$$Gain = G = 10log \left[e(\pi * D_{iameter}/\lambda)^2 \right] \tag{1.66}$$

where :

- G is the gain over an isotropic source in dB;
- e is the efficiency factor which is generally around 50% to 60%, i.e. 0.5 to 0.6;
- $D_{iameter}$ is the diameter of the parabolic reflector in metres;
- λ is the wavelength of the signal in metres.

The area of the aperture is:

$$A = \pi d^2/4 \tag{1.77}$$

Effective area of the aperture is:

$$A_e = eA \tag{1.18}$$

Gain of a parabolic reflector is directly related to the area of the aperture:

$$G = 4\pi A_e/\lambda^2 = e(\pi D_{iameter}/\lambda)^2 \tag{1.19}$$

- For example, for the parabolic antenna mentioned in HIRSCHMANN(Hit FESAT 65), the chord is 65cm. If we estimate it as the diameter, the gain is calculated as below:

  $A= \pi d^2/4= \pi*0.65^2/4=0.33m^2$

  $G= 10\log (e4\pi A/\lambda^2) =10\log (0.7*4\pi*0.33/.274^2) =35.87dB$

  It is very close to the real gain 36dB.

  The parameters of this antenna are presented in table 3.1.

1.5   Tracking

Tracking is adjusting the direction of antenna beam to the satellite in spite of movement of the satellite and the station. Every method of tracking has its own application and error.

1.5.1   The effect of antenna characteristics on tracking

The angular beamwidth has an important effect on choosing the type of tracking. The 3dB angular beamwidth in the used frequency should be small. Figure 1.21 shows the effect of the antenna size on the angular beamwidth in for different frequencies.
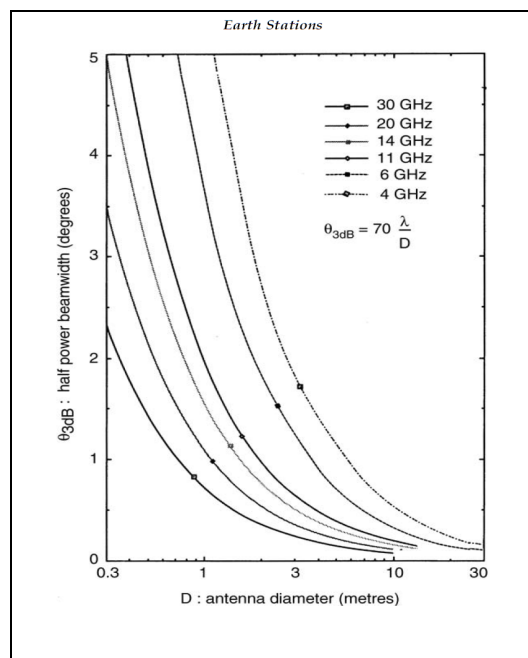
Figure 1.21 Half-power beamwidth θ_{3dB} versus antenna diameter D
Drawn from Maral et al. (1998, p. 400)

Depointing is associated with the satellite movement and direction of main beam. According to the equation below the depointing loss is related to the depointing angle θ and maximum gain. (Maral et al., 1998)

$$L = \Delta G = 12(\theta/\theta_{3dB})^2 \qquad (1.20)$$

The method of antenna installation and tracking depends on the variation of antenna gain with depointing.

The mass of antenna that relate to the antenna diameter is another antenna characteristic which affects the performance of the orientating device. Sometimes this amount is more than several tonnes. The mass and meteorological conditions cause deformation of antenna.

1.5.2   Types of Tracking

1.5.2.1   Fixed Antenna without Tracking

Tracking is not necessary for two cases:

- the antenna beamwidth is large compared to the station keeping box of a geostationary satellite;
- the antenna beamwidth is larger than the angle that contains the apparent movement of the satellite on inclined elliptical orbit.

The usable part of the beam can be defined at -0.1,-0.5, -1 or −ndB in according to the acceptable loss of gain. (Maral et al., 1998)

1.5.2.2   Programmed Tracking

In this kind of tracking, the antenna orientation control system provides the antenna pointing. For that the values of azimuth and elevation angles are calculated to predict apparent movement of the satellite. These amounts are stored in memory.

Programmed tracking is used for earth station antennas with large $\lambda/D_{iameler}$. Mostly these antennas have a large beamwidth, so high pointing accuracy is not necessary. For

geostationary satellite, programmed tracking uses station with mid rang of $\lambda/D_{iameler}$ at Ku band.

1.5.2.3 Computed Tracking

In this tracking method, the computer uses the orbit parameters like inclination, eccentricity, semi-major, right ascension of the ascendant node, and anomaly to evaluate the antenna orientation. The data is stored in memory and is refreshed if it is necessary.

CHAPITRE 2

LITERATURE REVIEW

2.1   Literature

Until now, various attempts have been done to replace or to modify the present 70-meter antennas. Several options studied to improve the traditional antenna for Deep Space Network (DSN) have been reported by JPL: (Jamnejad et al., 2002)

A.   Continue existing 70m stations with minor modifications:
- 70m antennas;
- 30 years old.

B.   Modify existing 70m stations for extended life and reliability:
- This option is similar to the option A, in addition of capability of receiving Ka-band.

C.   New 70m single aperture antenna:
- These antennas use wheel and track for azimuth and elevation motion.

D.   Array of four 34m antennas:
- This array antenna contains four 34m diameter antennas equivalent to one 70m antenna.

E.   Array of many small (e.g., 5m) dish antennas:
- It is an array of 5m aperture antennas equivalent to one 70m antenna.
- This array is large and contains many small dish antennas.

F.   Array of flat-plate antennas:

- This antenna array can be electronically steered.

G. Spherical reflector antennas:

- This antenna, which is called the SPHERE (Spherical Pair of High Efficiency Reflecting Elements), involves two elements that each one rotates only in azimuth never in elevation (Elevation is fixed).

Recently, planar array antennas are provided in order to replace by dish antennas because of the many advantages of the planar array antenna over the traditional ones such as higher reliability, near-instantaneous beam switching and steering capability. The problem with this kind of antenna is the cost. They contain many small reflectors or a few large ones. In the next decade, they will be developed to smaller configurations. (Jamnejad et al., 2002)

There are a number of phased array constructions which are presented below (option E, F and G)

2.1.1 Alternative Phased Array Configurations

2.1.1.1 Planar Horizontal Array

This type of array antenna is demonstrated in figure 2.1. Its characteristics are:

- it involves of small, low gain elements;
- the beam is toward zenith;
- the scan loss is depend on the sine of the elevation angle (0 dB at zenith and 3.0 dB at 30° and 7.6 dB at 10° elevation).

To have an equivalent array (with area S) with a 70m reflector (with area S_0) at 10° elevation:

$$S = S_0/sin(10°) = 5.8\ S_0 \tag{2.1}$$

or

$$D = 2.4\ D_0 = 168m \tag{2.2}$$

In this antenna the elevation is low and this makes a problem such as blind spot for scanning. It works good for scanning down to 30°(D=99m).
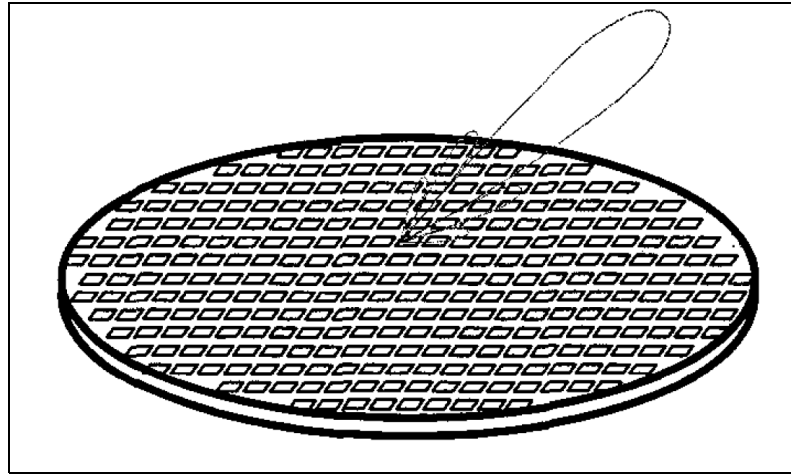
Figure 2.1 Schematic of a planar horizontal phased array with scanning range: ±80°
Drawn from Jamnejad et al. (2002, p. 5)

2.1.1.2 Hybrid mechanically/electronically steered array

This array uses planar arrays point at around 50° elevation angle. (Knittel, 1965)

- Figure 2.2.a shows the antenna which cover 10° to 90° elevation angle. The maximum loss is 1.16 dB for scan of ±40°. For 10° elevation:

$$S = S_0/sin(50°) = 1.3S_0 \tag{2.3}$$

or

$$D_{iameter} = 1.15D_0 = 80m \tag{2.4}$$

- In figure 2.2.b, each face of the antenna can be the same size. The loss is 1.5 dB at the edge of its coverage. For 10° elevation:

$$S = S_0/sin(45°) = 1.41S_0 \tag{2.5}$$

or

$$D_{iameter} = 1.19D_0 = 83m \tag{2.6}$$

- The antenna in figure 2.2.c shows the antenna with face angle of $60°$ relative to ground. For providing full hemispherical scan, it needs to scan $\pm30°$. In this antenna the loss is 0.6 dB at the edge of its coverage. For $10°$ elevation: (Knittel, 1965)

$$S = S_0/sin(60°) = 1.155\ S_0 \tag{2.7}$$

or

$$D_{iameter} = 1.075\ D_0 = 75m \tag{2.8}$$
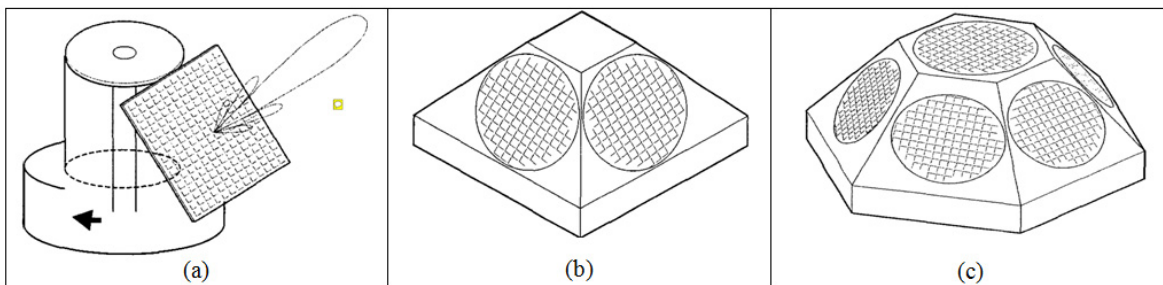
Figure 2.2 a) Schematic of a mechanically rotated 50°-tilted planar phased array with electronic scanning in elevation: ±40°, b) A four-face phased array arrangement: individual array scan: ±45°, c) A four-face phased array arrangement: individual array scan: ±30°
Adapted from Jamnejad et al. (2002, p. 6)

2.1.1.3   Phased-array fed lens antenna (dome antenna)

Dome antenna is another antenna that provides electrically hemispherical scan coverage. It contains a single horizontal planar phased array and a passive hemispherical microwave lens. It scans small angle around $30°$. This antenna is scanning down to a much lower elevation angle. Despite having advantages, the loss relates to the passive lens is high and the quality of the wavefront transformation makes some problem. (Jamnejad ,2002)
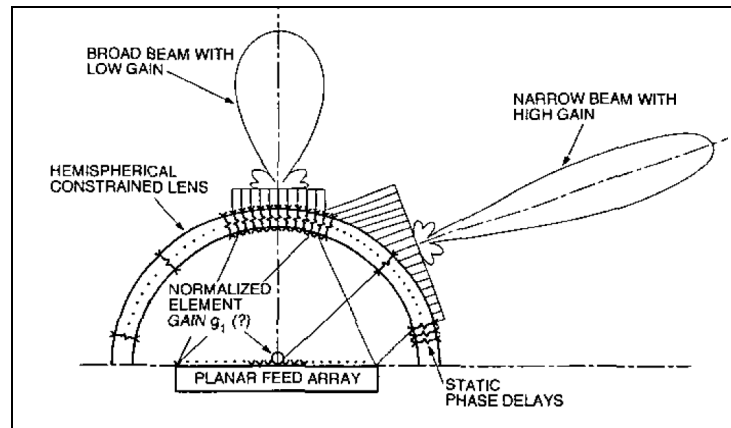
Figure 2.3 Schematic of a phased array fed lens antenna
Drawn from Jamnejad et al. (2002, p. 6)

2.1.1.4   Geodesic Sphere Phased Array Antenna

In this kind of antenna the element array placed on a spherical surface. The beam is made by switching on or off and providing phase shifter for each element. This antenna will be studied more in the future. (Jamnejad ,2002)
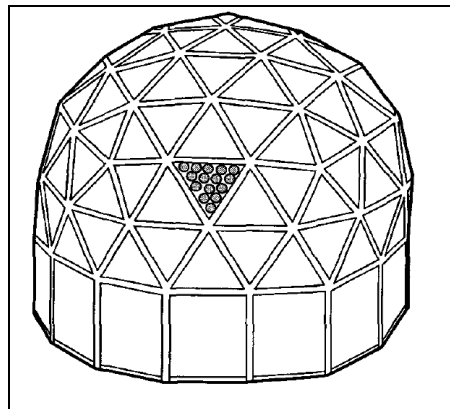
Figure 2.4 Schematic of a Geodesic sphere phased array antenna. Each face is a subarray
Drawn from Jamnejad et al. (2002, p. 7)

2.1.1.5   Phased Array of Mechanically Steered Reflectors

This antenna contains high gain directional elements. The act of scanning is done mechanically. This antenna is not as fast as electronically steered but faster than a very large reflector. The space between the elements should forbid making the blockage between the reflectors. The number of elements with diameter D which is equivalent to a 70-m reflector is $(D_{iamete}r/D_0)^2$. The minimum space between the elements is more than s=td/sin(a); number t is between 1.1 to 1.2 to account for diffraction effects and a is the minimum elevation angle. (Jamnejad et al., 2002)

For the diameter S of the circle consist of N element and 10° elevation:

$$S/D_{iameter} = 6.4D_0/D_{iameter} \qquad\qquad (2.9)$$

or

$$S = 6.4\, D_0 \qquad\qquad (2.10)$$
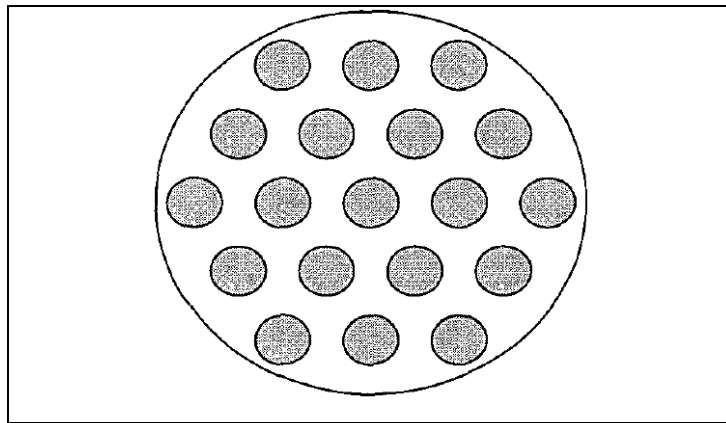
Figure 2.5 A hexagonal lattice of N reflector elements
Drawn from Jamnejad et al. (2002, p. 7)

2.1.1.6   Planar Reflect-Array

The planar reflect array has the ability of phase shifting. Its thin reflected surface contains many isolated microstrip patch elements. The elements do not need the network of power

division transmission line. The feed on the reflector illuminate these elements. This antenna can quickly scan the angle larger than 50˚ from the broadside. (Huang et al., 1998)

(a)

(b)
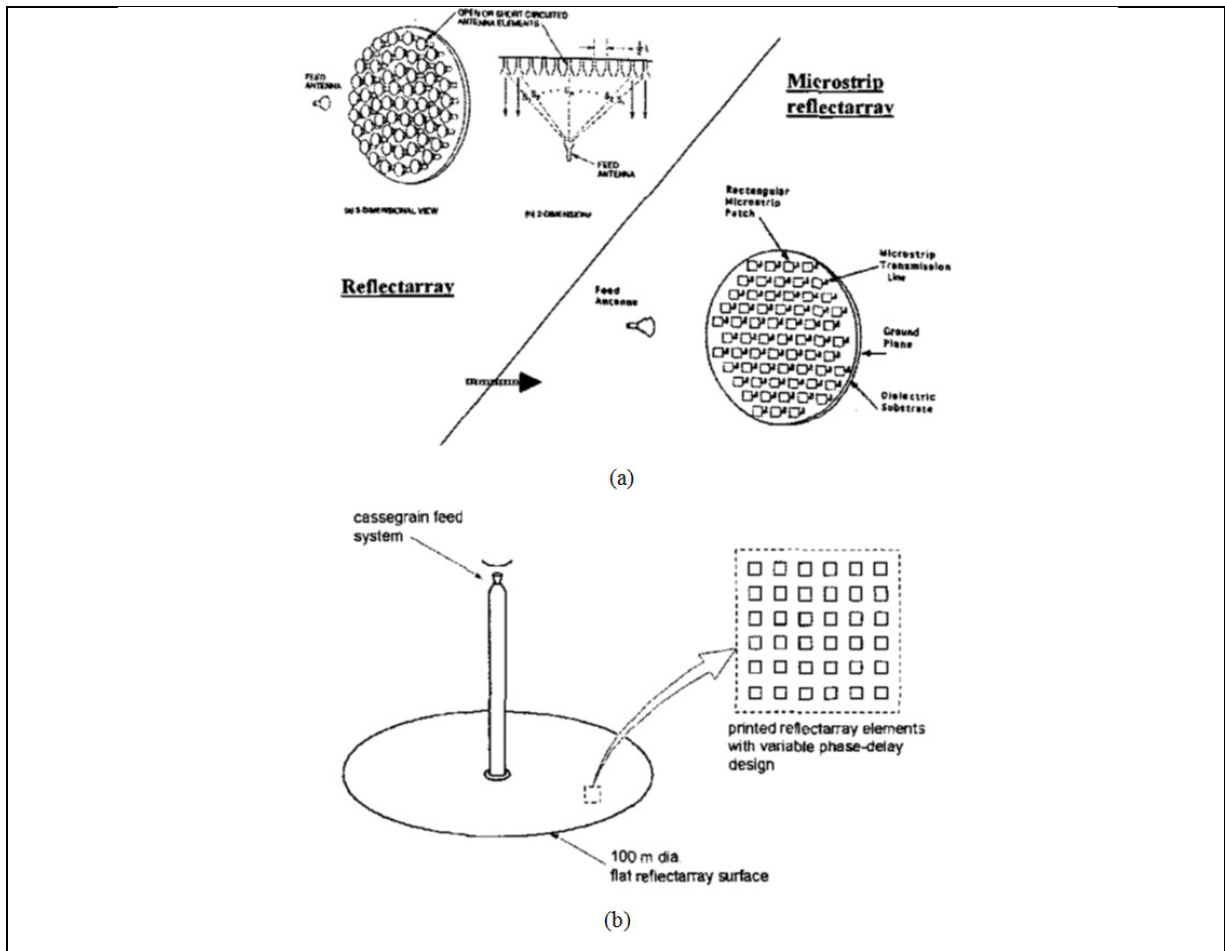
Figure 2.6 a) Concept of printed reflect-array antennas. b) Beam scanning can be achieved by
using electronic phase shifters or micro-machined motors
located underneath each patch element
Drawn from Jamnejad et al. (2002, p. 8)

There are some methods for the elements of reflector to adjust phase:

1- Uses of microstrip patches with different length phase delay lines. The different lines make different delays;

2- The method which works with circular polarization; the elements which polarizes circularly with different angular rotations make different feed path lengths.

An important drawback of the reflect array is having narrow bandwidth that effects on the phase delay lines and the array element spacing.

CHAPITRE 3

PLANAR ARRAY ANTENNAS

3.1   Planar Array Antennas

A planar array antenna is a linear array of linear arrays of radiating elements. For easier calculation we suppose that the elements of the array are placed on a regular lattice with equal spacing between rows and columns (figure 3.1). (Visser et al., 2005)
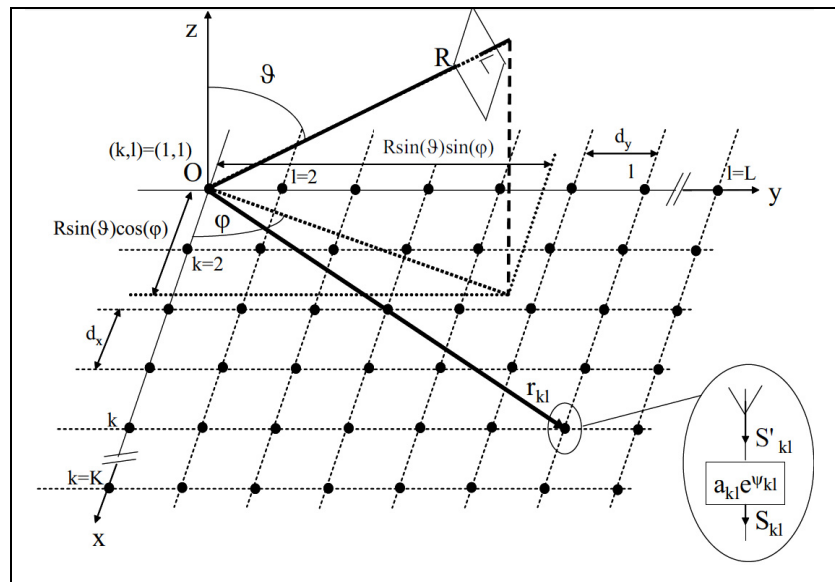
Figure 3.1 A planar array with K*L elements with the distance d_x between rows and the distance d_y between columns
Drawn from Visser et al. (2005, p. 242)

The position of an element in the array is shown by the vector r_{kl} , where k is the position of the element in the X direction (k=1,2,...,K) and l is its position in the Y direction (l=1,2,...,L) such that $r_{kl} = (k-1)d_x*u_x + (l-1)d_y*u_y$, where u_x and u_y are unit vectors in the x- and y-directions.
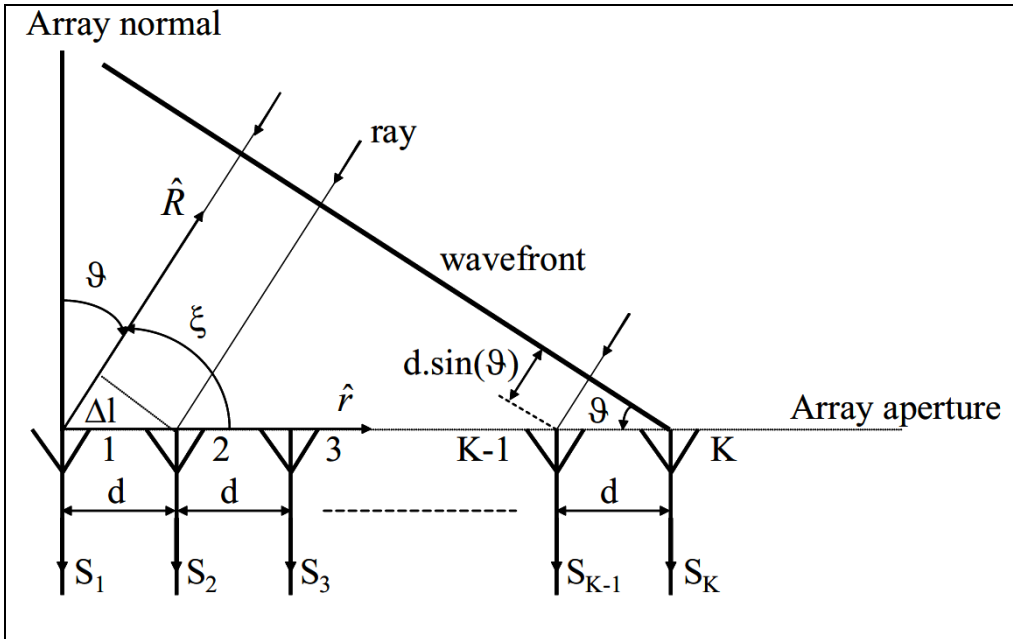
Figure 3.2 Linear array antenna of K elements at an inter-element spacing d, receiving a
plane wave from the direction R
Drawn from Visser et al. (2005, p. 244)

In order to analyse the total array, we will first analyse a linear sub-array (figure 3.2). It is convenient to take the phase reference $\psi=0°$ at element K and take the element $(k,l)=(1,1)$ at origin as the phase reference. Now we write the equations for the linear array and at the same time explain the vector projection.

In linear antennas the path length difference between two adjacent elements, ΔL, is the dot product of the plane wave direction $\hat{R}$ and the element position $\hat{r}$.

$$\Delta L = \hat{R}.\hat{r} = dcos(\xi) = dsin(\theta) \qquad (3.1)$$

where the angles ζ and θ are shown in figure 3.2.

The phase difference between two neighbouring elements, $\Delta\psi$, is:

$$\Delta\psi = k_0 dsin(\theta) \qquad (3.2)$$

with $k_0=2\pi/\lambda_0$, therefore the phase of element k relative to that of element 1 is:

$$\psi_k = k_0(k-1)dsin(\theta), for\ k = 1,2,\ldots,K \tag{3.3}$$

Equation 3.1 is easily translated to the planar array antenna. For element (k,l), the path length difference between two adjacent elements which are not weighted and not phased is:

$$\Delta L_{kl} = \hat{R}.\hat{r}_{kl} = (k-1)d_x\hat{R}.u_x + (l-1)d_y\hat{R}.u_y \tag{3.4}$$
$$= (k-1)d_x\ sin(v)cos(\varphi) + (l-1)d_ysin(\theta)sin(\varphi)$$

The phase of element (k,l) relative to element (1,1) is:

$$\psi_{k,l} = k_0(k-1)d_xsin(\theta)cos(\varphi) + k_0(l-1)d_ysin(\theta)sin(\varphi) \tag{3.5}$$

So the radiation pattern for the planar array antenna is:

$$F(\theta,\varphi) = f_e(\theta,\varphi)\sum_{k=1}^{K}\sum_{l=1}^{L}e^{j[k_0(k-1)d_xsin(\theta)cos(\varphi)+k_0(l-1)d_ysin(\theta)sin(\varphi)]} \tag{3.6}$$

where $f_e(\theta, \varphi)$ is the element radiation pattern.

The planar radiation pattern can be written as the product of an element factor $f_e(\theta, \varphi)$ and two linear array factors $A_{a1}(\theta, \varphi)$ and $A_{a2}(\theta, \varphi)$: (Figure 3.3)

$$F(\theta,\varphi) = f_e(\theta,\varphi)\ A_{a1}(\theta,\varphi)\ A_{a2}(\theta,\varphi) \tag{3.7}$$

$$A_{a1}(\theta,\varphi) = \sum_{k=1}^{K}e^{j[k_0(k-1)d_xsin(\theta)cos(\varphi)]} \tag{3.8}$$

$$A_{a2}(\theta,\varphi) = \sum_{l=1}^{L}e^{j[k_0(l-1)d_ysin(\theta)sin(\varphi)]} \tag{3.9}$$
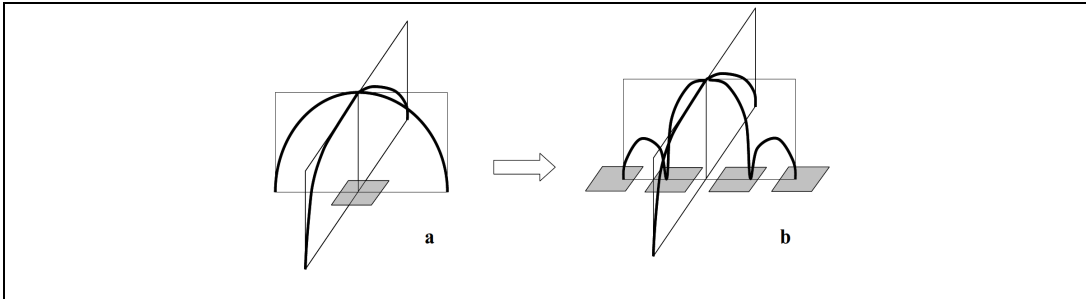
Figure 3.3 Normalized radiation patterns of a single element and a linear array consisting of these elements in the principal planes. a. Element. b. Linear array
Drawn from Visser et al. (2005, p. 246)

3.2   Effect of the Element Pattern on the Specifications of the Array

3.2.1   Pattern Multiplication

As the equation 3-7 shows, the array pattern is a result of multiplication of the array factor and the element pattern. For example figure 3.4 shows radiation pattern of a simple dipole, the array factor of a five elements array with 0.4λ, and the array radiation pattern. In this figure the overall radiation pattern is obviously different from the array factor as well as the element pattern. It shows that the dipole element affects the directivity and the beamwidth of the array.
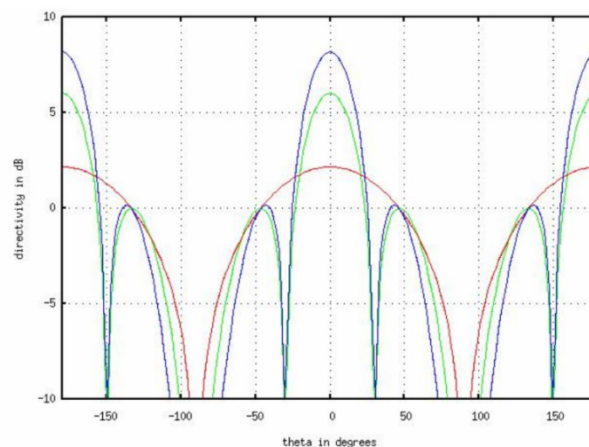
Figure 3.4 Dipole pattern (red), array factor (green), overall radiation pattern(blue)
Drawn from Moernaut et al. (2006, p. 6)

It is the same about the patch element; using the patch element has an important effect on the array antenna. The radiation pattern of a typical patch antenna is shown in figure 3.5.
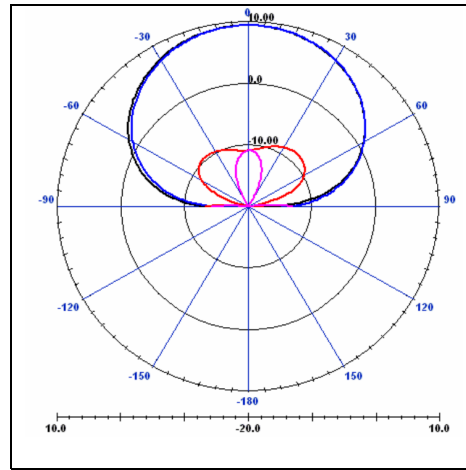
Figure 3.5 Radiation patterns for stacked Ku-band patch antenna
Drawn from Schippers et al. (2008, p. 346)

Mano et al., (1974) calculated mathematically the radiation pattern and the directivity of a planar array in xz plane. Using their work and transposing the array to the xy plane we have the element pattern as:

$$f_e(\theta, \varphi) \begin{cases} \sin(\theta)^p \sin(\varphi)^q & z \geq 0 \\ 0 & z < 0 \end{cases} \tag{3.10}$$

where p and q are arbitrary real numbers. The array is made of N_x elements in x-direction spaced by d_x and N_y elements in y-direction spaced by d_y. The scan angle is given by (θ_0, φ_0) and the main beam direction is given by (θ'_0, φ'_0).

The array factor is given by:

$$F = f_e(\theta, \varphi) . A_x(\theta, \varphi) . A_y(\theta) \tag{3.11}$$

where:

$$A_x = \frac{\sin N_x u}{N_x \sin u} \tag{3.12}$$

$$A_y = \frac{sinN_y v}{N_y\ sinv} \tag{3.13}$$

The u and v are given by :

$$u = \left(\frac{\pi d_x}{\lambda}\right)(sin\theta\ cos\varphi - sin\theta_0\ cos\varphi_0) \tag{3.14}$$

$$v = \left(\frac{\pi d_z}{\lambda}\right)(\ cos\theta - cos\theta_0) \tag{3.15}$$

The directivity is given by:

$$D(\theta,\varphi) = \frac{4\pi\left|f_e(\theta,\varphi)A_x(\theta,\varphi)A_y(\theta)\right|^2}{I(\theta_0,\varphi_0)} \tag{3.16}$$

The equation 3.16 shows that the element pattern has a direct effect on the directivity. In the next chapter we focus on the patch antenna and its pattern.

3.3 Comparison of Satellite Parabolic Antenna with Planar Array Antenna

In TV satellite reception, dish antennas are commonly used. They offer typical gain of 36dBi (IRSCHMANN, Hit FESAT 65) over a bandwidth of 10.7GHz to 12.7GHz. As mentioned before, these antennas are usually fixed and they are slow to be steered mechanically. Using a planar patch antenna array can help with steering, for example to allow tracking on a moving vehicle. However one must first establish what kind and what size of planar antenna array is required to provide similar performance to the dish antenna. This was done in Schippers et al., (2008) where it was determine that an array of 47.2*47.2 cm^2 is required.

Table 3.1 presents a comparison of the performance between the parabolic antenna mentioned in IRSCHMANN (Hit FESAT 65) and a corresponding patch array mentioned in Schippers et al., (2008). Every antenna is specified with some important parameters like the working frequency bandwidth, size, beamwidth, polarization, gain, directivity and efficiency. The beamwidth of the planar array antenna is 2 degrees whereas that for the parabolic one is 2.85 degrees. The beamwidth of the satellite antenna corresponds to the area of the Earth to be illuminated. It is related directly to the directivity. The efficiency of the planar array is around 50% which is 20% less than that of the parabolic antenna. Although the efficiency of

planar array is less than parabolic antenna, there are advantages to using them: (i) the area of the planar array is about 0.22 m^2 but the area of the parabolic antenna is around 0.33m^2. (ii) it can be steerable electrically, (iii) it is less expensive.

Table 3.1 Comparisons between the parabolic antenna and planar antenna

specifications	parabolic	Planar array
frequency	10.7-12.75	10.7-12.75
Gain	Min 36dB at 10.95GHz $G=10\log[k(d*\pi/\lambda)^2]=4\pi A_e/\lambda^2$	36dB
size	chord=65cm	d=11.8mm =0.5λ (12.7 GHz) 40(11.8mm)*40(11.8mm)=47.2*47.2cm^2
beamwidth	2.85º	2º
efficiency	70%	50%
Directivity D=G/e	37.55dB $4\pi A_e/\lambda^2$	10log(32400/2*2)=39.1dB
Polarization	dual linear (H & V)	dual linear (H & V)

3.3.1   Calculating the parameters of the planar array antenna

In this section we calculate the specifications of the planar array of Schippers et al., (2008) which is presented in table 3.1.

The specifications of the antenna are listed below:

- operating frequencies: 10.7-12.75 GHz;
- distance between the elements (d)=11.8 mm;
- N*N=40*40 (N is the number of elements in each side);
- current distribution: uniform;
- type of the Element: patch antenna.

Now we want to calculate the beamwidth with the help of the book.

Calculations:

Based on the formula reported in Balanis et al., (1982, p. 340), Array factor is:

2) $f = 1.144$

Base on figure 6-11 and equation 6-22a presented in Balanis (1982) we can obtained θ_h:

3) $\frac{\lambda}{L+d} = 1/20 \qquad \theta_h = 2.6°$

4) For uniform distribution:

$\theta_h = \theta_x \, Sec\theta_0 = 2.6 \, Sec\theta_0 \qquad$ for $\theta_0 = 0° \qquad \theta_h = 2.6°$

$\psi_h = \theta_y \, Sec\theta_0 = 2.6 \, Sec\theta_0 \qquad$ for $\theta_0 = 0° \qquad \psi_h = 2.6°$

$\Omega_A = \theta_h * \psi_h = 6.76$ steradian

The array is square, so $D_x = D_y$

$D_0 = \frac{32400}{\Omega_A} = \frac{32400}{6.76} = 4793 \qquad D_{dB} = 36.8$ dB

5) For Dolf-Tschebyscheff distribution:

$\theta_h = \theta_x \, Sec\theta_0 * f = 2.97 \, Sec\theta_0 \qquad$ for $\theta_0 = 0° \qquad \theta_h = 2.97°$

$\psi_h = \theta_y \, Sec\theta_0 * f = 2.97 \, Sec\theta_0 \qquad$ for $\theta_0 = 0° \qquad \psi_h = 2.97°$

$\Omega_A = \theta_h * \psi_h = 8.82$ steradian

$D_0 = \frac{32400}{\Omega_A} = \frac{32400}{8.82} = 3673.4 \qquad D_{dB} = 35.65$ dB

6) Efficiency $= P_r / P_r + P_{loss}$

The array radiation pattern is multiple of the single pattern and the array factor; so single pattern is very important. As it is told in part 1.3 the Multiplication of patch pattern in the array factor effects on the array pattern and also on the beamwidth. Schippers et al.,(2008) claims that it is 2 degree. But here we get the beamwidth of 2.6 degree. Because we did not consider the Pattern Multiplication effect.

As shown, the element plays an important role in the performance of the array. For microstrip patch array, the design of the individual element is the key to obtain good patterns. In the next chapter we discuss on the design of a microstrip patch element.

3.4   Number of Elements of the Array

According to the mentioned specifications for satellite antennas, the planar array antenna should provide a 36dB gain. To reach this amount of gain we need specific number of elements. This number depends on the element specifications and the location of the receiver relative to the satellite.

Figure 3.6 shows the geography of a geostationary satellite. To calculate the azimuth and the elevation of an antenna pointing to a geo-stationary satellite, the latitude and the longitude of the antenna and the longitude of the satellite should be defined. For example the latitude and longitude of Montreal, Canada (the location of the antenna) is: 45° 30' 0" N / 73° 35' 0" W.
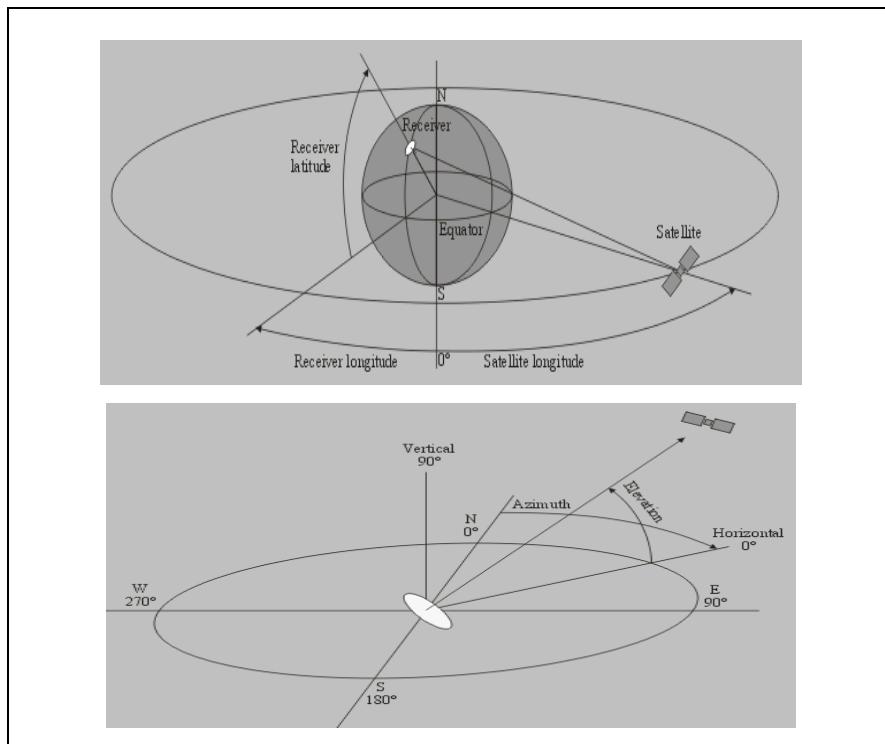
Figure 3.6 Calculating the azimuth and the elevation of an antenna
pointing to a geostationary satellite
Drawn from Cleto Pescia (2004)

If the angle φ_R and θ_R show the location of the receiver and the angle φ_S shows the location of the satellite, the azimuth and the elevation of an antenna can be calculated as:

$$\theta = tan^{-1} \frac{\cos(\varphi_R - \varphi_S) * \cos(\theta_R) - 0.1512}{1 - (\cos(\varphi_R - \varphi_S) * \cos(\theta_R))^2} \tag{5.1}$$

$$\varphi = 180 + tan^{-1} \frac{tan(\varphi_R - \varphi_S)}{\sin(\theta_R)} \tag{5.2}$$

Table 3.2 shows a list of the Canadian satellites.

Table 3.2 The satellites in Canada
Adapted from Wikipedia (2008)

satellite	Location	Type	Remarks
Ceil-2	129° W	Broadband	Leased to Echostar/Dish Network
Anik F3	11.8° W	Broadband	Ku-Band leased to Echostar/Dish Network
Anik F2	111.1° W	Broadband	Hybrid C/Ku/Ka-band satellite
Anik F1	107.3° W	Broadband	Hybrid C/Ku-band satellite; will be replaced by Anik F1R
Anik F1R	107.3° W	Broadband	Hybrid C/Ku-band satellite; will replace Anik F1
Nimiq1	91° W	Broadband	32 Ku-band transponders
Nimiq2	82° W	Broadband	Hybrid Ku/Ka-band satellite

CHAPITRE 4

MICROSTRIP PATCH ANTENNA

4.1   Microstrip Patch Antenna Basics

Microstrip antennas based on physical parameters are categorized in four groups of microstrip patch antennas: microstrip dipoles, printed slot antenna, and microstrip travelling-wave antennas which their characteristics are discussed by James et al., (1989). The most common group, Patch antenna or rectangular microstrip antenna, is a kind of antenna that is made of a rectangular sheet, or patch, over a large metal sheet (ground). Between these two sheets is a substrate.
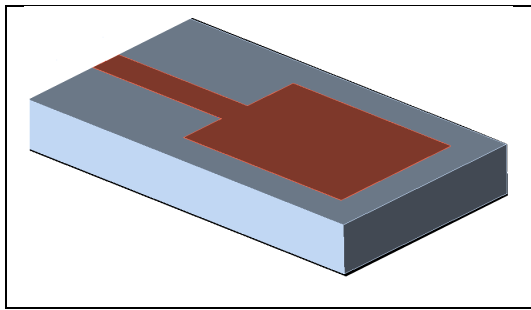
Figure 4.1   Microstrip patch antenna

Patch antenna has its own advantages and limitations. Here we present some of them (Garg et al., 2001):

Advantages:

- light weight;
- low fabrication cost;
- easily made Linear and circular polarization;
- easily made dual frequency and dual polarization;
- no need of backing cavity;
- easily integrated;
- feed lines can be fabricated within antenna structure.

Limitations:

- narrow bandwidth;

- low gain (5<gain<6);

- large ohmic loss in feed structure;

- most microstrip antenna radiate in half of the space;

- complex feed structure.

In spite of the difference in geometrical shape of the patches, the radiation pattern of them is similar to that of a dipole. Figure 4.2 shows the radiation pattern of a patch antenna.
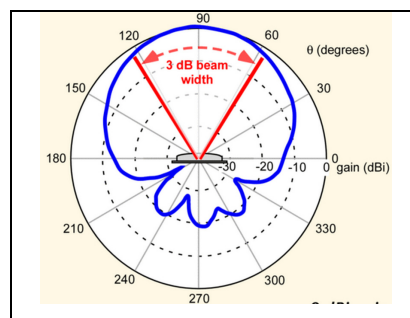
Figure 4.2 The radiation pattern of patch antenna
Drawn from Wikipedia (2012)

In fact, there is no specific simple formula for the patch radiation pattern. James et al., (1989) has calculated the radiation pattern for a large number of patches.

Normally, a patch has a gain between 5dB and 6dB, and a beamwidth between 70º and 90º. In patch antenna pattern, bandwidth, beamwidth, sidelobe level and gain don't change with frequency. But impedance changes fast with frequency.

4.2   Patch Shape

There are different patch shapes, which make them different in their bandwidth but with similar radiation patterns. The common patch shapes are annular ring, rectangular/square patch, quarter-wave (shorted) patch. (Figure 4.3)
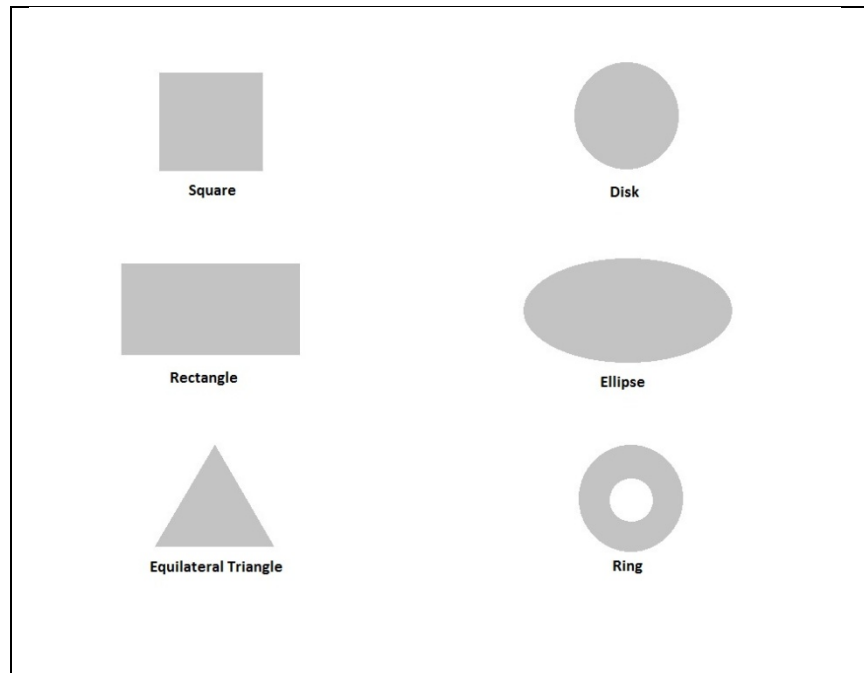
Figure 4.3 Common patch shapes
Adapted from Garg et al. (2001, p. 9)

4.3   Patch Feed

There are different kinds of feed methods for patch like coaxial feed, microstrip feed, proximity coupled microstrip feed, aperture coupled microstrip feed, and coplanar waveguide feed. Some of them are discussed here.

1. Coaxial Feed:

    The probe can connect to the patch antenna to feed it. The conductor of the covaxial line must be connected to the back side of printed circuit board and the center of the covaxial must be connected to the patch. (Figure 4.4)
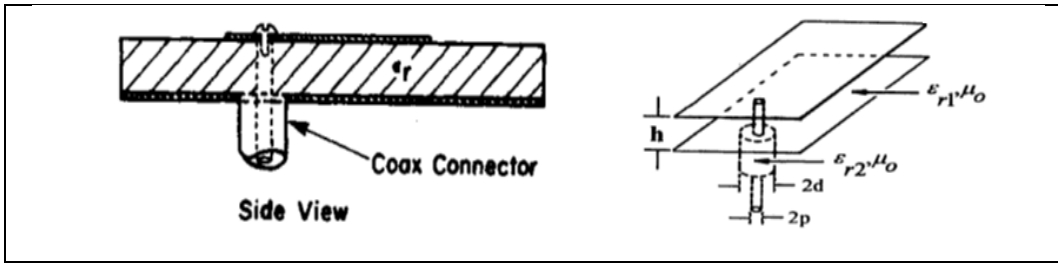
Figure 4.4 Probe feed to the patch
Drawn from Garg et al. (2001, p. 17)

Feeding by covaxial has some advantages like simplicity determining the input impedance by changing the position of probe. Also it has some disadvantages like difficult fabrication because of large number of solder points and much probe radiation in thick substrate.

2. Microstrip Feed:

In this method, a microstrip line is connected to the patch to feed. If the microstrip line connects directly to the patch (edge coupling) it makes a big limitation: the input impedance of the patch being higher than 50 ohm (figure 4.5.a). If the microstrip line connects by a narrow gap to the patch (gap coupling), it makes other problem of high radiation in the gap place (figure 4.5.b).
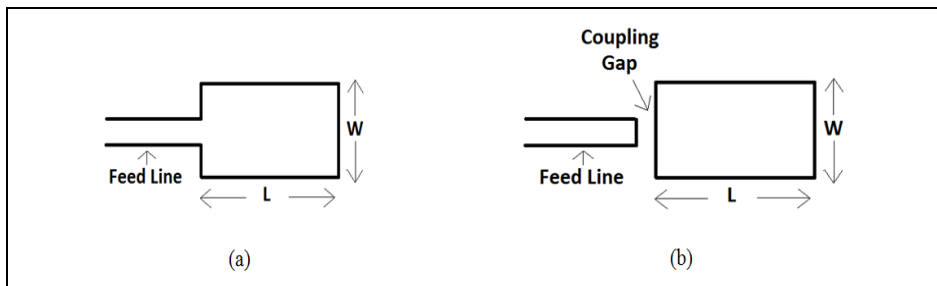
Figure 4.5 (a) Edge coupling, (b) Gap coupling
Adapted from Garg et al. (2001, p. 21 and p. 22)

3. Microstrip Inset Feed:

In this method a microstrip line is inserted to the patch. The feed position is selected such that the input impedance is 50 ohm. This method overcomes the limitations of the microstrip feed. The result of this method is as the same as probe method.(Figure 4.6)
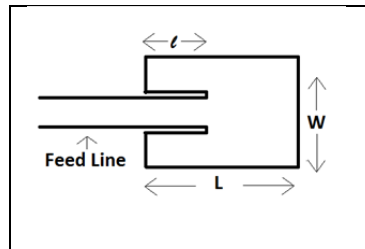
Figure 4.6 Microstrip inset feed
Adapted from Garg et al. (2001, p. 23)

4. Proximity Coupled Microstrip Feed:

This noncoplanar feed method is shown in figure 4.7. It uses two layers of substrate. The patch is on the upper layer and the microstrip line is on the lower layer. This method can increase the bandwidth up to 13%. The microstrip line can be connected to the stub and the stub parameters can change the bandwidth. In addition the substrate parameters also can effect on the bandwidth. By choosing thin lower substrate we can reduce spurious radiation from the open end of the microstrip; also two layer substrate can make more bandwidth for the patch.
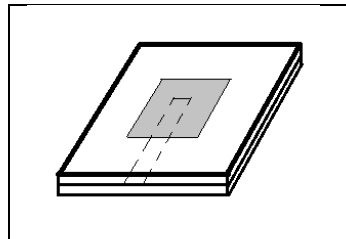
Figure 4.7 Proximity coupled microstrip Feed
Adapted from Garg et al. (2001, p. 25)

5. Aperture Coupled Microstrip Feed :

    This feed method is shown in figure 4.8. It uses two layers of substrate. The microstrip line on the lower substrate is electromagnetically coupled to the patch on the upper substrate by the slot aperture in the ground plane. The slot can be in any shape and it can increase the bandwidth. Because of the existence of the ground plane, the radiation from the open end of the feed line can not interfere with the radiation of the patch and they can act independently. For this we can chose the substrate parameters in a way to optimise the patch and feed functions. For example the thicker substrate for patch can make larger bandwidth and that of low dielectric constant can increase the efficiency of the patch where as the substrate for the feed should be thin with high dielectric constant. This method improves the polarization purity also.

    The coupling slot should be centered to the patch because the magnetic field of the patch is more in the center. In addition of the substrate parameters, the shape and the length of the slot, the width of the feed line, and stub length also effect on the bandwidth. Garg et al., (2001) has reported the increase of 21% bandwidth for the unstacked patch.
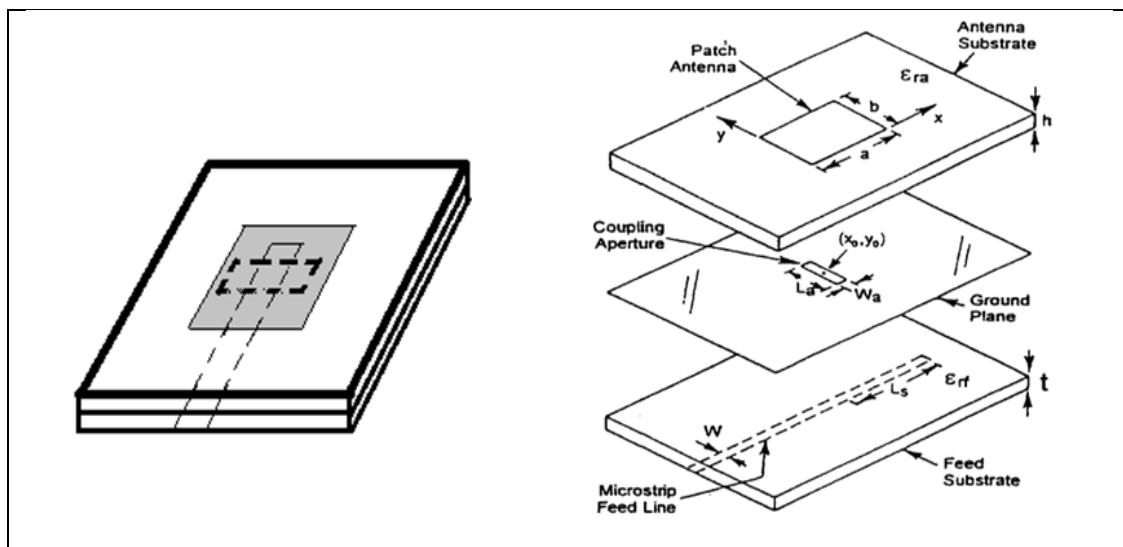
Figure 4.8 Aperture coupled microstrip feed
Adapted from Garg et al. (2001, p. 26 and p.540)

4.4 Patch Array Loss

Losses in patch antennas are caused by dielectric losses and conductor losses. Losses in the feed lines and patches and losses due to feed radiation, surface wave generation, mutual coupling and design and manufacturing tolerance error are the factors which reduced the gain of patch arrays.

- the total feed losses L_f in a two dimensional patch array is: (Wikipedia, 2012)

$$L_f = \frac{\alpha d}{\lambda_m}(\sqrt{N} - 1) + n_t l_t + n_b l_{b} + l_c \qquad (4.1)$$

$\alpha = \alpha_d + \alpha_{er}$,N is the total number of elements, d is the element spacing, l_t , l_b and l_c are the radiation losses in db of a T-junction, bend and coax to microstrip transition respectively. n_r is the number of a T-junction; n_s is the number of bends.

- the thickness of the substrate and dielectric constant and feed impedance also effect on the overall array loss. The figure 4.9 shows that overall array loss increases with increasing substrate height, decreasing dielectric constant and feed impedance.
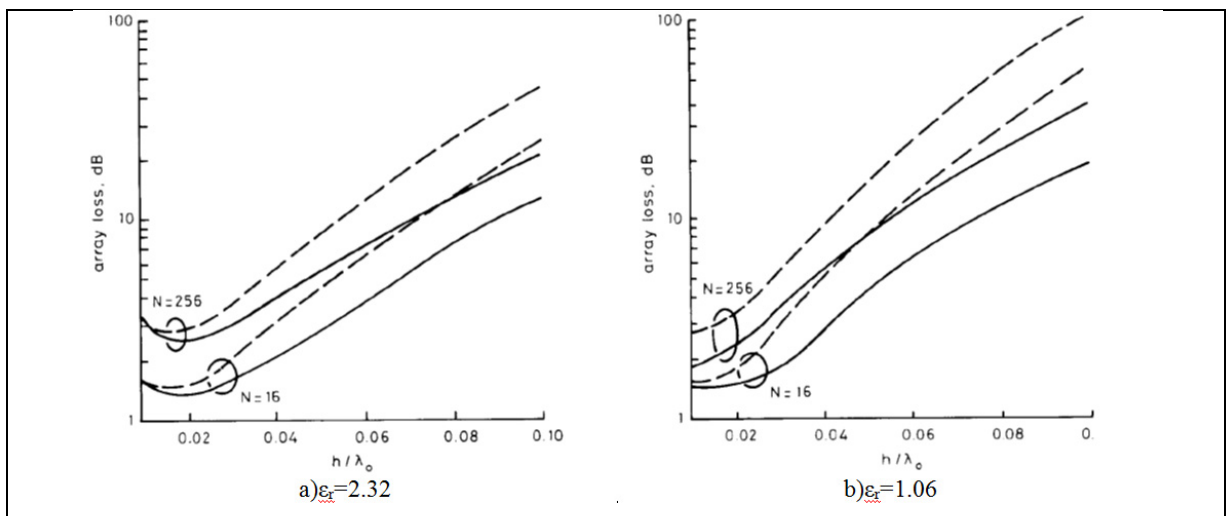
Figure 4.9 Overall loss of corporately fed microstrip array (element spacing = 0.8 λ)
_____ feed impedance = 100 Ω
_ _ _ feed impedance = 50 Ω
Drawn from Hall et al. (1988, p. 5)

4.5   Size Restriction of Patch

There are some restrictions for the place and size of patch elements. The available power of every element of array depends on the previous one, so we need an element with large emission efficiencies. However, the maximum patch width is restricted by the frequency domain and the minimum distance between the patches and between the columns to suppress coupling effect. (Schoebel et al., 2010)

For small patch widths, a reliable determination of the emission efficiency is difficult, because the radiated power is small and comparatively large measurement or numerical errors can easily occur in the development process. In general, the maximum achievable sidelobe suppression is a function of the maximum and minimum available patch widths.

An additional complication results from the matching of the patch elements, which requires a length adjustment as a function of patch width. Hence, for equidistant position of the patches, phase errors are introduced which deteriorate a low-sidelobe pattern. Adjusting the position of the elements to ensure a uniform phase distribution will also affects on the antenna pattern as the spacing becomes non-uniform. (Schoebel et al., 2010)

4.6   Patch Polarization

The polarization of a rectangular patch is linear. Circular polarization is also obtained by suitably placed the feed point of the nearly squared patch. Polarization of the antenna can be changed mechanically and physically. (Garg et al., 2001)

Microstrip antennas have good potential for making dual-polarized antennas due to their several attractive features including low profile, lightweight, conformability to mounting structure and compatibility with integrated circuit technology. (Ryu et al., 2008)

4.7   Patch Bandwidth

An antenna has some characteristics such as gain, side lobe level, beamwidth, and VSWR, which can be changed with frequency; but the input impedance of the patch changes fast with the frequency. So it defines the bandwidth of the patch antenna.

For a type of parallel resonance the half power bandwidth is obtained from equation 4.2. (Garg et al., 2001)

$$BW = \frac{2G}{\omega_0 \left.\frac{dB}{d\omega}\right|_{\omega_0}} \qquad (4.2)$$

where input impedance Y is equal to G+jB. Impedance bandwidth can be defined also in term of VSWR=2 where the half power bandwidth for a patch with transmission line feed is 2.4.

$$BW = \frac{VSWR - 1}{Q\sqrt{VSWR}} \qquad (4.3)$$

Q is the quality factor of the patch which is less than 2 for bandwidth of 78%. (Garg et al., 2001)

Other than impedance bandwidth, the cross polarization is the other most important factor that limit the bandwidth. (Garg et al., 2001)

In this thesis, BW is referred to the 10dB return loss bandwidth.

4.7.1   Increasing the Bandwidth of the Patch Antenna

The main disadvantage of these microstrip patch antennas is their limited bandwidth. So the researchers try a lot to enhance the bandwidth of patch antenna to being useful for broadband satellite communication.

There are several methods for increasing the bandwidth of the patch which are discussed below.

4.7.1.1   Effects of Substrate Parameters

According to equation 4.3, the impedance bandwidth has an inverse relation to Q. So the parameters of substrate such as thickness and the dielectric constant can effect on the bandwidth. Q can be defined as bellow:

$$Q = \frac{\text{Energy stored}}{\text{power lost}} \tag{4.4}$$

By increasing the thickness of the substrate, the bandwidth is increased and by increasing the dielectric constant, the bandwidth is decreased. But changing these factors made some bad effects which limited the change domain. Increasing the thickness and decreasing the dielectric constant, cause to make surface waves. These waves radiate from the surface and the efficiency being low and etc.

Figure 4.10 is shown two plots of variation of radiation Q for a rectangular patch antenna as a function of thickness and dielectric constant of the substrate.
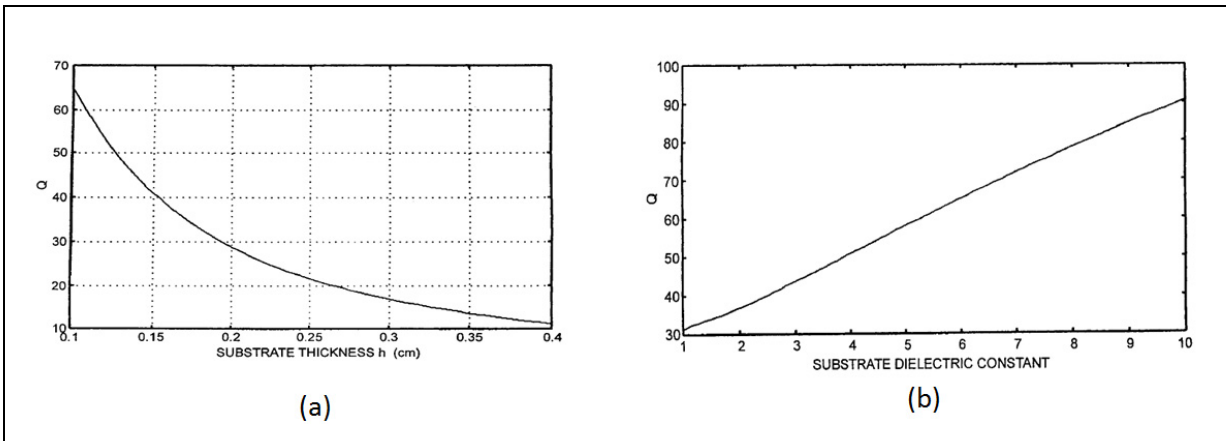
Figure 4.10 W=0.9 L, f=3 GHz (a) Q as a function of the substrate thickness, ε=2.2
(b) Q as a function of the dielectric constant, h=1.59mm
Drawn from Garg et al. (2001, p. 536 and p. 537)

4.7.1.2   Choosing Suitable Patch Shape

The shape of the patch can also affect Q as well as the bandwidth. Table 4.1 compares the bandwidth of different shapes of patch.

Table 4.1 Comparison of VSWR=2 bandwidth
ε_r=2.32, h=1.59 mm, f=2 GHz (Garg et al., 2001)

Element shape	Element size	Bandwidth%
Narrow rectangular patch	L=4.924 cm, W=2 cm	0.7
Wide rectangular patch	L=4.79 cm, W=7.2 cm	1.6
Square patch	L=W=4.82 cm	1.3
Circular disk	a=2.78 cm	1.3
Annular ring	b=8.9 cm, a=4.45 cm	3.8
Quarter-wave patch	L=2.462 cm, W=2 cm	1.05

4.7.1.3   Using Stacked Elements

In this method, we put some sheets in different sizes up and below the main patch which are separated by foam or other space filler. It reduces the impedance variation of the antenna with frequency. Thick laminates of low permittivity provide the largest bandwidth and surface wave efficiency. (Schippers et al., 2008) These sheets should stand in a special distance to be coupled to the exited patch. Dimensions of every stack should be a little different to make a different resonant. A little shift in x or y dimension of the patch seriously affect impedance bandwidth and radiation pattern. Figure 4.11 consists of several resonant patches with different sizes. There is no specific rule for the distances between the layers. Every layer is exited with the other patch. Each patch has its own resonant frequency but close to each other and it makes an overall large bandwidth for the whole system.
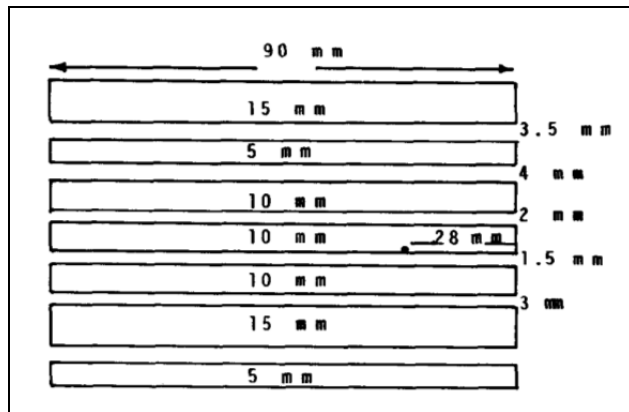
Figure 4.11 Parasitic coupled patch antenna
Drawn from Aanandan et al. (1990, p. 1582)

Here we present the results of several simulations performed in order to investigate the effect of the stacked elements on the bandwidth. All these circuits were designed for the resonant frequency of 11.7GHz on the 951Green Tape substrate, which is used in LTCC technology with the electrical constant of 7.8. These simulations are done with Momentum 3D planar electromagnetic simulator (Agilent). The results of simulation are presented in APPENDIX I.

The first design is a patch over one layer of substrate with a 1.6mm thickness. The results show a 0.694 GHz bandwidth and an efficiency of 40.145%. (APPENDIX I: Figure-A I-1)

The second design contains two patches. In this design there is one additional patch element. Each patch is over the substrate with the thickness of 0.224mm. Each layer is separated from the other one with an air gap. The result shows a 0.106 GHz bandwidth and an efficiency of 46.751%. (APPENDIX I: Figure-A I-2)

The third design is a patch with two stacked elements. In this design there are two additional patches over the substrate with a thickness of 0.224mm. Each layer is separated from the other layers with an air gap. The result shows a 0.162 GHz bandwidth and an efficiency of 55.483%. (APPENDIX I: Figure-A I-3)

The fourth design is a patch with three stacked elements. In this design there are three additional patch elements over the substrate with the same characters. They are separated

from the other layers with an air gap with the thickness of 0.508mm; there is one more patch element below the main patch which is separated with an air gap of 0.308mm. It shows 0.193 GHz bandwidth and an efficiency of 61.953%. (APPENDIX I: Figure-A I-4)

The fifth design is a patch with four stacked elements. In this design there are four additional patch elements over the substrate with the same characters which are separated with an air gap with the thickness of 0.508mm from the other layers; there is one more patch element below the main patch which is separated with an air gap of 0.308mm. It shows a 0.271 GHz bandwidth and an efficiency of 67.410%. (APPENDIX I: Figure-A I-5)

Table 4.2 shows the comparison of these systems with different layers.
Figure 4.12 shows patches with Different Number of Stacked Elements

Table 4.2 Comparison between Patches with Different Number of Stacked Elements

Number of Layers	Bandwidth (GHz)	Efficiency%
one	0.059	69.329
two	0.106	55.483
three	0.162	55.483
four	0.193	61.953
five	0.271	67.410

One layer   Two layers   Three layers

Four layers   Five layers
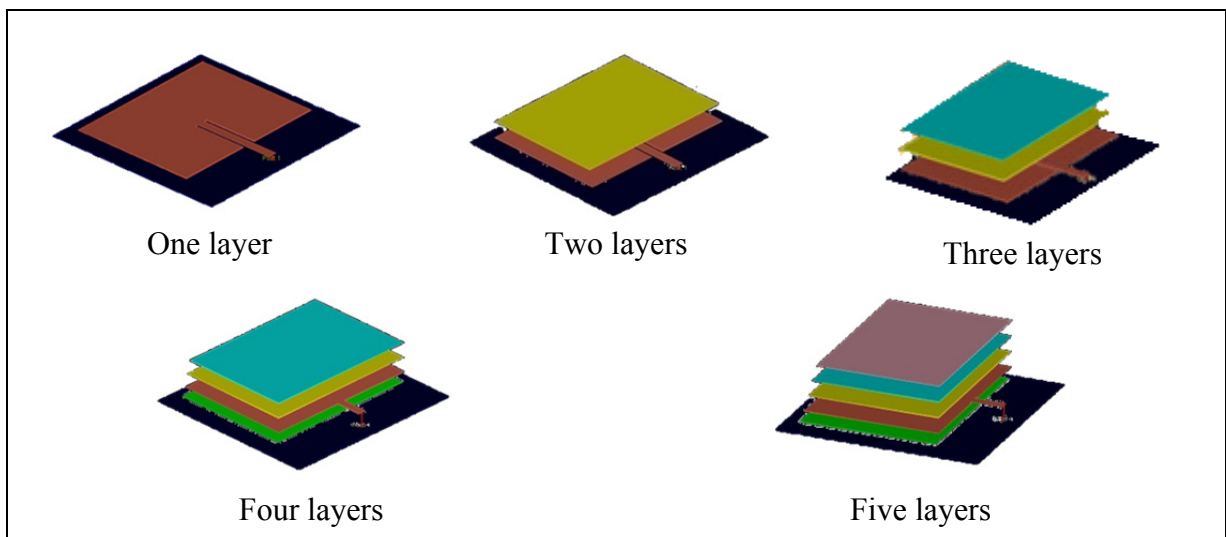
Figure 4.12 Patches with different number of stacked elements

Table 4.2 shows that increasing the number of stacked elements increase both the efficiency (except for the one layer) and the bandwidth. For more than five layers we did not get a good result. It seems that with this structure we can not get a better result.

4.7.1.4   Choosing Suitable Feeding Technique

As it was discussed in part 4.1.2, there are different methods for feeding the patch antenna. These methods can have important effect on the bandwidth. Among these feeding techniques, aperture feeding is used more in broadband antennas. Because it has many adjustable parameters like width, length, shape of the aperture and stub parameters.

Table 4.3 Comparison between different feed techniques for patch antennas
Drawn from Stutzman et al. (1998)

Characteristics	Microstrip Line Feed	Coaxial Feed	Aperture Coupled Feed	Proximity Coupled Feed
Spurious Feed Radiation	More	More	Less	Minimum
Reliability	Better	Poor due to soldering	Good	Good
Ease of fabrication	Easy	Soldering and drilling	Alignment require	Alignment require
Impedance Matching	Easy	Easy	Easy	Easy
Bandwidth achieved with Impedance Matching	2-5%	2-5%	2-5%	13%

In this part we investigated about the effect of different aperture feed lines on the bandwidth. The aperture shape is one of the important parameters that adjust the input impedance and bandwidth. The aperture can be circular, square, rectangular, or other shapes. We used Momentum software to simulate patches with different aperture shapes and found out that for

my design structure, the rectangular shape, which is the most popular one, is the best aperture shape. For maximum coupling the patch, should be centered over the aperture. The feed line is also positioned in the center of the aperture. Various feed lines can affect the patch bandwidth. The traditional feed line for aperture feeding is a simple line. The width of the line is 50 ohms generally. The length of the line can adjust the input impedance. The problem of this kind of feeding is having a narrow bandwidth. The result of the simulation of the patch with the regular feed line is shown in figure-A II-1.

Another feed line which has been proposed recently is a cross shape one. This kind of feed line has several advantages. In addition of having a larger bandwidth than the simple line, it has adjustable parameters like width, length and position of cross line relative to the other line and to the aperture which make effect on the bandwidth. The result of the simulation of this kind of feed line is presented in figure-A II-2.

Because the cross feed does not provide enough bandwidth, we proposed another shape for the feed line; there are two proposed patch feeds. One is like a patch and the other one is like a patch with inset. Existence of an inset can help to adjust the imaginary part of the impedance and result in a larger bandwidth. The simulation result of the first one is presented in figure-A II-3 and the simulation result of the second one is presented in figure-A II-4.

Table 4.4 and 4.6 show the characteristics of the two different patches and table 4.5 and 4.7 show the comparison between the mentioned different feed lines. We can see that the proposed patch feed shape with inset (patch A) make better result and larger bandwidth up to 2.5 GHz.

About patch B, existence of inset does not work well. But with the patch feed shape we can reach up to 2.9 GHz bandwidth.

Figures 4.13 and 4.14 show these mentioned types of feed lines.

Table 4.4 Characters of the patch element A

Er(patch)=2.2	H(patch)=60mils	Patch size=6.8*8.3mm	Feed width= 0.588mm
Er(feed)=7.1	H(feed)=20mils	Aperture size= 2.7*3.7mm	λ(2.2)=17.32mm

Table 4.5 Comparison between the different feed line for patch A

	Types	Directivity	Gain	Efficiency%	polarization	BW(GHz)	fc(GHz)
1	Line feed	7.66	6.19	71.3	linear	1.26	12
2	cross feed	7.36	5.9	71.4	linear	1.28	11.3
3	Patch feed	7.36	6.14	75.4	linear	1.29	12.4
4	Patch-inset feed	7.9(11.3) 6.8(13) 7.36(11.7)	5.8(11.3) 5.8(13) 6(11.7)	74.16(11.3) 78.9(13) 73.6(11.7)	linear	2.5	11.26 & 13
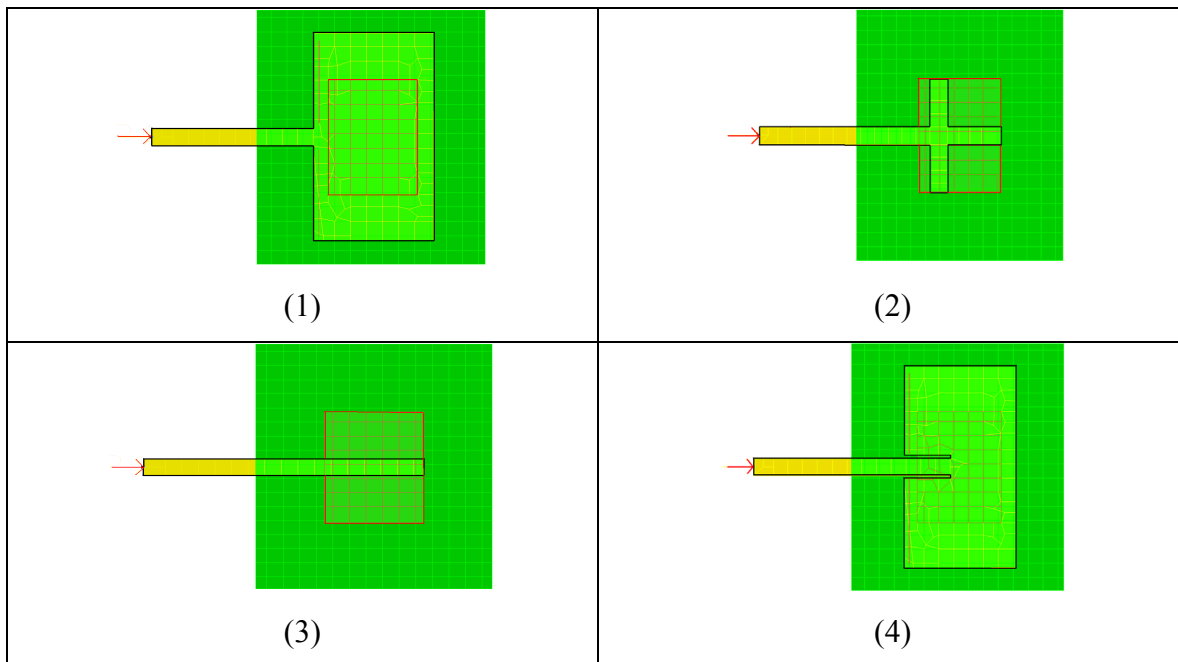
Figure 4.13 Different feed line for patch A

Table 4.6 Characters of the patch element B

Er(patch)=2.2	H(patch)=60mils	Patch size=6.8*8.3mm	Feed width= 0.777mm
Er(feed)=2.2	H(feed)=20mils	Aperture size=2.85*3.75mm	λ(2.2)=17.32mm

Table 4.7 Comparison between the different feed lines for patch B

	Types	Directivity	Gain	Efficiency%	polarization	BW(GHz)	fc(GHz)
1	Line feed	7.1	5.6	71.1	linear	0.9	11.3
2	Cross feed	7.57	6.11	71.4	linear	1	11.6
3	Patch feed	7.1	5.6	71.5	linear	2.9	11.7, 13.7
4	Patch feed2	7	5.6	72.4	linear	2	11.13, 12.5
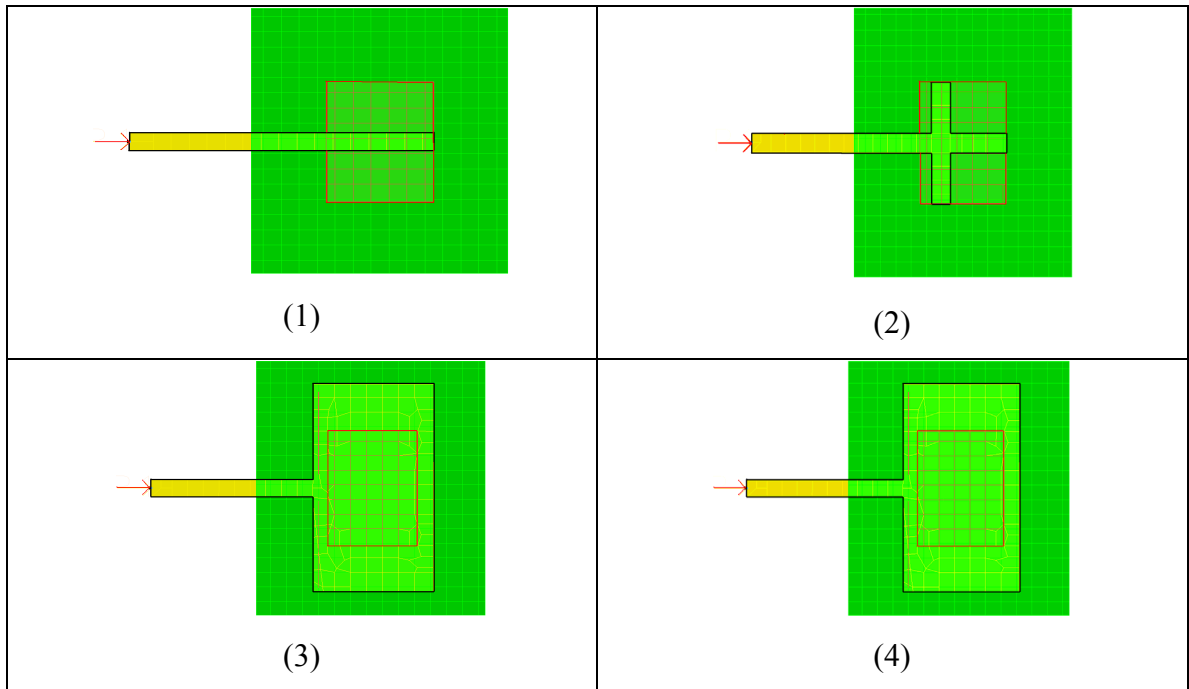
Figure 4.14 Different feed line for patch B

CHAPITRE 5

DESIGN OF A WIDEBAND PATCH ELEMENT ANTENNA

5.1   New Linear Polarized Patch Antenna A

We proposed a new kind of feed line for aperture feeding which has many advantages. This method of feeding can provide large bandwidth around up to 19% for one layer patch, which is considerable. Another important characteristics of this structure is the possibility to easily adjust the real and imaginary parts of the input impedance. In this structure, the aperture is rectangular. The feed line is like a patch which makes a large bandwidth. This structure is useful because, in addition of a adjusting the input impedance and the resonance frequency by the aperture size, we can also adjust the imaginary part by changing the dimension d and adjust the real part by changing the s and r dimensions. (figure 5.1)
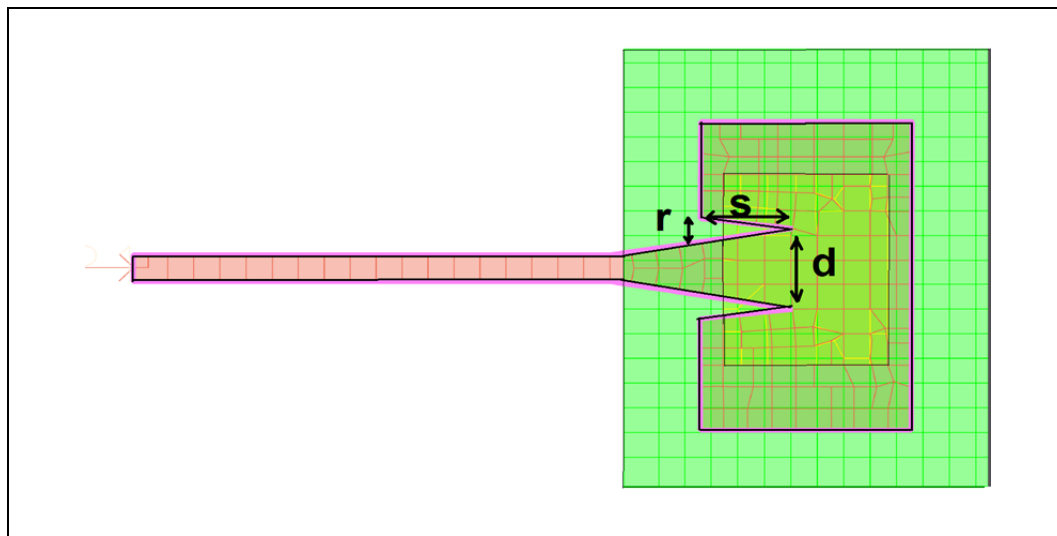
Figure 5.1 New linear polarized patch antenna A

In this design the feed dielectric is composed of two layers of 10 mils material 951 Green Tape with a dielectric constant of 7.8 to use in LTCC (after shrinkage it beings 17mils). Patch dielectric consists of one layer of 65mils dielectric Rogers RT5870 with the dielectric constant of 2.3 and two layers of substrate 951 Green Tape with dielectric constant of 7.8. The substrate is shown in figure 5.2.
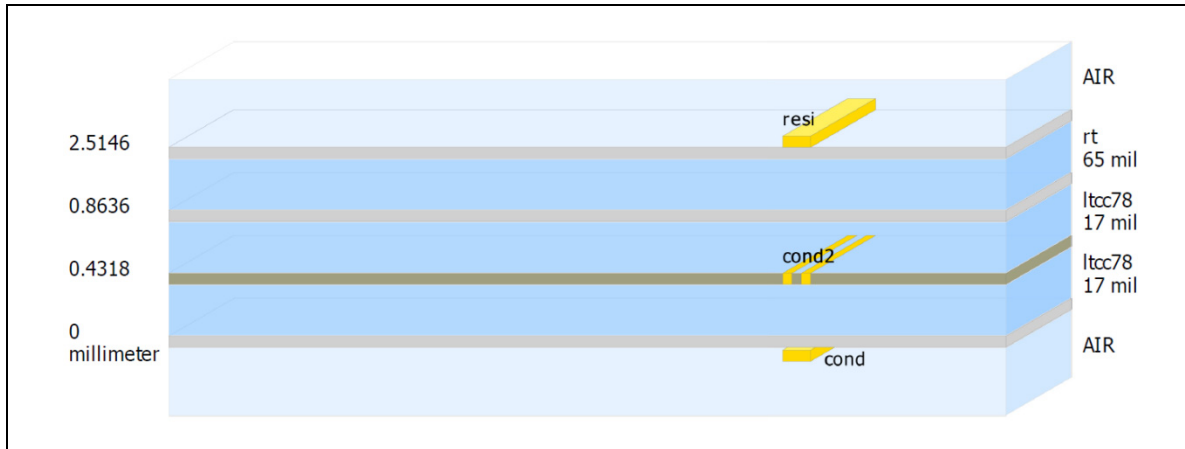
Figure 5.2 Patch antenna substrate I

This patch is designed for a center frequency of 11.7GHz. Figure 5.3 shows the S11 parameter and the input impedance. For this antenna the bandwidth is 1.92GHz, the input impedance at the center frequency is $Z_0(0.975+ j0.064)$ Ohms and the efficiency is 58.57%.
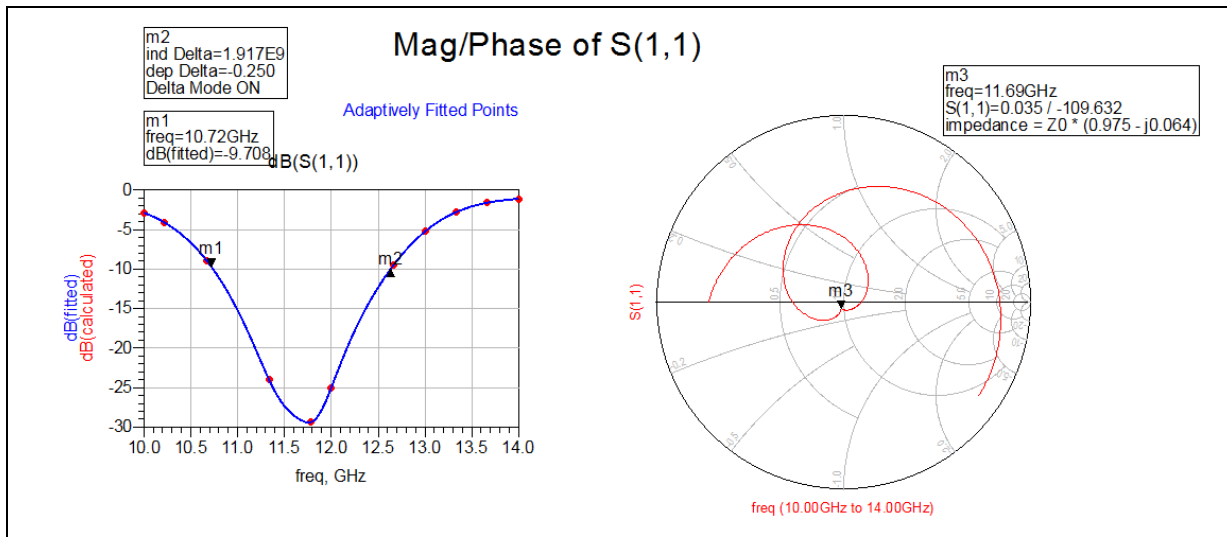
Figure 5.3 S11 Parameter and input impedance plot of the patch antenna A

5.2　　New Linear Polarized Patch Antenna B

This antenna shown in figure 5.4 is a little different compare to the previous one with the same characteristics:
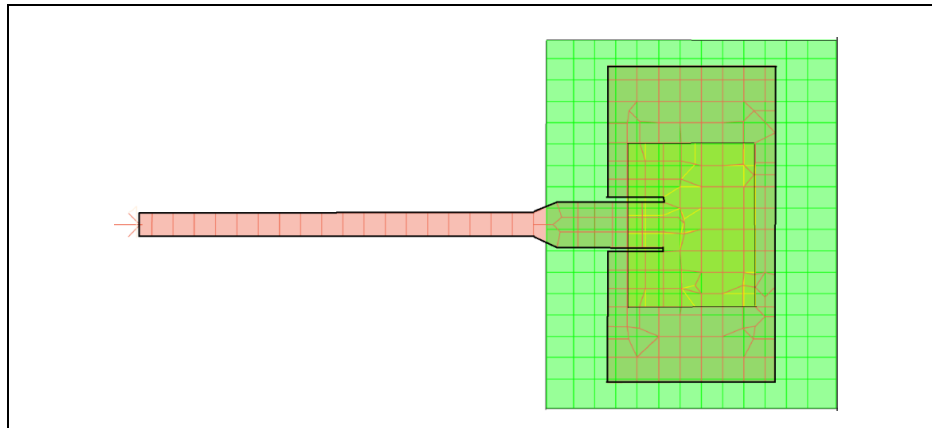
Figure 5.4   Linear polarized patch antenna B

This patch is designed for a center frequency of 11.7GHz. Figure 5.5 shows the S11 parameter and the input impedance. For this antenna the bandwidth is 1.94GHz, the input impedance at the center frequency is $Z_0(1.004- j0.036)$ Ohms and the efficiency is 57.31%.
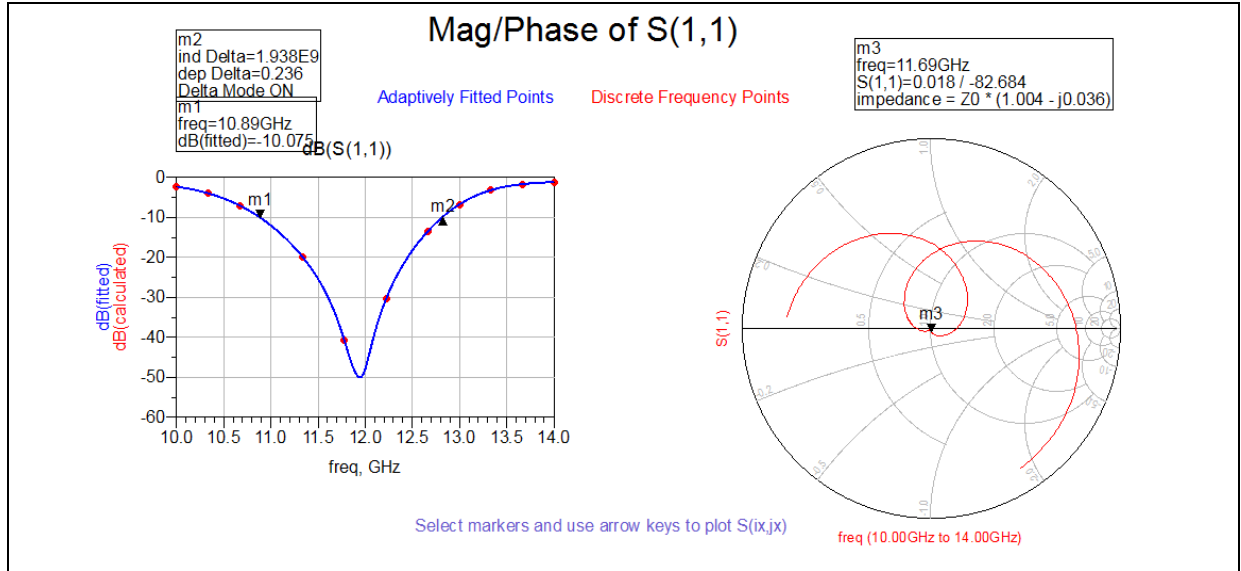
Figure 5.5 S11 Parameter and input impedance plot of the patch antenna B

5.3   New Dual Polarized Patch Antenna C

To have a dual polarized antenna we need a symmetric structure. In this structure the aperture is changed from a square to a square frame. The substrate is the same as before. (figure 5.6)
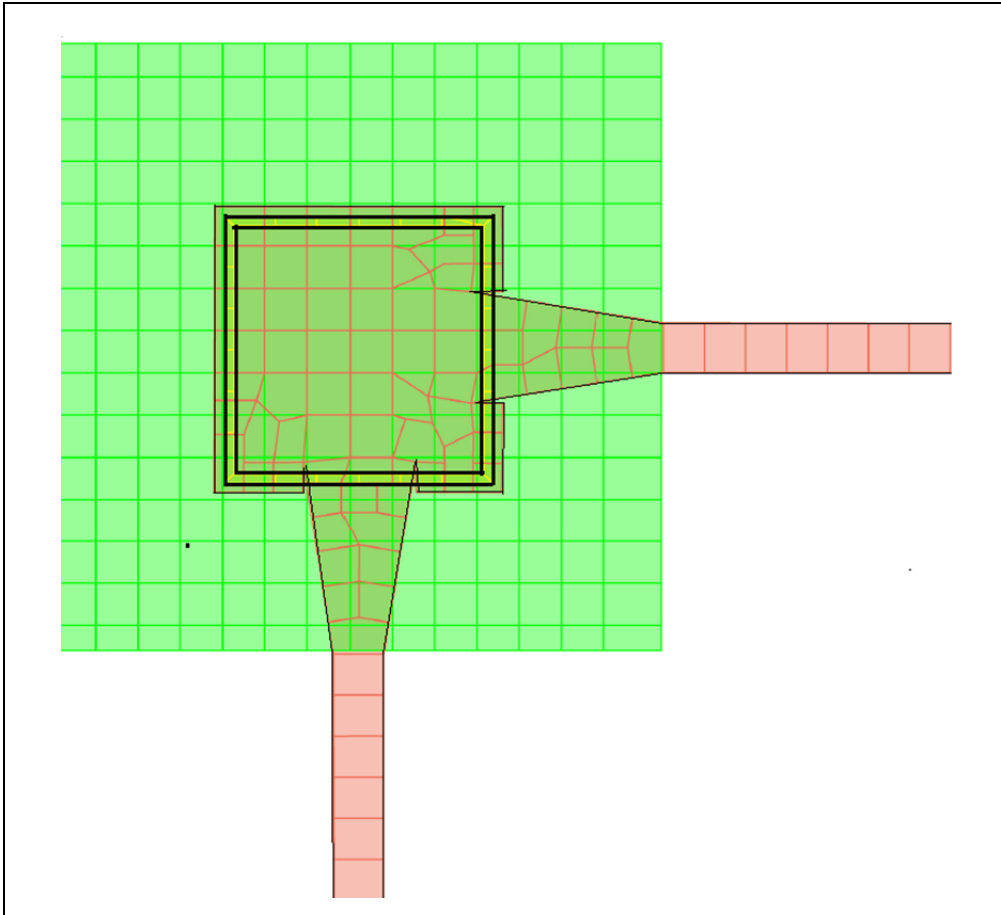
Figure 5.6 New dual polarized patch antenna

This patch is designed for center frequency of 11.7GHz over the substrate I. Figure 5.7 shows the S11 parameter and the input impedance. For this antenna the bandwidth is 2.17GHz, input impedance in center frequency is $Z_0(0.967- j0.030)$ Ohms with the efficiency of 58.20%.
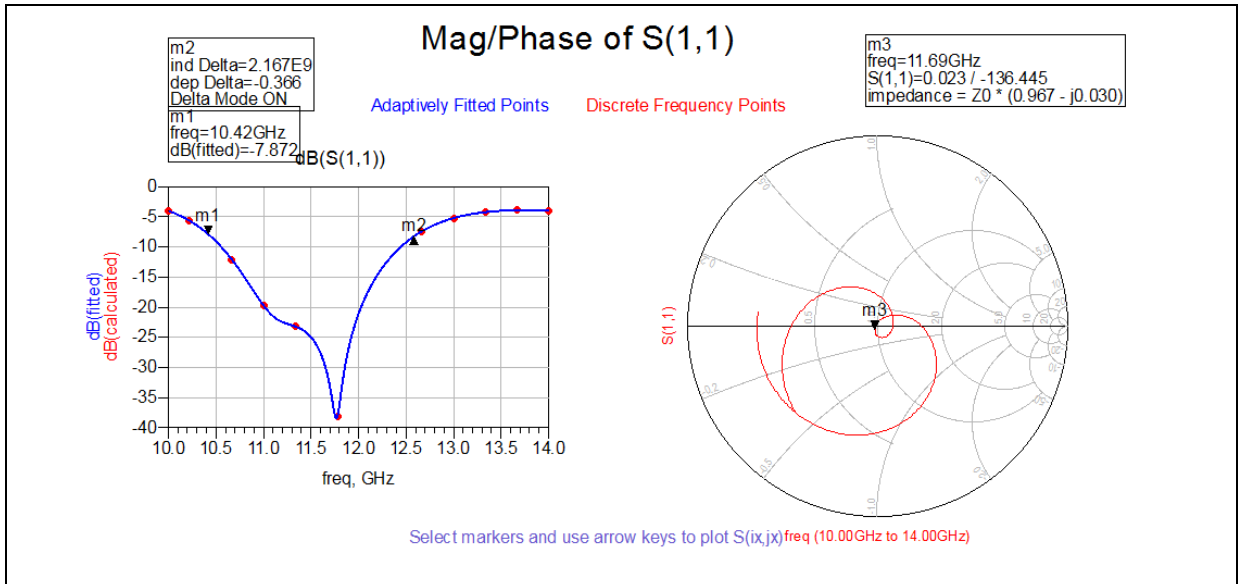
Figure 5.7 S11 Parameter and input impedance plot of the dual polarized patch antenna on the 65mils substrate of Rogers RT5870

5.3.1 Dual Polarized Patch Antennas and the Divider

For connecting the patch elements to each other and make an array antenna we need dividers. In this structure we used from the divider.

5.3.1.1 Divider

A microstrip divider provides equal splits (3dB) and low loss. It consists of two quarter wave lines with impedance $Z_0\sqrt{2}$ at the center frequency. It needs one lumped $2z_0$ resistor between the output ports. For the divider used for an array antenna, because of symmetry we do not need this lumped resistor. Figure 6.8 shows the designed divider for connecting two patch elements. (figure 5.8)
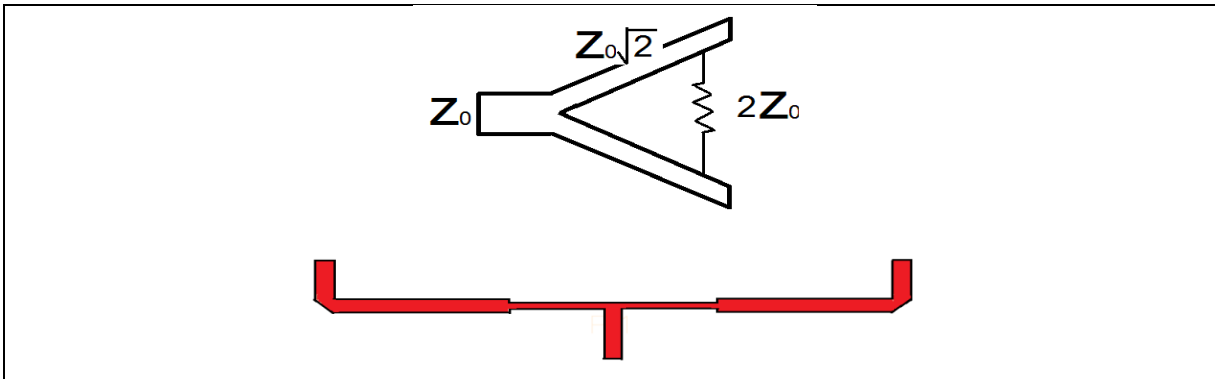
Figure 5.8 Divider

5.3.1.2 Two Patch Antenna Connect to the Divider

Figure 5.9 shows two patch elements which are connected to a divider and its S11 parameter.
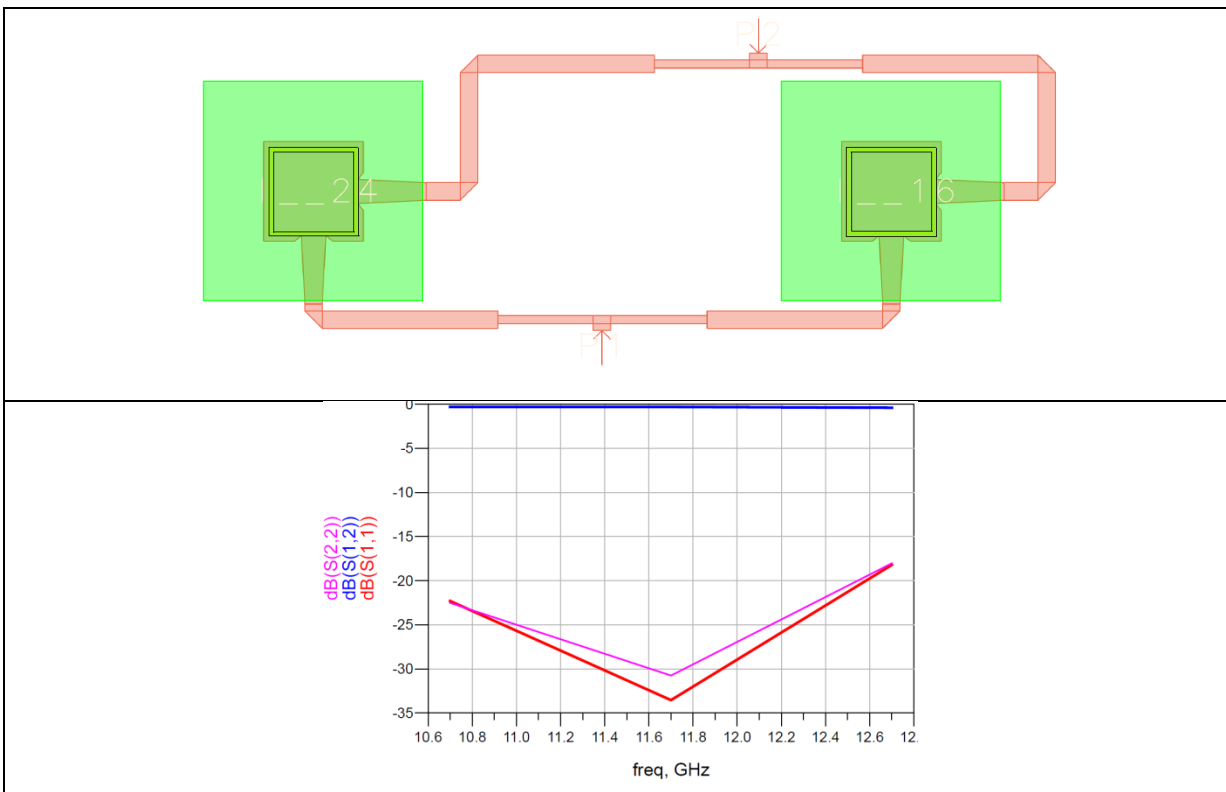
Figure 5.9 S-Parameters of the two dual polarized patch antennas
connected to each other

5.3.2   Dual Polarized Patch Antenna D

Figure 5.11 shows the S11 parameter of another two patch element with different substrates. The patch dielectric is 80mils of Rogers RT5870. The substrate is shown in figure 5.10.

The bandwidth of this patch antenna is 2GHz with the input impedance of $Z_0(1.070- j0.011)$ Ohm. The efficiency of this structure is 63.92% which is better than the previous one.
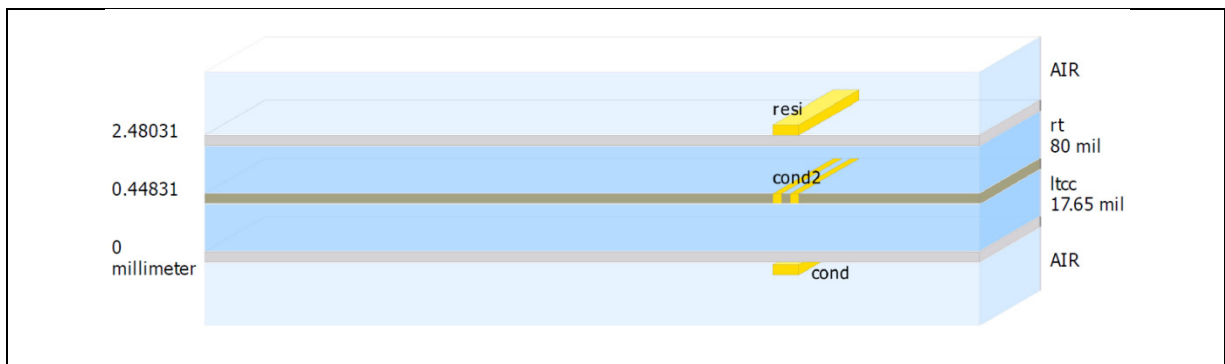
Figure 5.10 Patch antenna substrate II
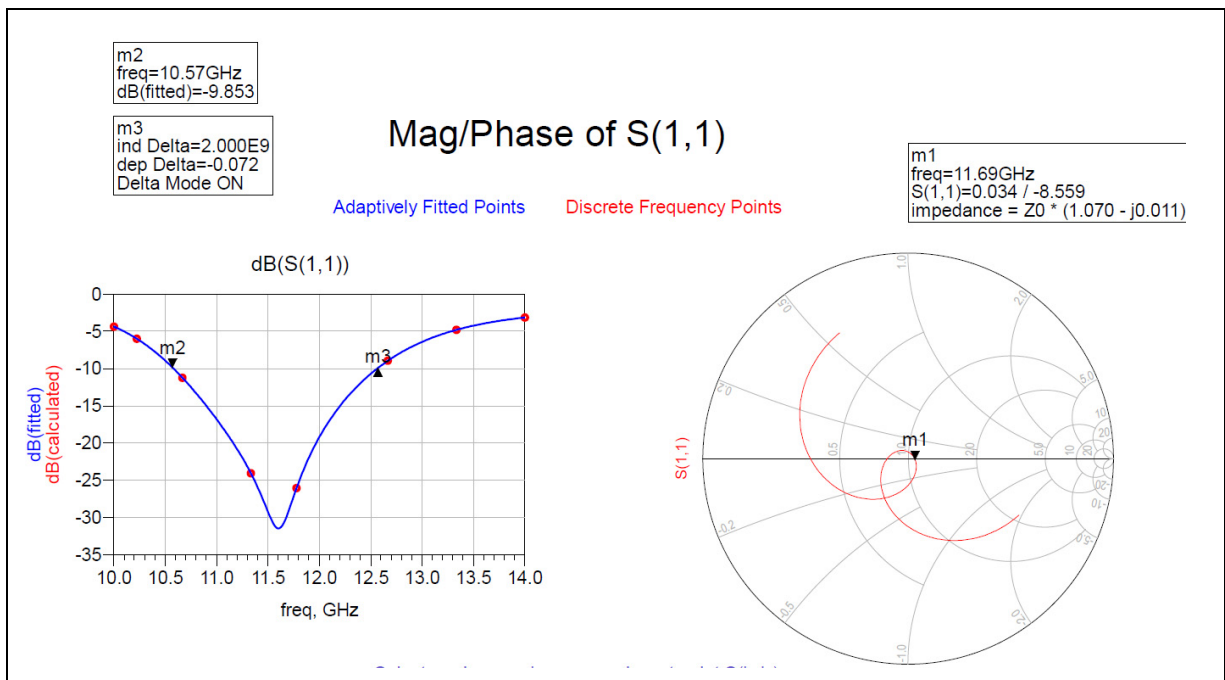
Figure 5.11 S11 Parameters of the two dual polarized patch antennas connected to each other on the 80mils substrate of Rogers RT5870

5.4　　　Calculating the number of the elements of the array of patches

As discussed in section 3.4, to have a planar array of equivalent gain, we must take in to account the element pattern. Having developed a patch element we can now calculate the number of required patch elements to achieve equivalence with the dish. This will determine the size of the planar array.

To calculate the number of elements to provide a 36dB gain, we need to know the gain and the efficiency of an individual element. The efficiency of my designed dual polarized patch (figure 5.6) is 58.2% and that of the other designed patch (figure 5.9) is 63.9%. The patch gain also is considered as 0.58. We used this amounts to calculate the number of elements.

Usually the distance between two elements is around 0.72 to 0.8λ. We suggest d=0.75 λ.

For uniform distribution based on Balanis, (1982) we can obtain the h beamwidth:

$$\theta_h = cos^{-1}\left[\cos\theta_0 - 0.443\frac{\lambda}{L+d}\right] - cos^{-1}\left[\cos\theta_0 + 0.443\frac{\lambda}{L+d}\right] \qquad (5.3)$$

L is the length of the array. For this antenna we should provide 2 degrees for θ_h and φ_h.
There is a relation between the bandwidth in polar coordinate system and xyz coordinate system:

$$\theta_{x0} = cos^{-1}\left[\cos\theta_0 - 0.443\frac{\lambda}{Md+d}\right] - cos^{-1}\left[\cos\theta_0 + 0.443\frac{\lambda}{Md+d}\right] \qquad (5.4)$$

$$\theta_{y0} = cos^{-1}\left[\cos\theta_0 - 0.443\frac{\lambda}{Nd+d}\right] - cos^{-1}\left[\cos\theta_0 + 0.443\frac{\lambda}{Nd+d}\right] \qquad (5.4)$$

$$\varphi_h = \sqrt{\frac{1}{\theta_{x0}^{-2}\sin^2\varphi_0 + \theta_{y0}^{-2}\cos^2\varphi_0}} \qquad (5.5)$$

$$\theta_h = \sqrt{\frac{1}{\theta_{x0}^{-2}\cos^2\varphi_0 + \theta_{y0}^{-2}\sin^2\varphi_0}} \qquad (5.6)$$

Ω is the space angle. It can be obtained as:

$$\Omega = \theta_h \varphi_h \qquad (5.7)$$

In addition of the beamwidth we need to provide 36dB gain. For this we can fix the directivity in x direction and change the directivity in y direction. In other words we can fix the number of the rows in the array and adjust the number of column to get 36dB gain.

$$D_0 = \pi\cos(\theta_0)\,D_x D_y\,, \qquad (D_0 = \frac{32400}{\Omega_A}) \qquad (5.8)$$

$$G_0 = e\,D_0 \qquad (5.9)$$

The Matlab M-program of these calculations is presented in APPENDIX V.

This program uses the location of the receiver and the satellite as the inputs and calculates the number of elements, directivity, gain, beamwidth, and the phases of the elements. In this program the patch efficiency is considered to be 58% and the number of elements varies depending on the position of the receiver and the satellite. In general, for a receiver placed in Montreal, this number varies between 210 and 270, which can be a square or nearly-square geometry.

As an example the output of this program for the satellite Ceil-2 and the receiver placed in Montreal is as follows:

$\theta = 15.121$ degree ($0° =$ north, $90° =$ east, $180° =$ south, $270° =$ west)

$\varphi = 244.207$ degree ($0° =$ horizontal, $90° =$ vertical)

$N_x = 15$

$N_y = 18$

D_x= 22.387 ,   13.500 dB

D_y= 26.499 ,   14.232 dB

G_x= 13.029 ,   11.149 dB

G_y= 15.422 ,   11.882 dB

θ_x= 1.476

θ_y= 2.230

θ_h= 2.000

φ_h= 1.561

To provide the antenna gain in the direction (15.121º, 244.207º), the elements must have the phase distribution given in table 5.1 where the amplitude is uniform.

Figure 5.12 shows the phase of the elements by the intensity of color. 0 degree is white and 360 degrees is black.

Table 5.1 Phase of each element in uniform array in degrees

0	31	61	92	123	153	184	215	245	276	306	337	8	38	69
63	94	125	155	186	217	247	278	309	339	10	41	71	102	132
127	157	188	219	249	280	311	341	12	43	73	104	135	165	196
190	221	252	282	313	343	14	45	75	106	137	167	198	229	259
254	284	315	346	16	47	78	108	139	169	200	231	261	292	323
317	348	18	49	80	110	141	172	202	233	264	294	325	355	26
21	51	82	112	143	174	204	235	266	296	327	358	28	59	90
84	115	145	176	207	237	268	298	329	360	30	61	92	122	153
147	178	209	239	270	301	331	2	33	63	94	124	155	186	216
211	241	272	303	333	4	35	65	96	127	157	188	219	249	280
274	305	335	6	37	67	98	129	159	190	221	251	282	313	343
338	8	39	70	100	131	161	192	223	253	284	315	345	16	47
41	72	102	133	164	194	225	256	286	317	347	18	49	79	110
104	135	166	196	227	258	288	319	350	20	51	82	112	143	173
168	198	229	260	290	321	352	22	53	84	114	145	176	206	237
231	262	293	323	354	24	55	86	116	147	178	208	239	270	300
295	325	356	27	57	88	119	149	180	210	241	272	302	333	4
358	29	59	90	121	151	182	213	243	274	305	335	6	36	67
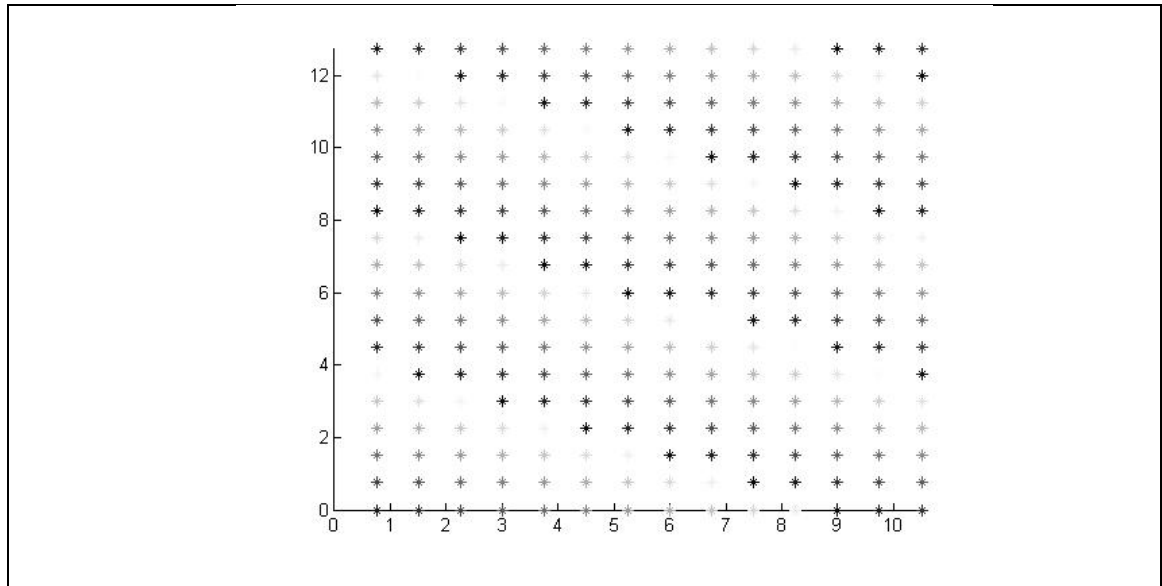
Figure 5.12 The element phase shown by the color intensity

CHAPITRE 6

FABRICATION

6.1   Low Temperature Co-Fired Ceramic Technology

For the fabrication of these components we used Low Temperature Co-fired Ceramic (LTCC) technology besides using printed circuit board (PCB).

LTCC multilayer technology is a popular technology to produce highly integrated, complex multilayer modules and circuits. This technology is appreciated for its flexibility in realizing an arbitrary number of layers with easy-to-integrate circuit components like via-holes,   thick film resistors, cavity-buried or top-mounted Surface Mount Technology (SMT) components or even chip devices. (Holzwarth et al., 2001)

LTCC multilayer technology has great benefits in microwave applications: high level of integration, buried components, low losses, robustness, cavities for mounting MMICs, temperature coefficients close to that of GaAs, good thermal conductivity due to a thermal management and others. (Wolff et al, 2009)

The LTCC fabrication process comprises the following main steps as present in KEKO EQUIPMENT and as shown in figure 6.1:

1. via punching: vias may be punched or drilled with a laser;
2. via filling: vias can be filled with a conventional thick film screen printer or an extrusion via filler. In the first case, the tape has to be placed on a sheet of paper that lies on a porous plate; a vacuum pump holds the tape on its place and it is used as an aid for via filling;
3. Conductor printing: cofireable conductors are printed on the green sheet using a thick film screen printer;

4. stacking: opposite to the process where each layer is placed in turns over tooling pins or where some processors use heat pliers to fix the sheets in turns one on top of the other, the sheets are stacked one by one;

5. laminates: There are two possibilities of laminating the tapes in the process of LTCC production. The first one is uniaxial lamination; the tapes are pressed between heated plates at 70°C, 200 bar for 10 minutes. The second way is to use an isostatic press; The stacked tapes are vacuum packaged in a foil and pressed in hot water at pressure about 350 bar;

After laminating, the parts are usually cut into the individual pieces;

6. co-firing: laminates are fired in one step on a smooth, flat setter tile.

The temperature of sintering is below 900° C for the LTCC glass-ceramic. This relative low temperature enables the co-firing of gold and silver conductors. The melting points of Au and Ag are 960° C and 1100° C respectively. (Wolff et al., 2009)
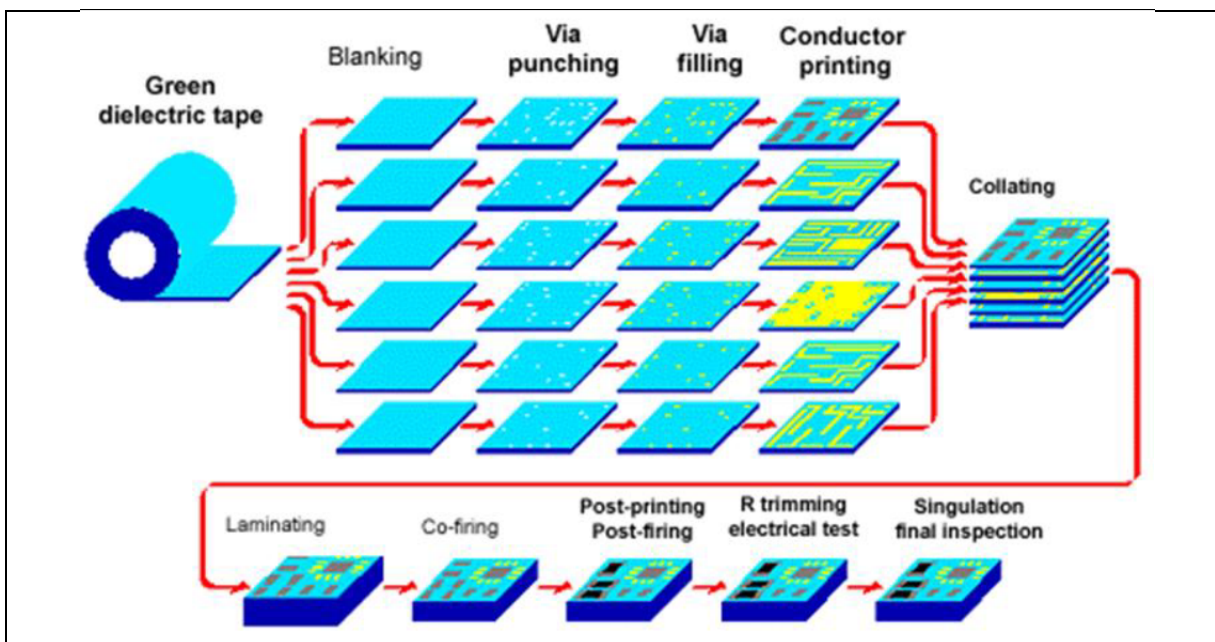
Figure 6.1 Technology steps for fabricating a LTCC circuit
Adapted from Wolff et al. (2009, p. 3)

For fabricating of the patches designed in chapter five, we use two kinds of ceramic type which are available at the LTCC laboratory of École de technologie supérieure namely: 951 Green Tape and 9K7 Green Tape. The datasheets for these two ceramics are presented in APPENDIX VI.

There are some rules for designing in LTCC which should be considered such as the size limitation and shrinkage of each part which help us to reach the expected dimensions. These rules are available at the LTCC laboratory and were followed in our design.

6.2 LTCC Fabrication

The feed part of my patch is fabricated with LTCC technology. At first we chose substrate 9K7 Green Tape with a dielectric constant of 7.1 and a thickness of 20 mils. To decrease the feed loss it is better to choose a substrate with low dielectric constant and low thickness. Every layer in LTCC has 10 mils thickness and total the thickness of the LTCC element must not to be less than two layers to ensure mechanical robustness. For the first design we used two layers of substrate 9K7 Green Tape. The thickness after shrinking is 17.65mils. Figure 6.2 shows the layout of the design of the feed of two patches which are connected to each other by a divider.

The four corner vias are for adjusting the alignment of the LTCC and PCB parts.
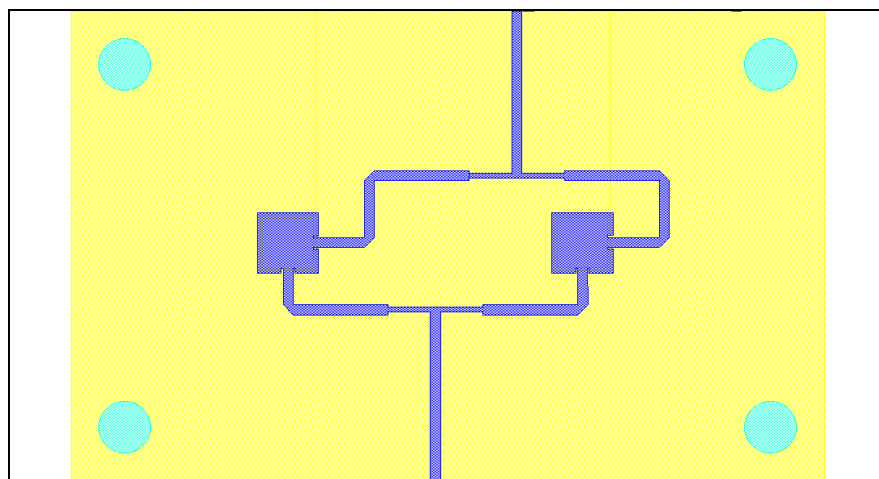
Figure 6.2 The design of the feed of two patches D which are connected to each other by a divider in Momentum

Figure 6.3 shows the bottom view of fabricated LTCC feed component with the material 9K7 Green Tape while figure 6.4 shows the top view of the same circuit.

Figure 6.3 Bottom view: the feed of two patches D connected to each other with a divider over substrate 9K7 Green Tape in LTCC
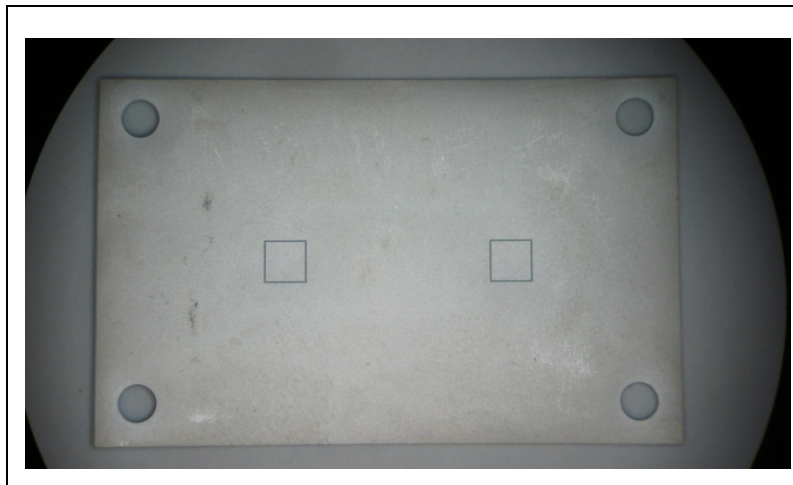
Figure 6.4 Top view: the slots of the two patches D in ground over substrate 9K7 Green Tape in LTCC

In the process of fabricating this component we faced some problems. Although it had two LTCC layers, this component was very thin which made it very fragile and difficult to fabricate. For example it had been broken in some parts (Figure 6.5) and was distorted (not flat) particularly near the edges (Figure 6.6). These problems had me use another material,

the 951 Green Tape, which has better rigidity and flatness but a higher dielectric constant of 7.8. We also used four layers instead of two layers and we had no fragility or flatness issue.
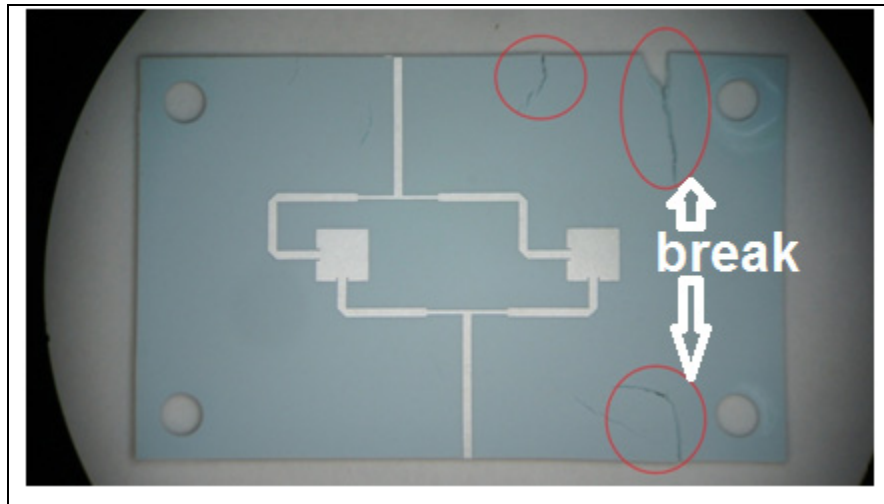
Figure 6.5 The LTCC device being broken in the fabrication process because of very thin thickness

Figure 6.6 Side view of the LTCC fabrication broken in the fabrication process because of very thin thickness

Figure 6.7 shows the mask for the circuits using the 951 substrate. We reproduced the design of the divider, two dual polarized patches C connected to each other with a divider, one dual polarized patch C element, and two different linear polarized patches A and B. Every mask is around 10cm by 10cm before shrinkage. The design includes a ground layer in the middle of stack of four layers. The PCB part is designed on the Rogers substrate separately. The details about the simulation were presented in part 6.1.

Again, the corner vias are for adjusting the alignment of the LTCC and PCB parts.
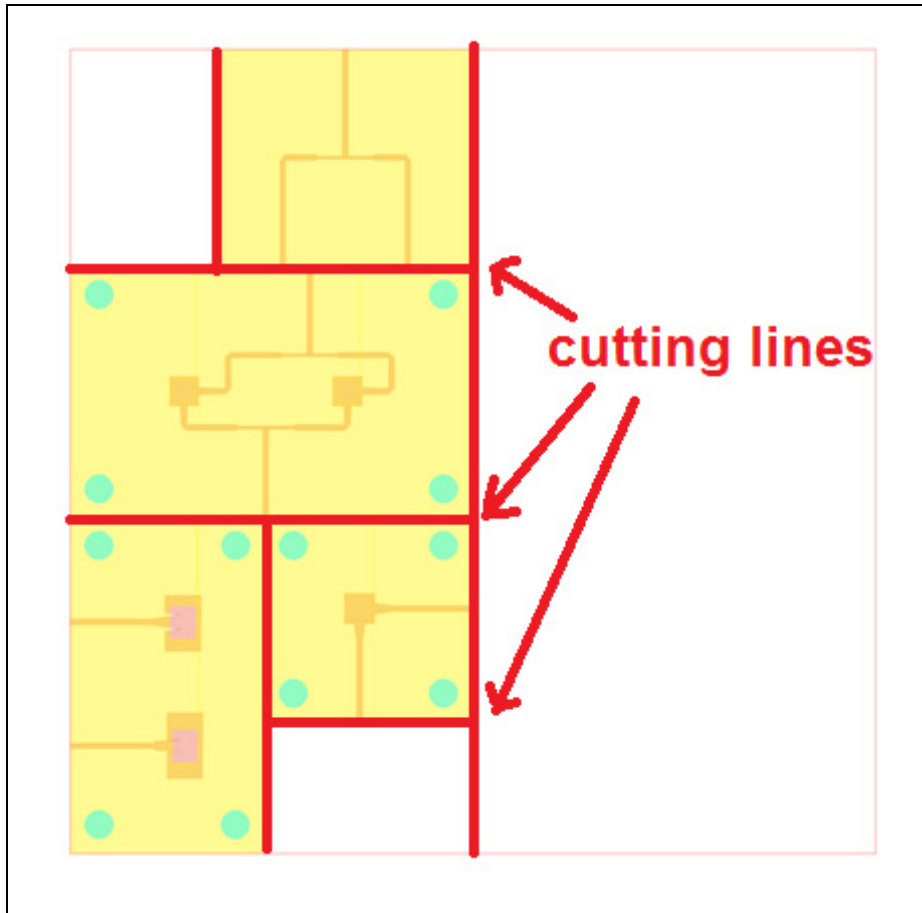
Figure 6.7 The momentum design for LTCC on the substrate 951 Green Tape

The circuit of figure 6.7 was fabricated and cut along the cutting lines. Figure 6.8 shows the fabricated divider on the 951 substrate.
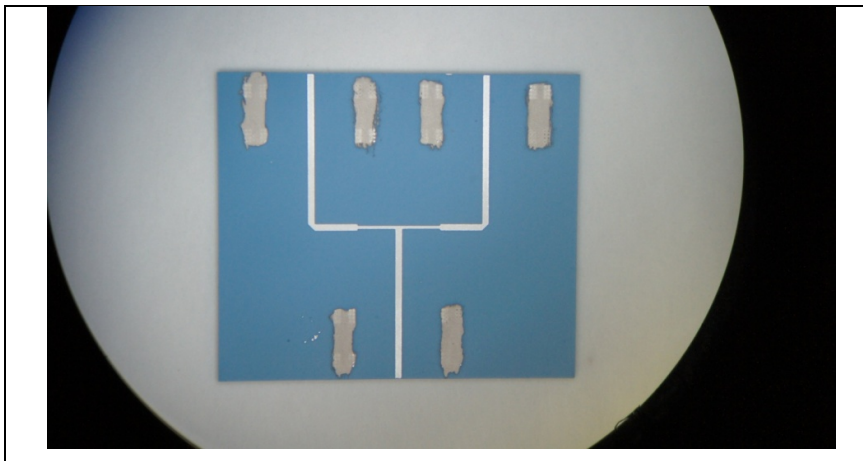
Figure 6.8 The divider over the substrate 951 Green Tape

To ensure that we have access to the ground in the LTCC stack, via holes and silver paste were added next to the lines at the ports of each circuits as shown in figure 6.8-6.11.

Figure 6.9 shows the feed of two patches C which are connected to each other by a divider on the substrate 951 Green Tape. Figure 6.10 shows one dual polarized patch C fabricated on the substrate 951 Green Tape. Figure 6.11 shows two linear polarized patches, A and B, fabricated on the substrate 951 Green Tape.
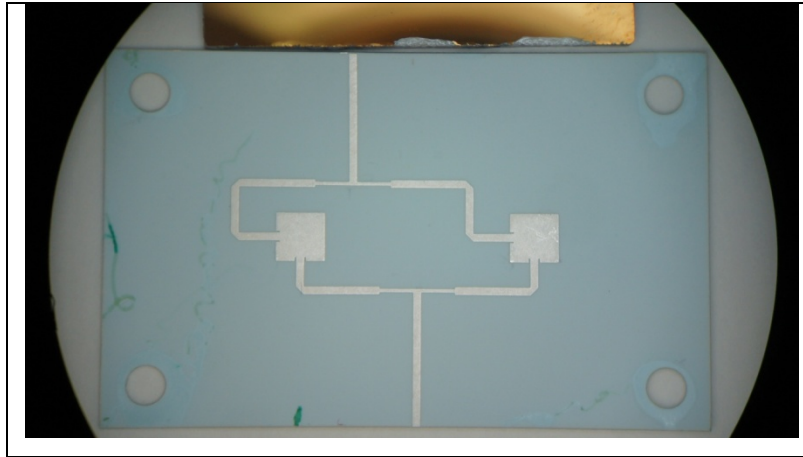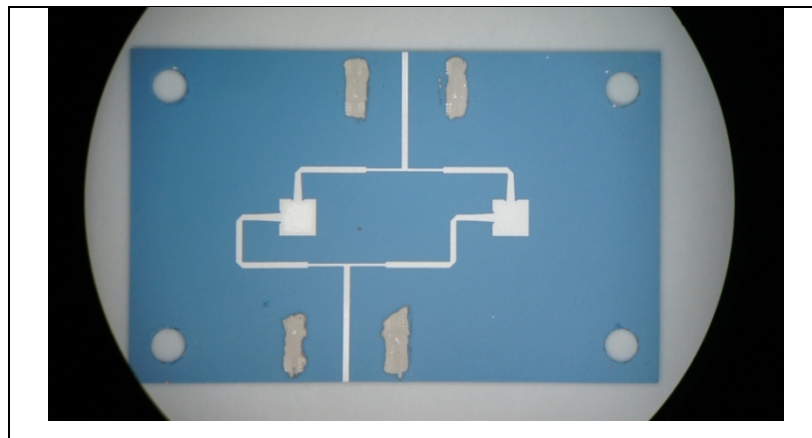

Figure 6.9 The feed of two patches connected to each other with a divider over substrate 951 Green Tape in LTCC
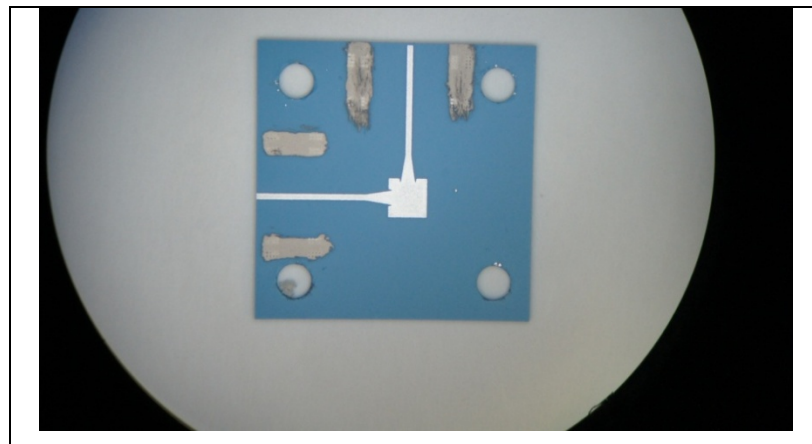
Figure 6.10 The dual polarized patch on the substrate 951 Green Tape
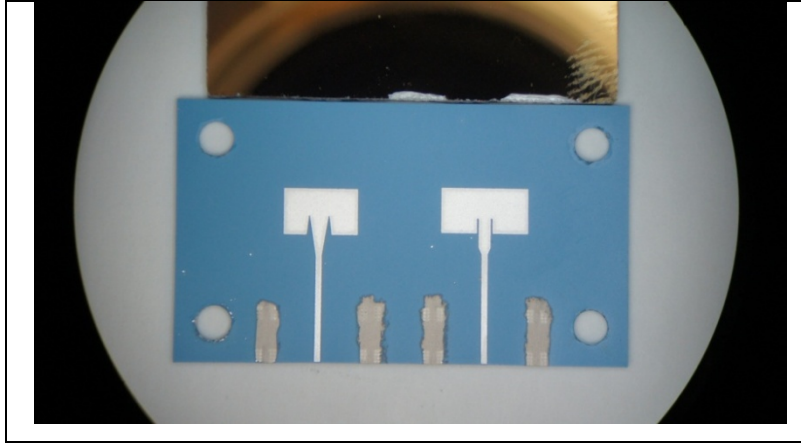
Figure 6.11 Two linear polarized patches on the substrate 951 Green Tape

6.3   Differences in Predicted Dimensions

After fabricating the LTCC components we noticed that the dimensions were different from the expected ones. It happened because the shrinkage factor used was not accurate. Because the alignment of the PCB and LTCC component is critical, we needed to have precise dimensions. Therefore, we measured every dimension manually using a microscope. At first we used vernier caliper for measuring, then for more precision we used an optical technology by taking photos of the components and comparing to the photo of the standard scale (figure 6.12b) using GIMP software.

Figure 6.13 and 6.14 show the measurement results using the vernier caliper (black and pink numbers), using the optical technology (red and violet numbers), and compare them to original desired dimensions of Momentum (green numbers). Based on these measurements, we redesigned the PCB parts for the better alignment.
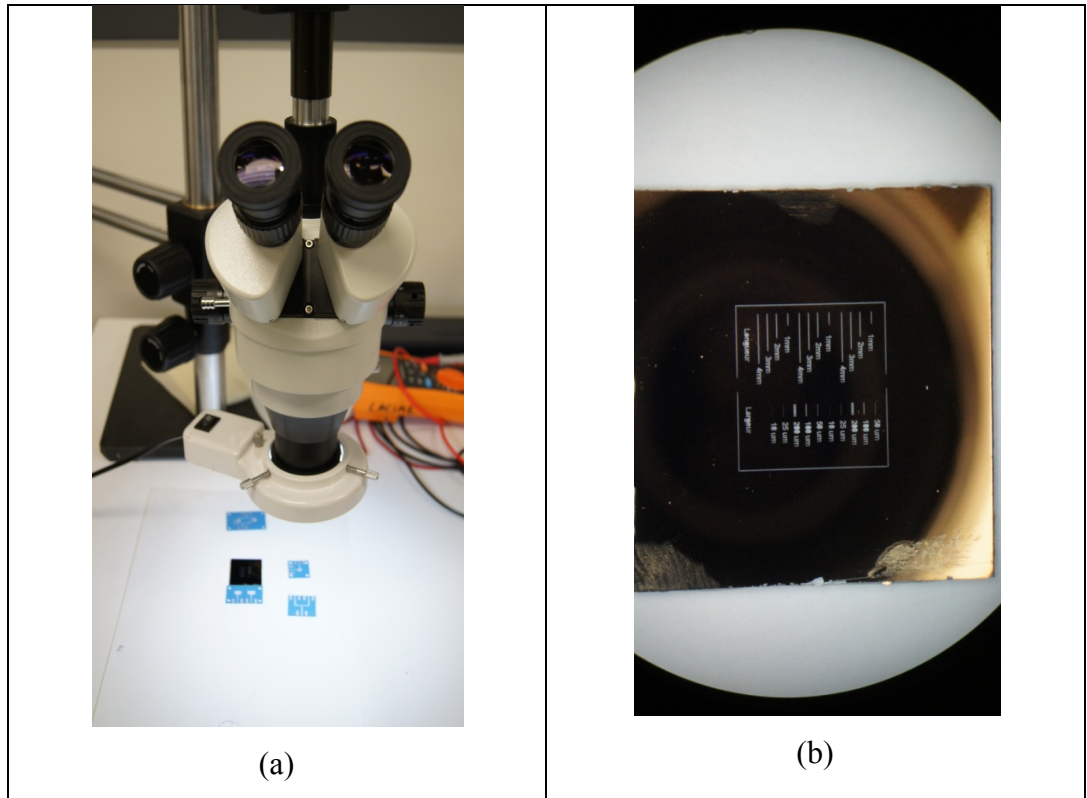
Figure 6.12 (a) Measuring using microscope (b) the standard scale
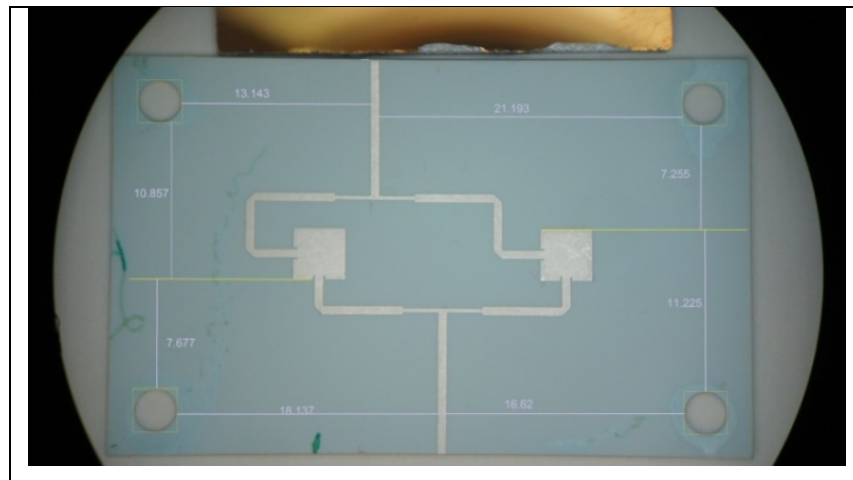
Figure 6.13 Measurements from the photos of the component over
the substrate 9K7 Green Tape
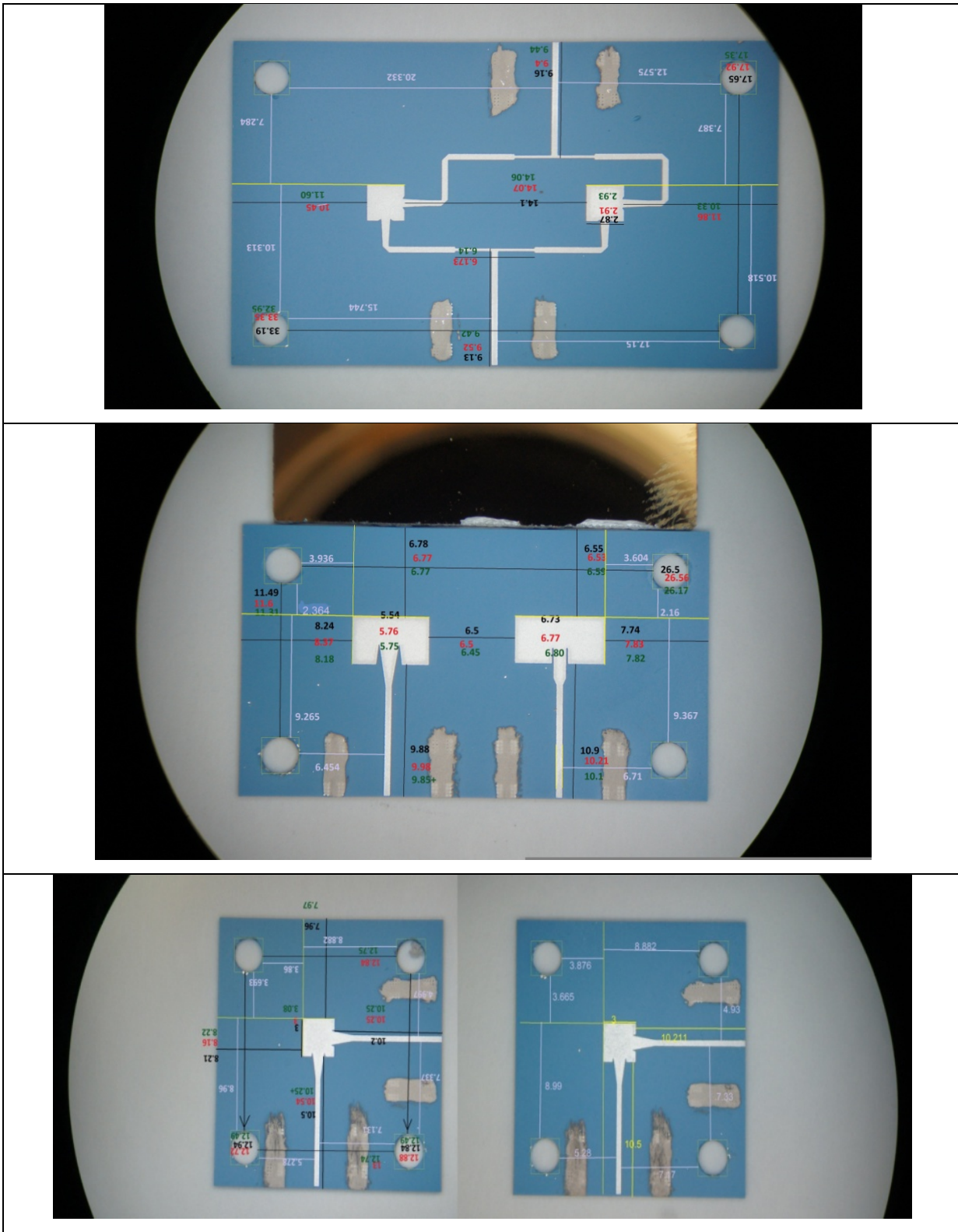
Figure 6.14 Different measurements of the components over the substrate
951 Green Tape

6.4 PCB Fabrication

As studied, our antenna consists of a stack having feed element in LTCC and a radiating patch in PCB. In this step we used the Rogers substrate with dielectric constant of 2.33. The datasheet for this substrate is presented in APPENDIX VI.

We designed two PCB patches, one for the 9K7 substrate and one for the 951 substrate. For the LTCC feed on 9K7 Green Tape (substrate I) we needed 80 mils Rogers RT5870 substrate to achieve the bandwidth required as shown in figure 5.10. To reduce the effects of the existence of air gaps between the LTCC and PCB parts, we used a special glue (speed set Epoxy). The thickness of the glue was estimated around 1mil and its dielectric constant was close to 2.33 so that it would not affect the patch function.

Figure 7.15 shows PCB part which contains the two patches to be mounted on the 9K7 feed circuit.
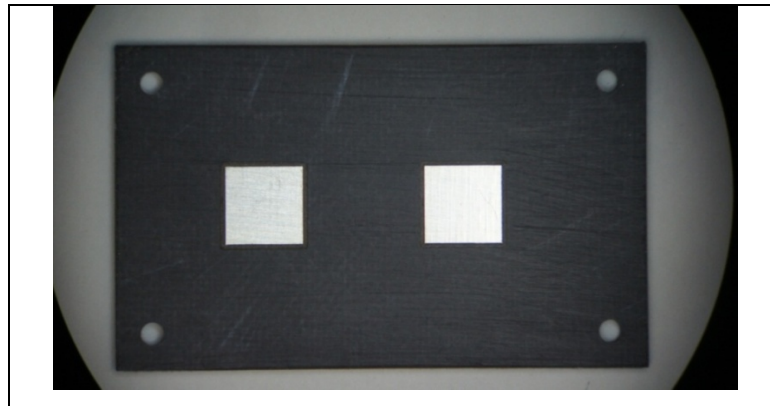
Figure 6.15 Two patches over the 80 mils Rogers RT5870

Similarly, for the 951 Green Tape, a PCB circuit was designed using the same Rogers RT570 substrate with 65mils thickness as presented in figure 5.2. Figure 6.16 shows the PCBs for the feed components over the substrate 951 Green Tape for the two dual polarized patch C (figure 6.16a), for the two linear polarized patch A and B (figure 6.16.b), and for the single dual polarized patchC(figure 6.16c).
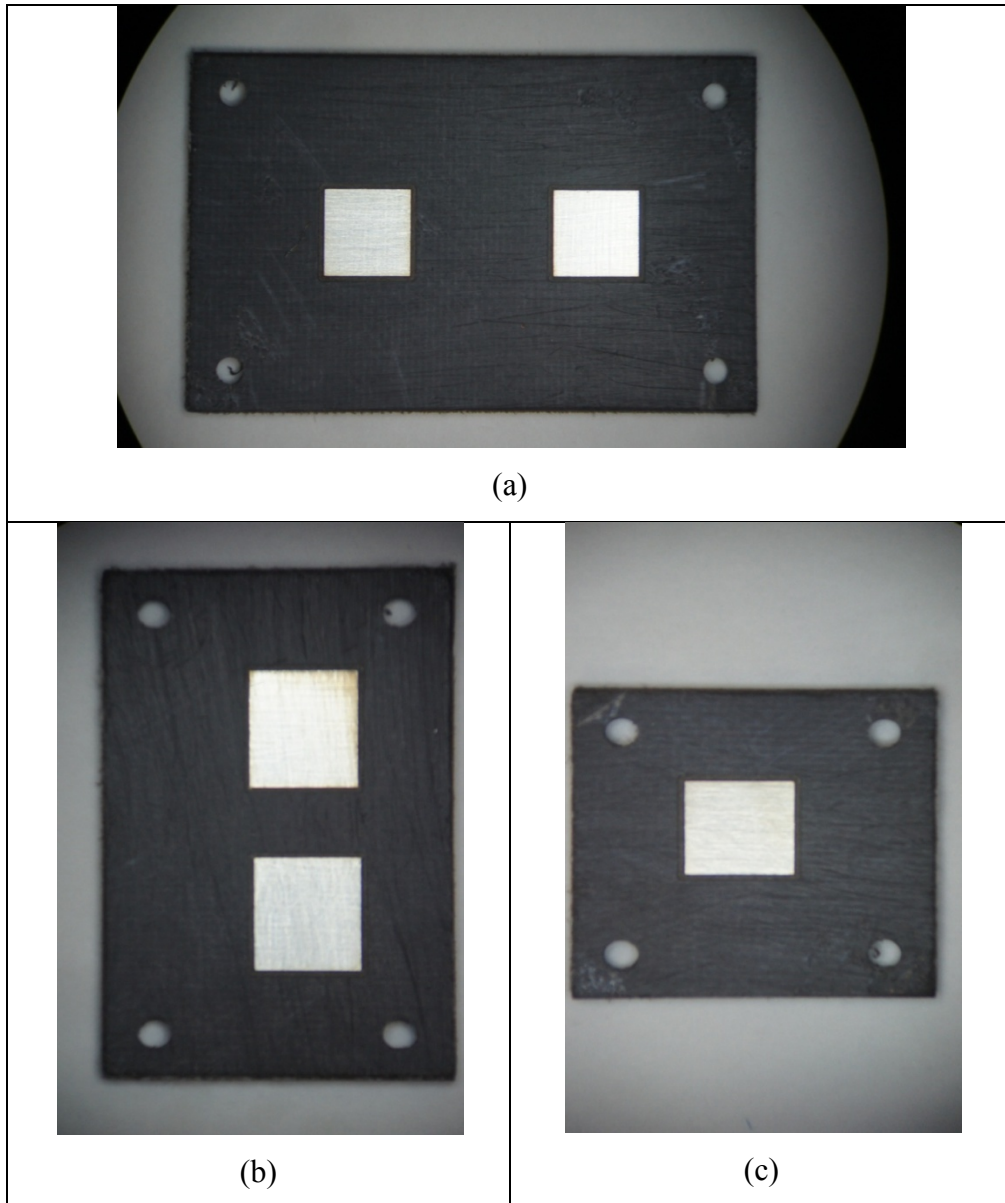
Figure 6.16 PCBs of: (a) two dual polarized patchC (b) two linear polarized patch A&B
(c) single dual polarized patchC

6.5   Integration of the Multilayer Antenna

The final step of fabrication of these patch antennas was connecting the PCB part to the LTCC part. This step was the most difficult step. All the dimensions should be very precise, especially the dimensions of vias to ensure the best alignment of the PCB part to the LTCC part. For this purpose we used screws to fix the two parts together.

For connecting the SMA connectors, some parts of the PCB were cut away. In addition, to connect the SMA ground to the LTCC ground, via holes were added to the LTCC components at the positions of the SMA ground pins. In this way the connectors could be properly connected.

Figure 6.17 and 6.18 show the final fabricated and integrated components with the 951 Green Tape while figure 6.19 shows with the 9K7 Green Tape.
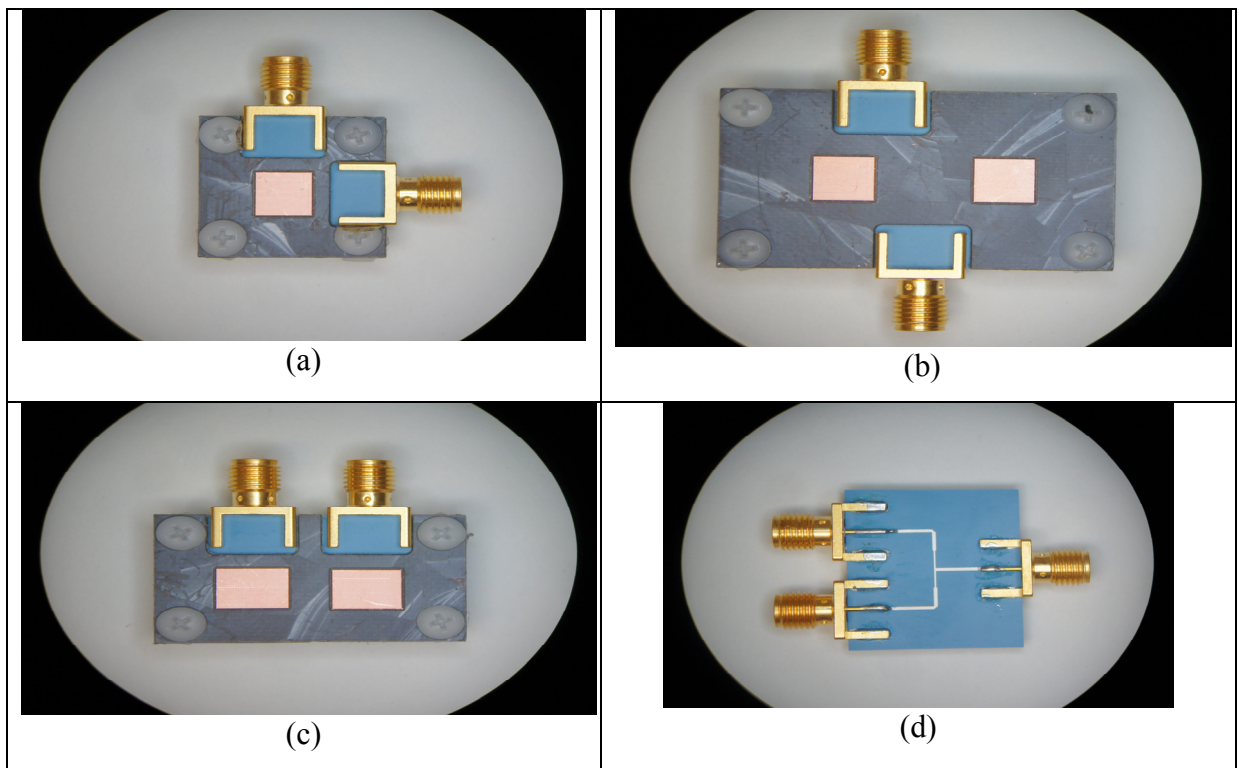
Figure 6.17 (a) Dual polarized patch antenna (b) Two dual polarized patch antennas connected by a divider (c) Two linear polarized antennas A and B (d) Divider
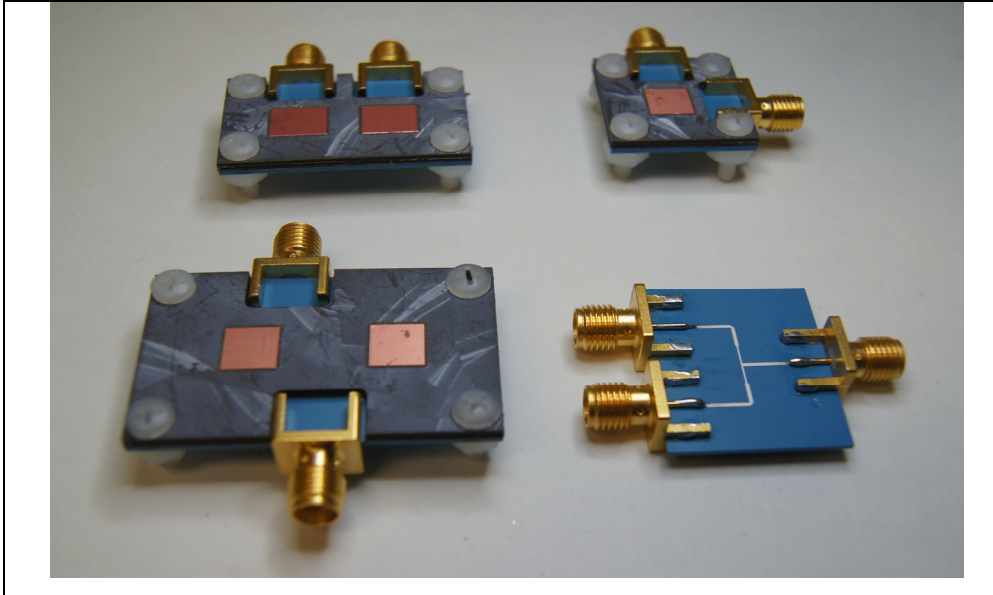
Figure 6.18 Fabricated components on substrate I
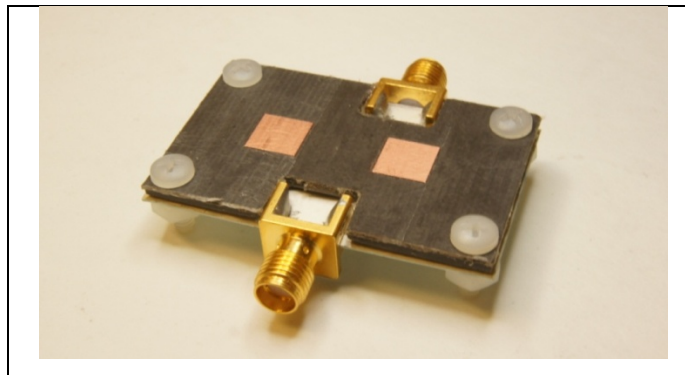
Figure 6.19 Two dual polarized patch antennas connected by a divider
fabricated on substrate II

6.6   Experimental Measurement

In this section we discuss the overall measurement approaches and instrumentations used. Measurement results will be presented in subsequent sections.

6.6.1   S-parameters Measurement

To measure the S-parameters of the component we used a Network Analyser system, Agilent 8722ES (figure 6.20). After calibrating the system, we measured the S-parameters in the 9GHz to 18GHz frequency range. The important frequency domain of my circuit is 10.7GHZ to 12.7GHz but due to the probability of shift frequency we measured S-parameters up to 18GHz.
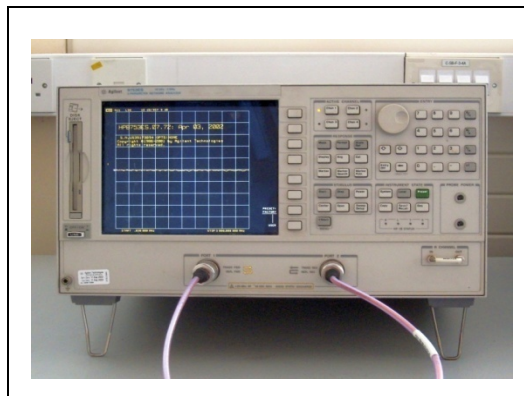
Figure 6.20 Network Analyser system, Agilent 8722ES

6.6.2   E-Pattern Measurement

There are two pattern measurements for each antenna; the E-horizontal pattern and the E-vertical pattern. Every antenna also has a co-polarization and a cross polarization radiation pattern. A good linear patch antenna has a large co-polarization pattern and a small cross one; but the dual polarized antenna has both of them simultaneously. These measurements were done in the Anechoic antenna testing chamber in École Polytechnique de Montréal (figure 6.21). For each antenna, the measurements for the frequencies between 9GHz to 18 GHz with the step of 0.1GHz were done. To calibrate these measurements, another measurement of a standard horn, with definite gain, was done. By comparing the measurements of our patch antennas with the standard horn antenna, we could obtain the gain of our components. The data analysed using Matlab software and the algorithm is attached in APPENDIX V. This code gets the data file of each antenna and by comparing to the standard antenna draws the horizontal and vertical radiation patterns. These patterns are drawn for the frequencies

where the gain is maximum, the frequency 11.7GHz which is the circuit center frequency and the frequencies where the S11 is minimum.
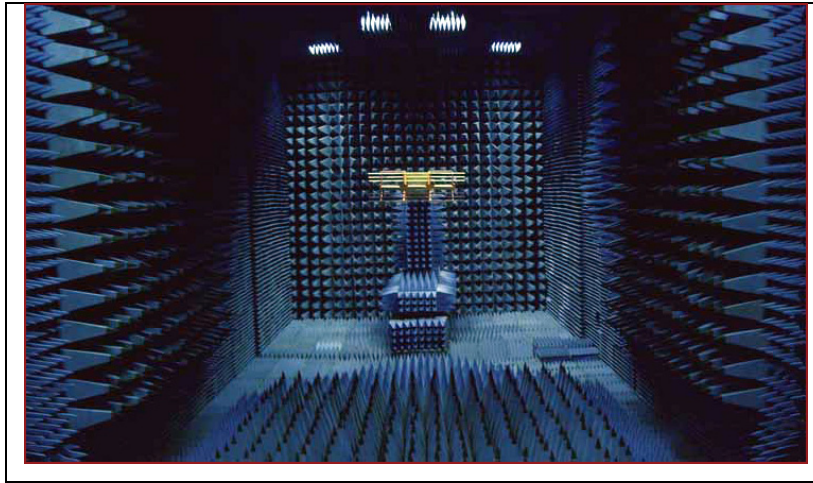
Figure 6.21 Anechoic antenna testing chamber

6.7   Measurement Results

6.7.1   S-parameters of the Divider

Figure 6.22 shows the measured S-parameters of a divider on the 951 substrate. This divider is designed for the center frequency 11.7GHz. At this frequency, the measured S11 and S22 are -3.3dB and S12 is -6.7dB. It is totally different from the simulation results.   The simulation results of this divider are shown in figure 6.23 where S11 is below -10dB and S12 and S13 are around -3dB for the entire band.

At high frequency there are a lot of options that potentially affect the circuit performance. One option that can cause this problem is the place of the vias beside the pins to reach the ground. A second option is soldering the connectors to the circuit which can cause mismatching. A third option is the type of connectors that we used for this frequency. A forth option is the limited ground in reality which was considered unlimited in the simulations. These options also affect the performance of the other components as will be explained later.

Note1:

To test if the SMA connector is good or not for this substrate at this frequency, I designed another divider on the PCB of substrate 31mils with dielectric constant of 6.15. The disagreement between the simulation and the measurement was very similar. So it is strongly supposed that the reason for not getting good results for all the components is the SMA connectors. The part number of the used SMA was 142-0701-881 (JOHNSON company) which was not good for thin planar structure at high frequency.
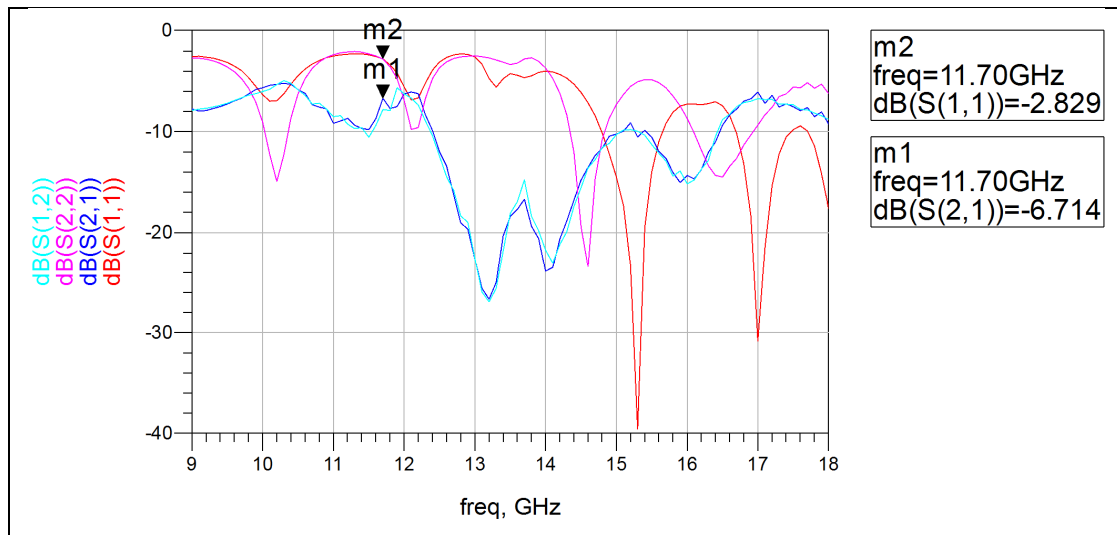
Figure 6.22 Measured S-parameters of the divider
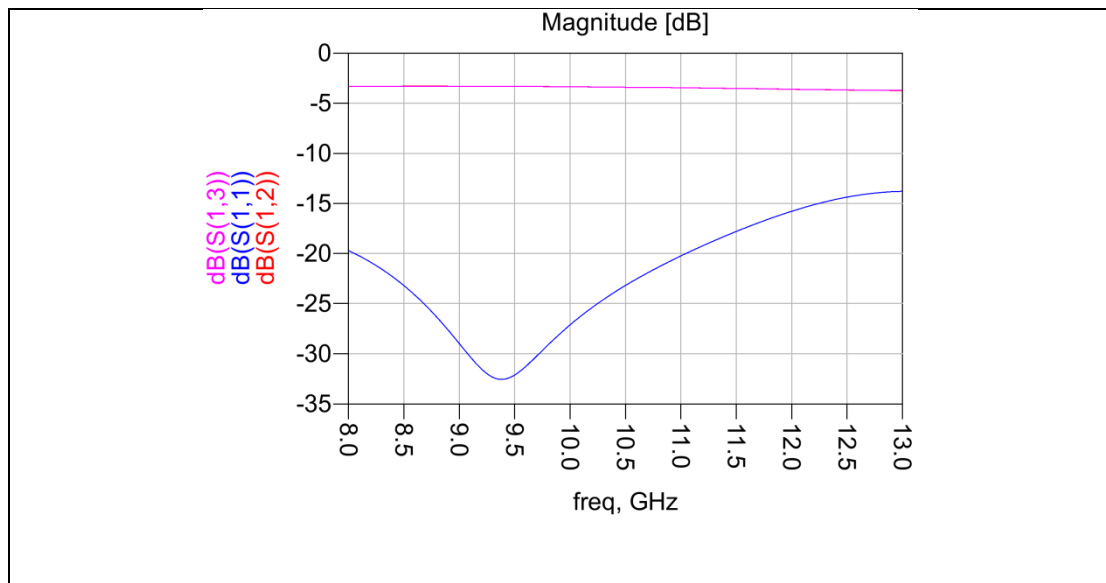
Figure 6.23 Simulation result of the divider

6.7.2   Linear Polarized Antenna A

6.7.2.1   S-parameters

Figure 6.24 shows the measured S-parameters for the linear polarized antenna A. The behaviour of the circuit between the frequency 10.7 GHz to 12.7GHz is similar to the simulation but the value of S11 is higher than what we expected (around -3dB which shows a big loss). But for the frequency 15.5GHz to 16GHz the S11 is below -10 dB. So we have 0.5 GHz bandwidth at this frequency. This can happen because of the propagation of other wave modes.
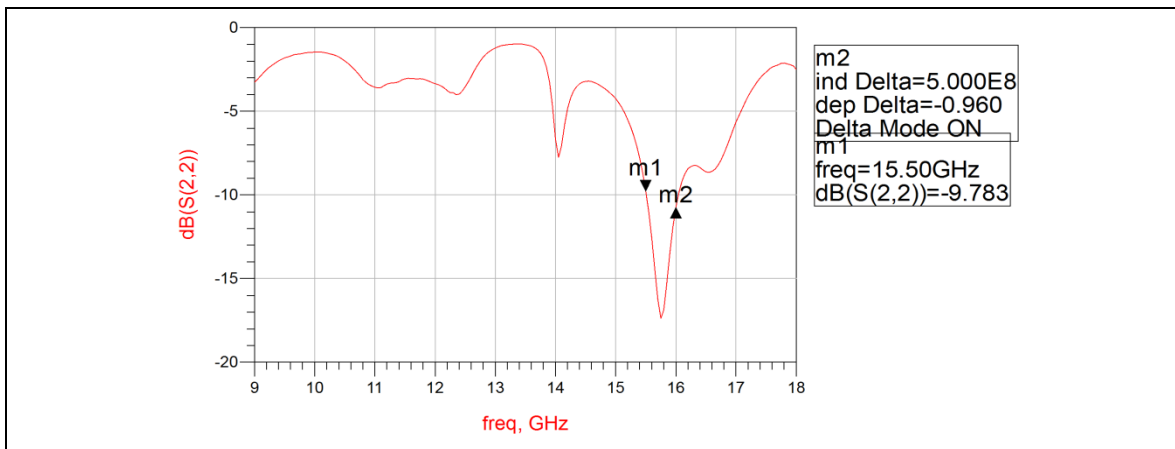
Figure 6.24 Measured S11 of linear polarized patch A before cutting the pin

After testing the antennas we underestand that the length of the connector pin can disturb the function of the components. At first it was thought that the length of the pin connected to the 50 Ohm line is not important; but because of the existance of the slot in ground plane, the pin can affect the circuit function. So we tested the antenna after cutting the connector pin. Figure 6.25 shows the S11 of the antenna after cutting the pin. It shows that the value of S11 being lower than the S11 before cutting the pin. In the frequency domain 10.7GHz to 12.7GHz the behaviour is similar the simulation but the value of S11 is still not low enough.

Note2:

Because of the existance of a slot in the ground, the lenght of the feed line can affect on the circuit function. So it is better to consider longer transmition line to decrease the sensitivity of the antenna to this parameter.
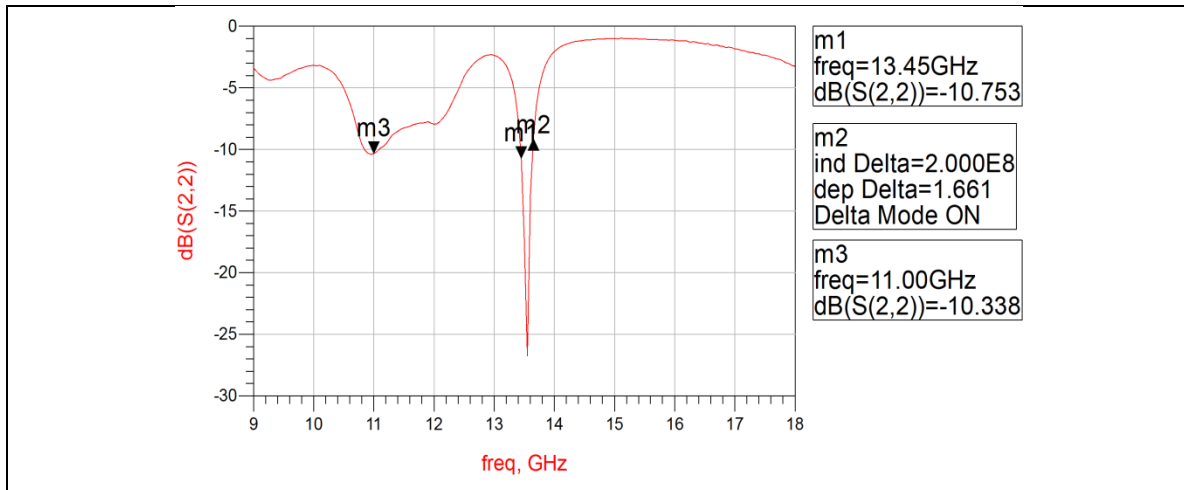
Figure 6.25 Measured S11 of linear polarized patch A after cutting the pin

6.7.2.2   Radiation Pattern

To draw the radiation patterns we wrote a Matlab program, which is attached in APPENDIX V. This code computes the maximum gain in the 9GHz to 18GHz frequency range and draws the pattern at the frequency of maximum gain. It also draws the pattern at frequency 11.7 GHz which is the center frequency of the circuit. We also drew the antenna pattern at the frequencies where S11 is minimum. There are two horizontal and vertical patterns for each antenna. Each pattern has also co-polarization and cross polarization patterns. In a linear antenna, co-polarization is the polarization in which the antenna is intended to radiate but for the dual polarization both of them should radiate.

Figure 6.26 shows the radiation patterns of antenna A before cutting the pin and figure 6.27 shows the patterns after cutting the pin. It is shown that cutting the pin makes not much difference in the shape of patterns but some changes in the gain.

Figure 6.26 (a) Horizontal and (b) vertical pattern of the linear polarized patch A before cutting the connector pin (ε_r:7.8) (___co-polar ....cross-polar)

In this antenna maximum gain happened at 11.4GHz which is around 5dB.

Figure 6.27 (a) Horizontal and (b) vertical pattern of the linear polarized patch A after cutting the connector pin (ε_r:7.8) (___co-polar ....cross-polar)

For the antenna after cutting the pin, the maximum happened at 11.4GHz again. The gain after cutting the pin is increased up to 6.5dB.
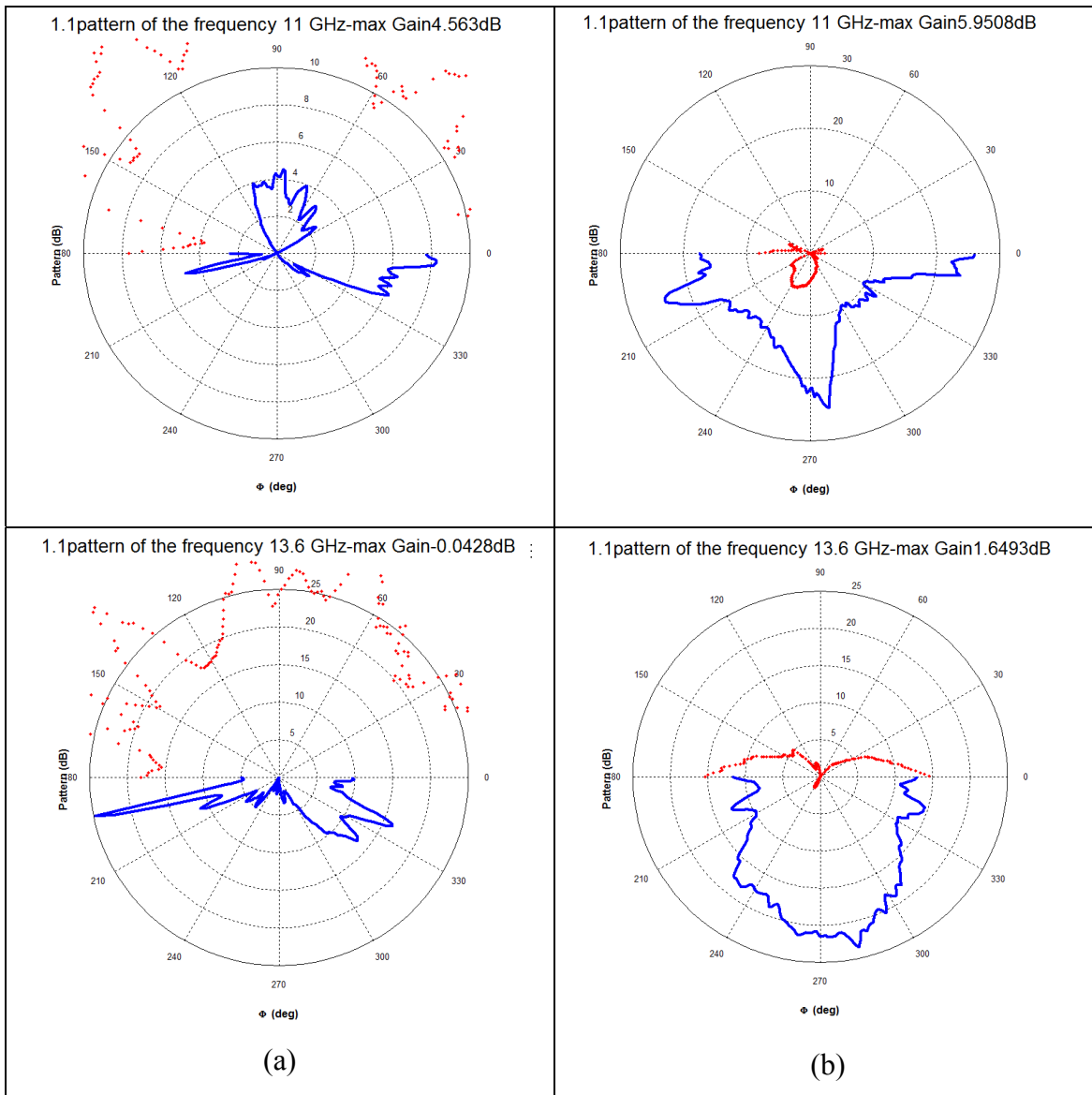
Figure 6.28 (a) Horizontal and (b) vertical pattern of the linear polarized patch A after cutting the connector pin in the minimum S11 points (ε_r:7.8) (___co-polar ....cross-polar)

Figure 6.28 shows the patterns for 11GHz and 13.6GHz. In these points the S11 has the minimum value so the radiation should be better than the other points. The shape of the pattern for 11GHz is what we expected from a patch antenna; because it is in the band for which it was designed. But at 13.6GHz, in spite of having good S11, the radiation pattern is not as expected for a patch since this frequency is outside the design band.

6.7.3   Linear Polarized Antenna B

6.7.3.1   S-parameters

Figure 6.29 shows the measured S11 for the linear polarized antenna B before cutting the connector pin. The behaviour of S11 is the same as simulation; it shows dual band between 10.7GHz and 12.7GHz. Also it shows a 0.65GHz at 10dB bandwidth.
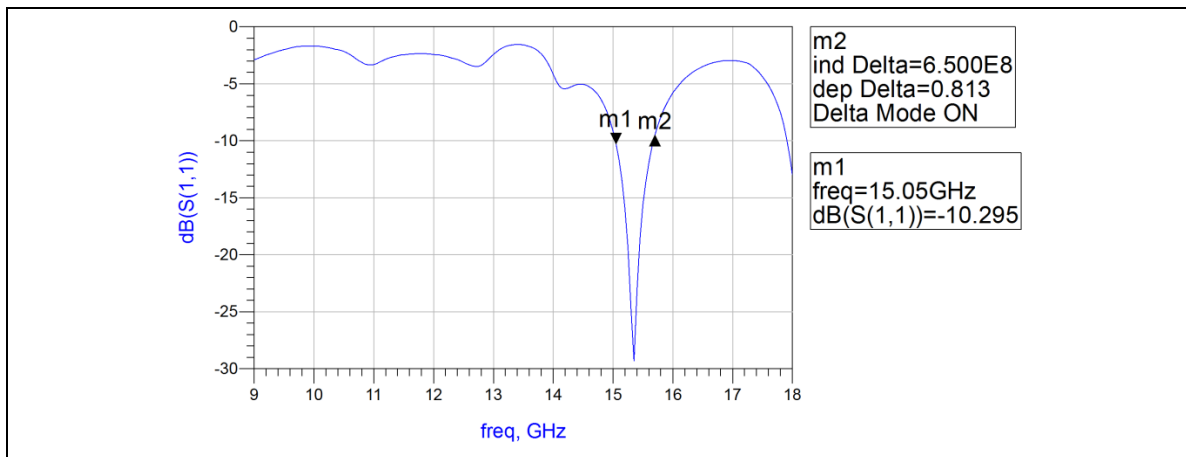
Figure 6.29 Measured S11 of linear polarized patch B before cutting the pin

Figure 2.30 shows S11 after cutting the connector pin. The same as antenna A, the result is better than S11 before cutting the pin.

Figure 6.30 Measured S11 of linear polarized patch B after cutting the pin

6.7.3.2   Radiation Patterns

Figure 6.31 shows the radiation pattern at 11.4GHz which the gain is maximum (5dB) and at 11.7GHz. The patterns are similar to the antenna A.

(a)

(b)

Figure 6.31 (a) Horizontal and (b) vertical pattern of the linear polarized patch B before cutting the connector pin (ε_r:7.8) (___co-polar ....cross-polar)

Figure 6.32 shows the pattern at 11.4GHz and 11GHz after cutting the pin. The vertical pattern is changed but the horizontal one is not changed. The gain is also increased.
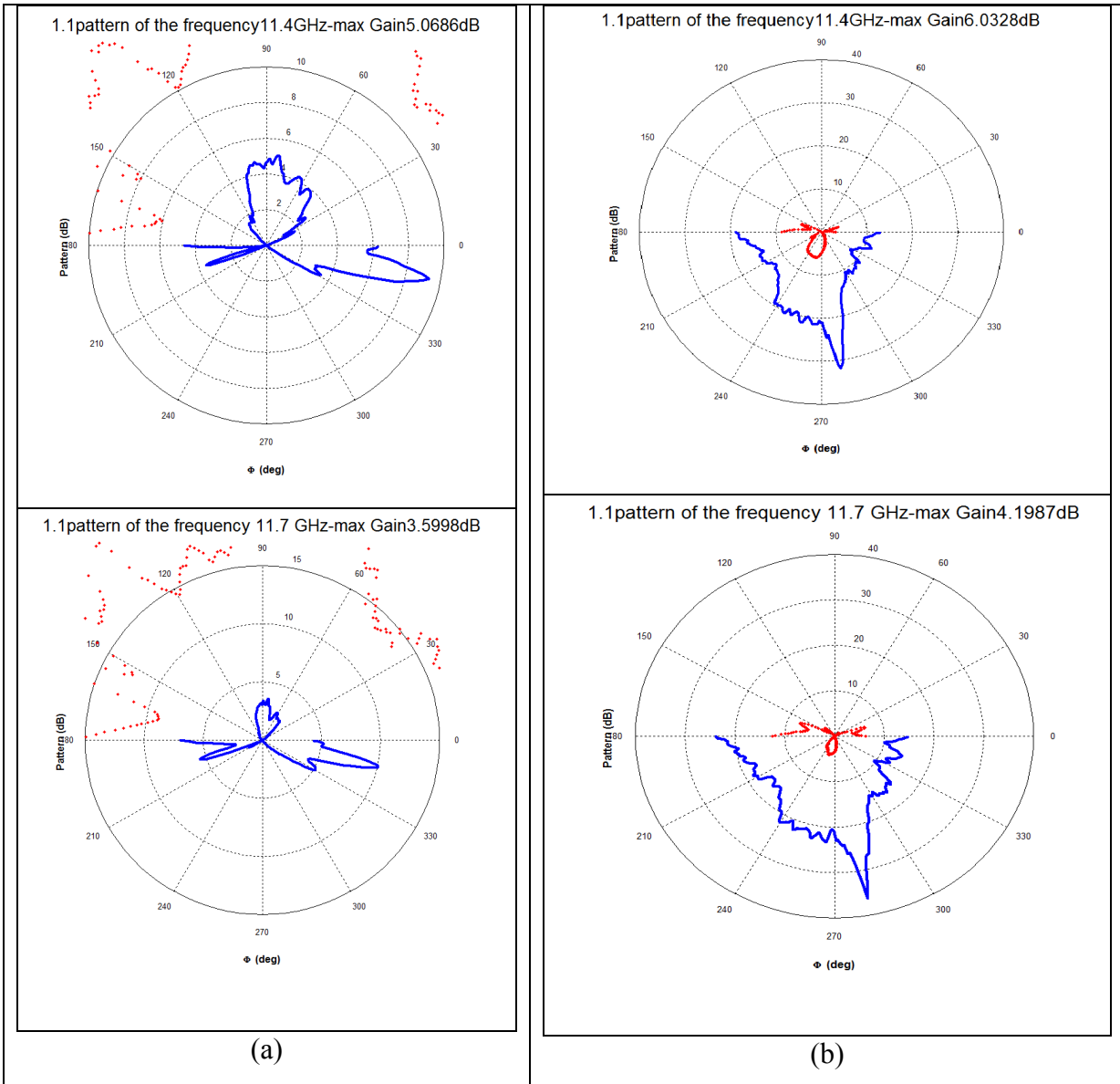

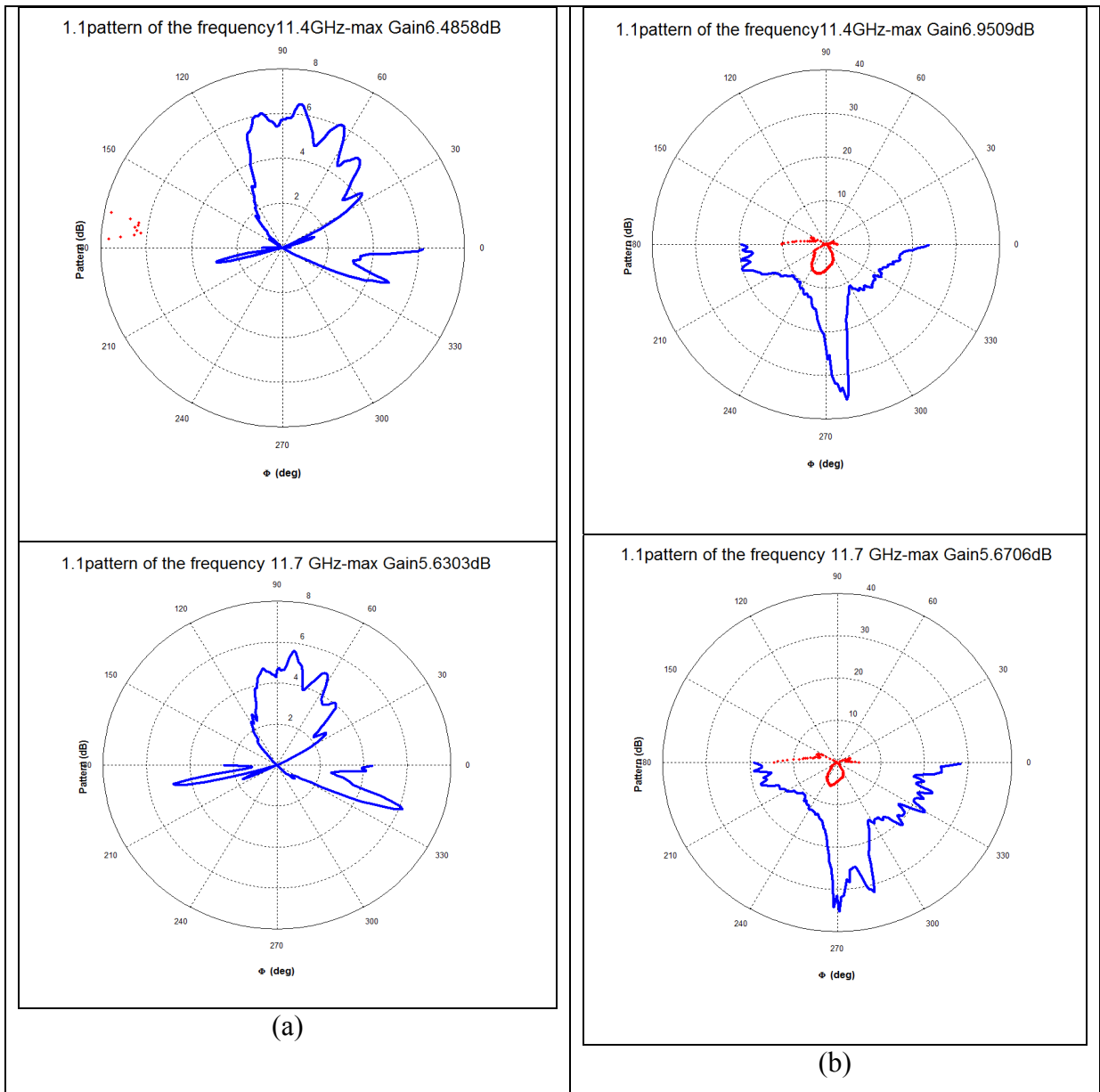| (a) | (b) |

Figure 6.32 (a) Horizontal and (b) vertical pattern of the linear polarized patch B after cutting the connector pin (ε_r:7.8) (___co-polar ....cross-polar)

Figure 6.33 shows the patterns at 10.7GHz and 13.4GHz. At these frequencies the S11 is minimum so the radiation should be good. The vertical pattern in these frequencies is changed but the horizontal patterns are similar.

1.1pattern of the frequency 10.7 GHz-max Gain4.0422dB

1.1pattern of the frequency 10.7 GHz-max Gain4.3049dB

1.1pattern of the frequency 13.4 GHz-max Gain2.0667dB

1.1pattern of the frequency 13.4 GHz-max Gain-1.3746dB

Figure 6.33 (a) Horizontal and (b) vertical pattern of the linear polarized patch B after cutting the connector pin in the minimum S11 points (ε_r:7.8) (___co-polar ....cross-polar)

6.7.4 Dual Polarized Antenna C

6.7.4.1 S-parameters

Figure 6.34 shows the S-parameters for the single dual polarized patch antenna over the substrate 951 Green Tape. It shows that S12 and S21 from 10GHz to 15GHz is below -15dB,

it means the ports are almost isolated from each other. This circuit is symmetric and it was expected that S11 matches to S22 but after the soldering process they had been changed. S11 in figure 6.34 shows 1.5GHz bandwidth at 13.5GHz. It is supposed to be at 11.7 GHz but it shifted to13.5GHz. The S22 shows 0.4GHz bandwidth at 10.5GHz.

Note3:

Soldering can easily affect the function of the components at high frequency.
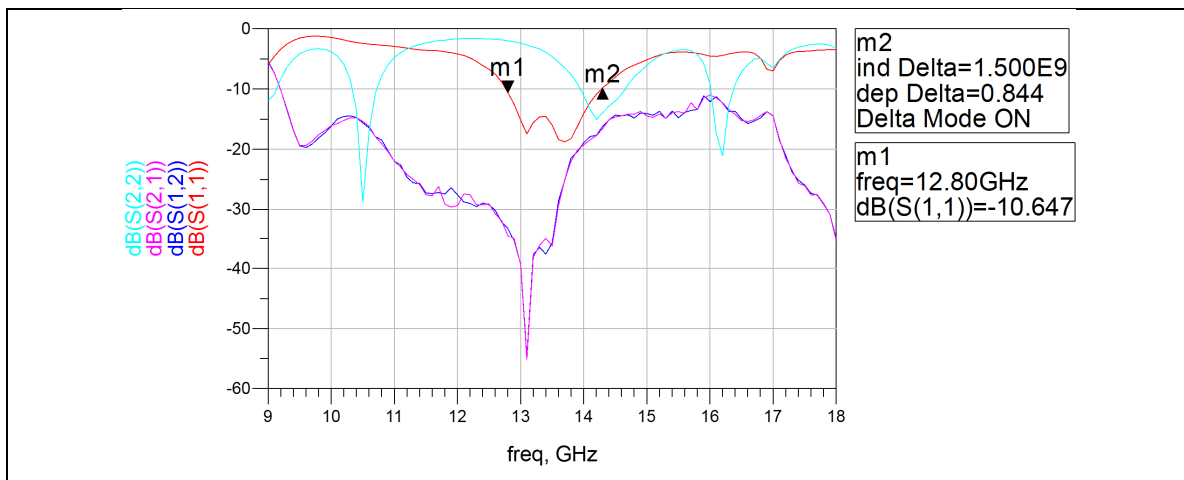
Figure 6.34 Measured S-parameters of dual polarized patch antenna before cutting the pin

Figure 6.35 show the S11 after cutting the pin. It shows 0.8GHz at14GHz. Here we present just port one because the other port was damaged in the process of soldering.
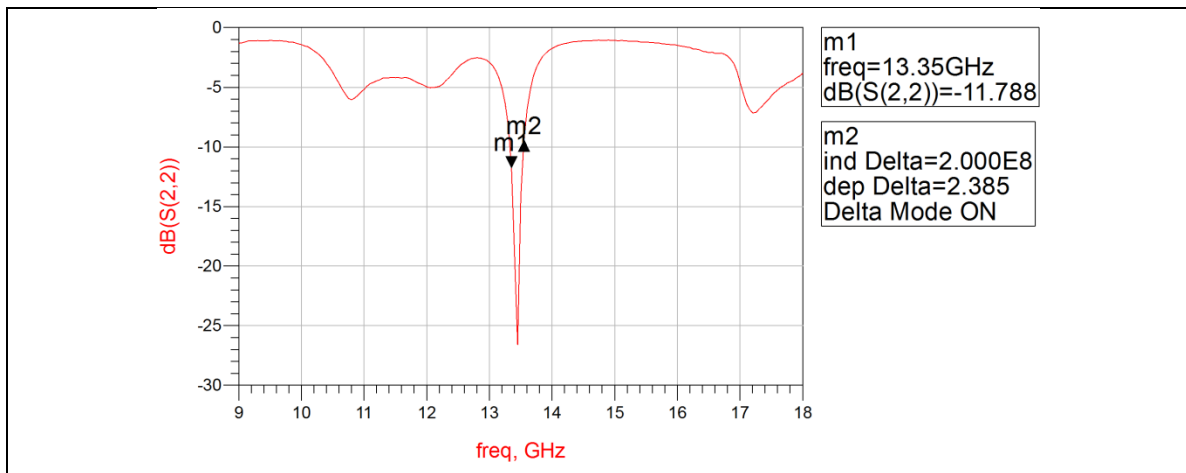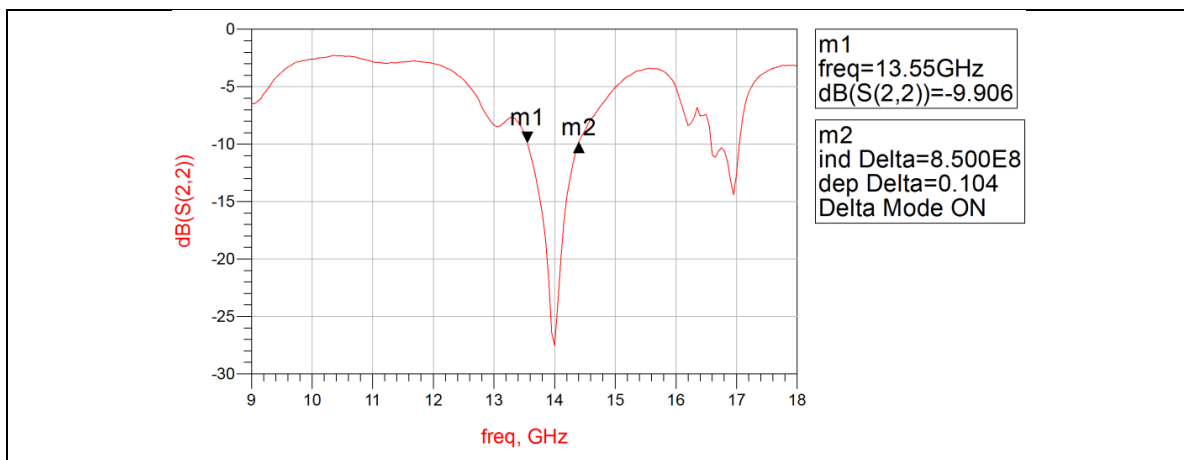

Figure 6.35 Measured S11 of dual polarized patch antenna after cutting the pins

6.7.4.2   Radiation Pattern

Figure 6.36 shows the radiation patterns for a dual polarized antenna over the substrate 591 Green Tape at 9.3 GHz, which is the frequency of maximum gain, and at 11.7GHz. Figure 6.37 shows the same measurements with the other port of the patch. For this antenna the polarization should be dual. It means that we want both co and cross polarization. In comparison with antenna A, the cross polarization in vertical pattern is increased.
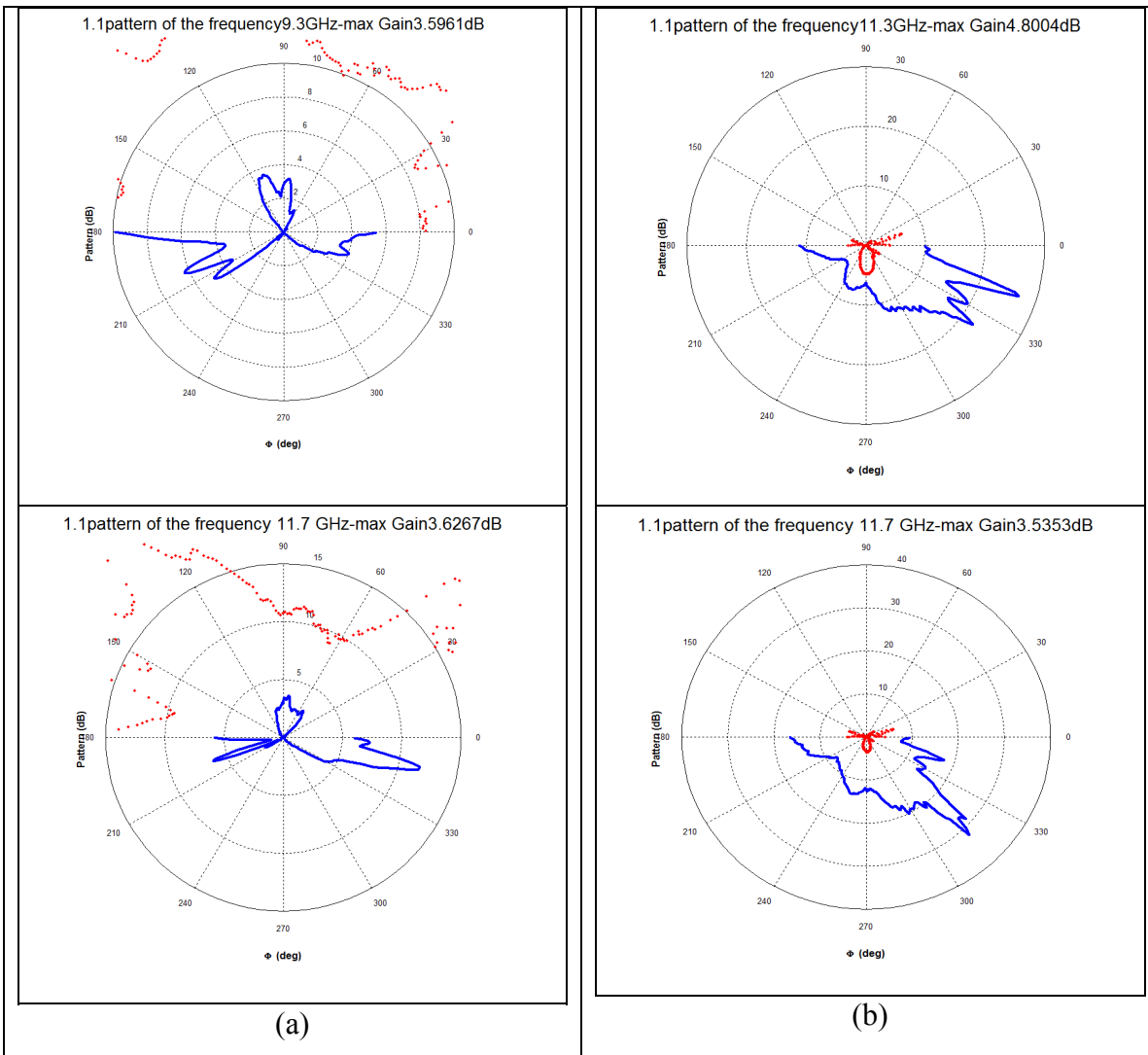
Figure 6.36 (a) Horizontal and (b) vertical pattern of the dual polarized patch, port1 before cutting the connector pin (ε_r:7.8) (___co-polar ....cross-polar)
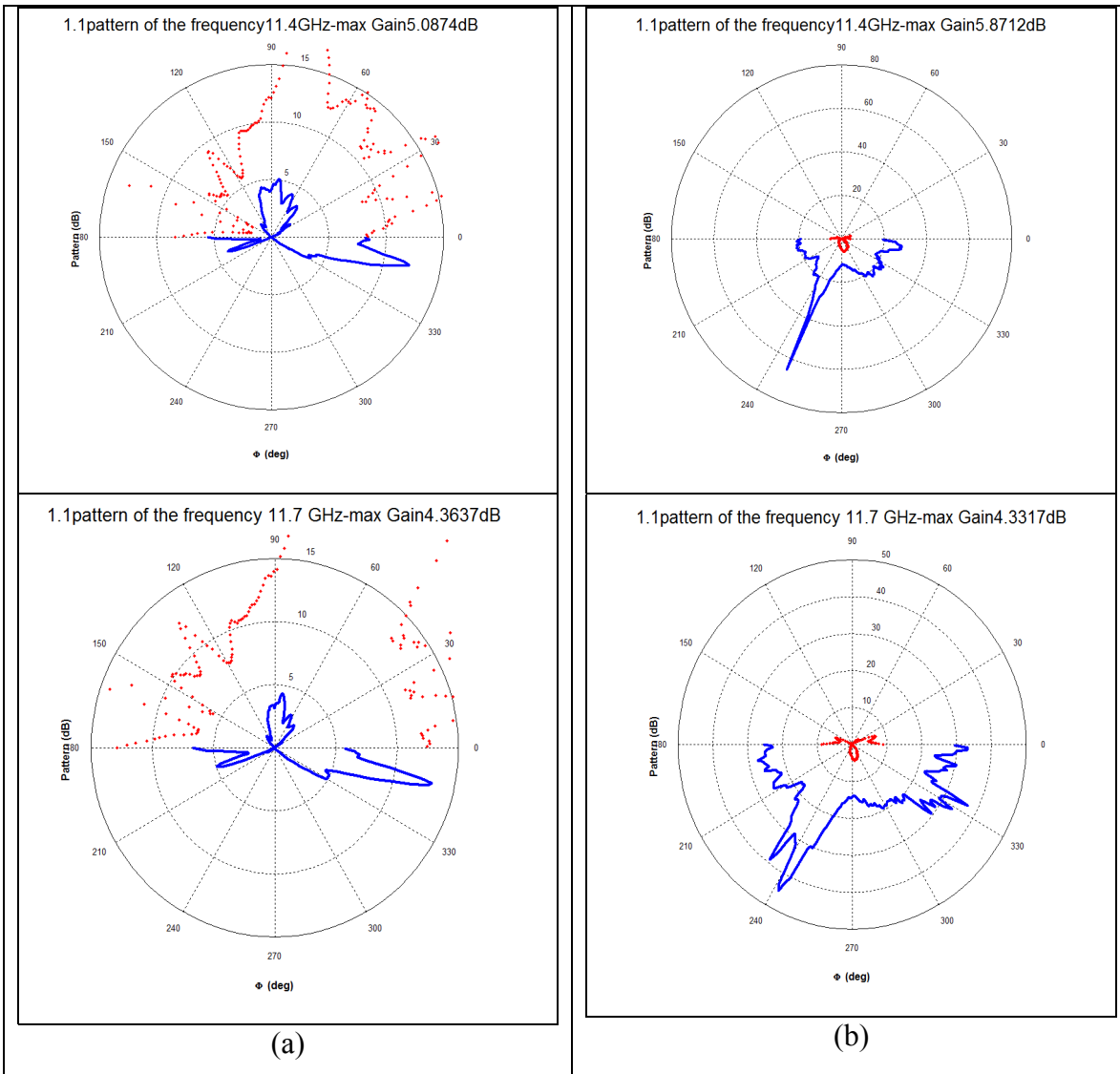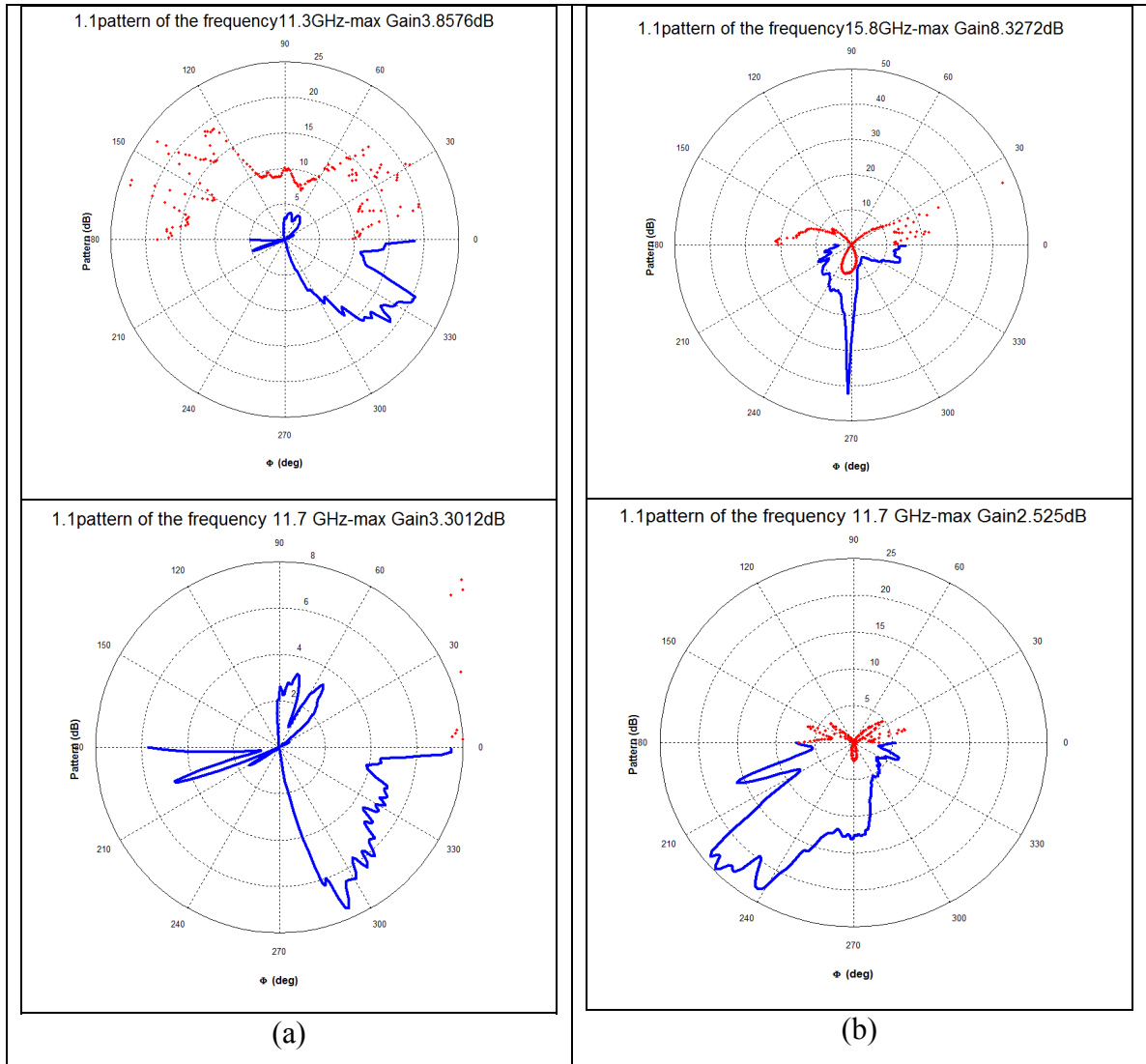
Figure 6.37 (a) Horizontal and (b) vertical pattern of the dual polarized patch, port2 before cutting the connector pin (ε_r:7.8) (___co-polar ....cross-polar)

The gain for the patch C is below 4dB. Even after cutting the pins, this value did not change so much (figure 6.37 and 6.38). It can be caused because the element was damaged in the soldering process.

108

Figure 6.38 and 7.39 shows the pattern after cutting the pin.
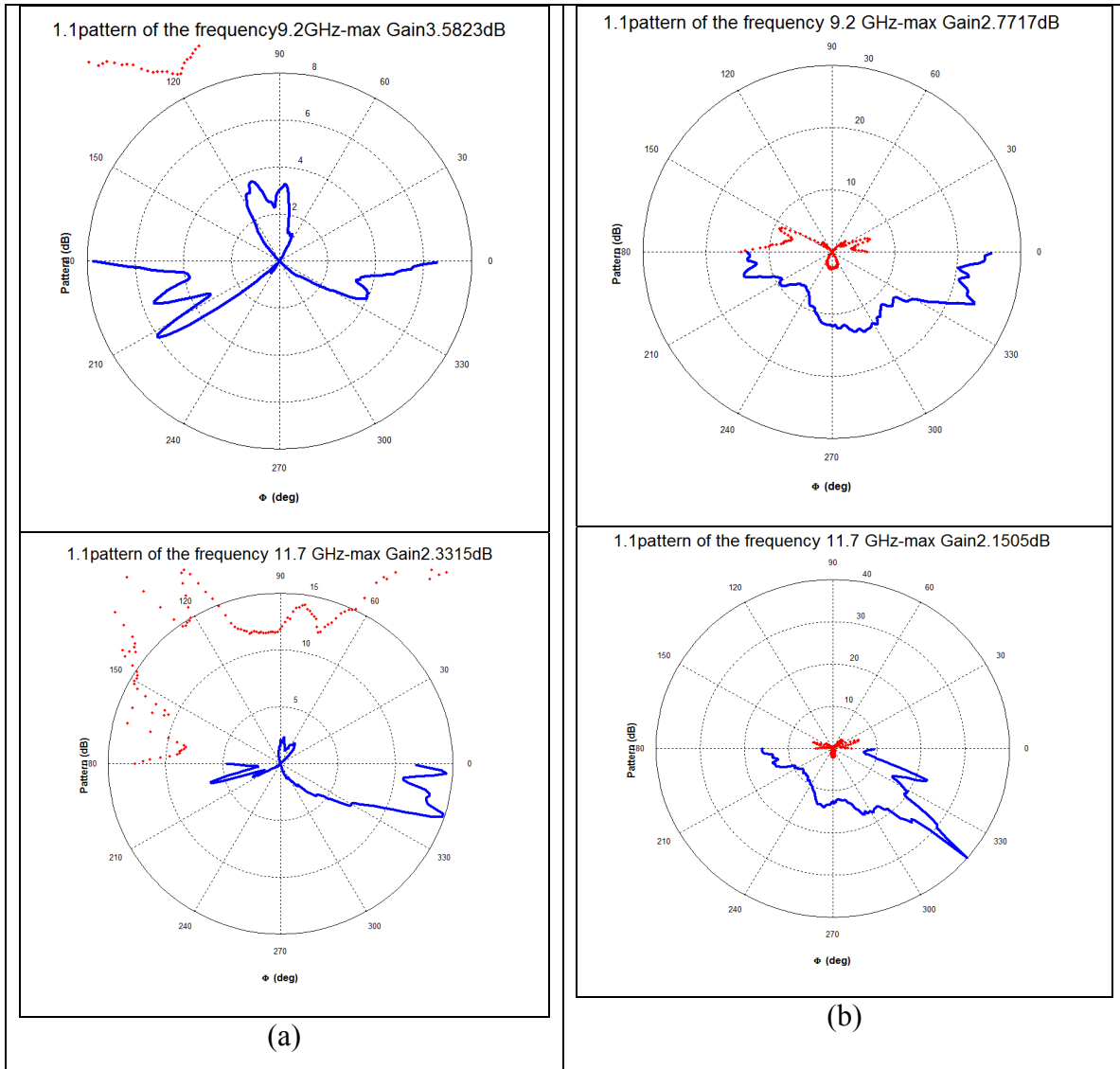
Figure 6.38 (a) Horizontal pattern (b) vertical pattern of the dual polarized patch, port1 after cutting the connector pin (ε_r:7.8) (___co-polar ....cross-polar)
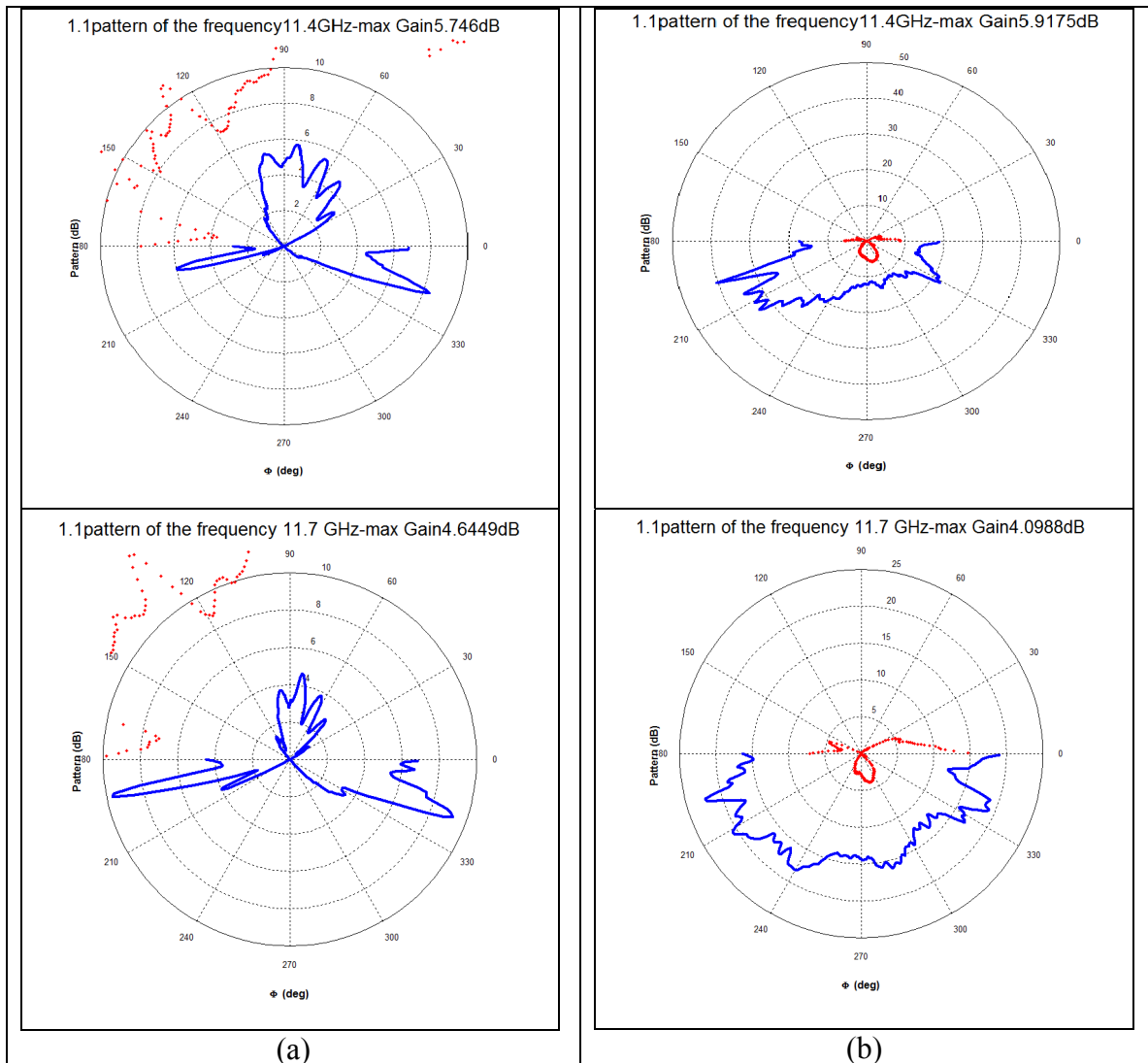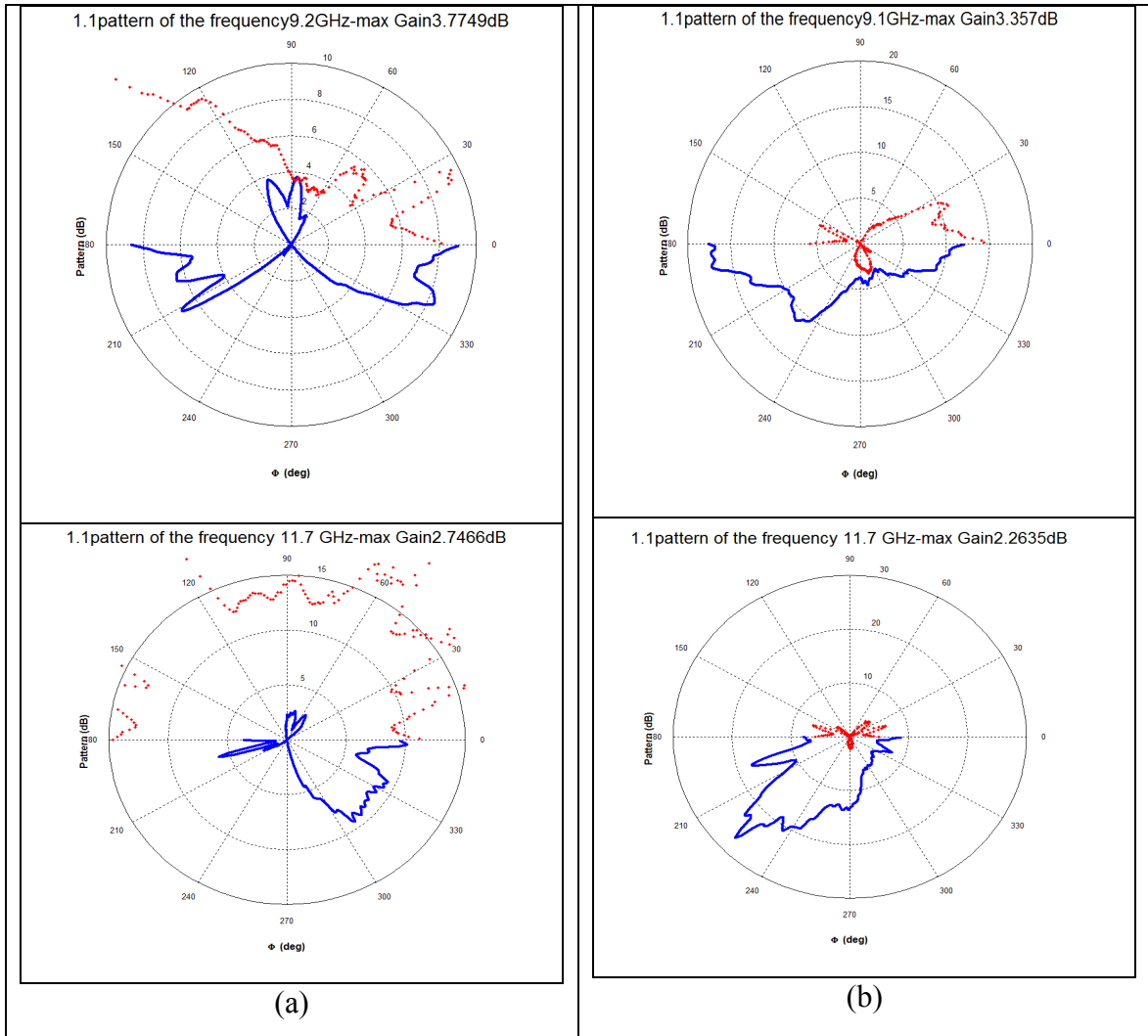
Figure 6.39 (a) Horizontal and (b) vertical pattern of the dual polarized patch, port2 after cutting the connector pin (ε_r:7.8) (___co-polar ....cross-polar)

Figure 6.40 shows the radiation pattern at 10.5GHz, 13.1GHz, 13.7GHz, 14.2GHz and 16.2 GHz which are the frequencies that S11 has the minimum value for the patch before cutting the pins. At these points the duality of the polarization and the shape of the pattern can show itself better. The gain at 13.7GHz is 4.68dB and the gain at 14.2GHz is 5.7dB; these two frequencies have proper pattern shape and gain. For 10.5GHz,13.1 and 16.2GHz the pattern shape is totally different. It may have happened because the circuit was damaged during the soldering process.
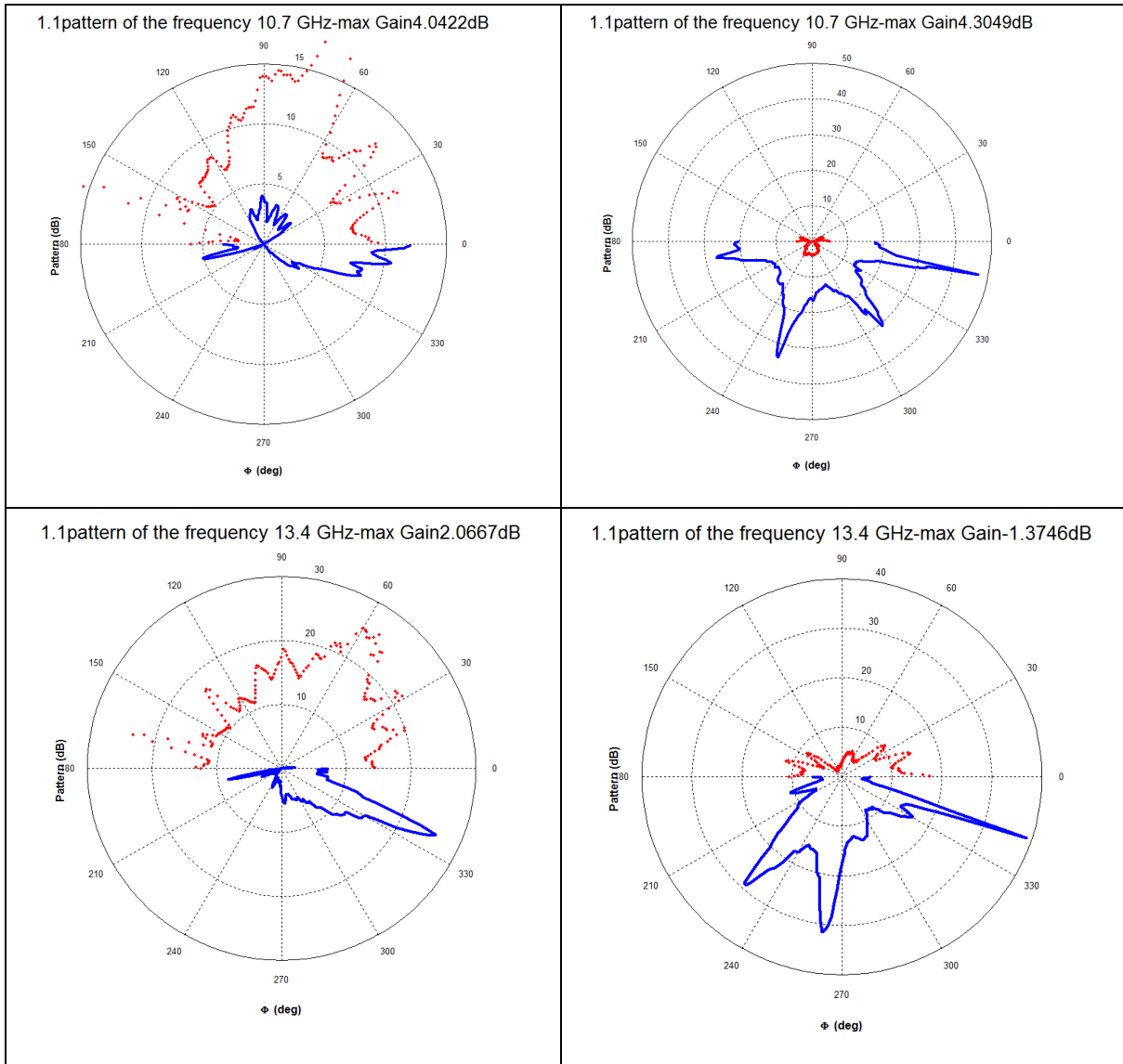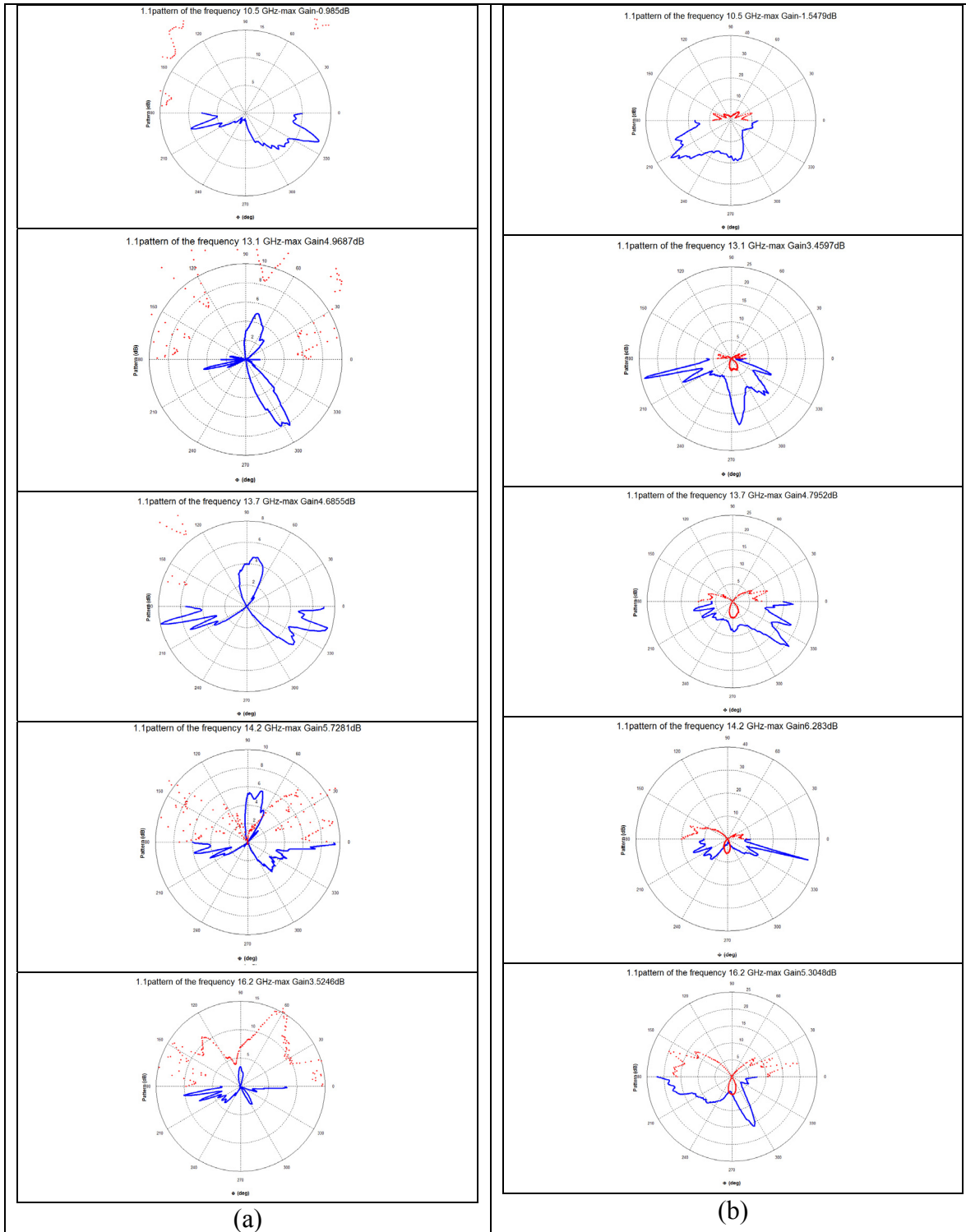
Figure 6.40 (a) Horizontal and (b) vertical pattern of the dual polarized patch after cutting the connector pins in the minimum S11 points (ε_r:7.8) (___co-polar ....cross-polar)

6.7.5   Two Dual Polarized Antennas C over the Substrate 951GreenTape

6.7.5.1   S-parameters

During the testing of the two dual polarized patches C connected by the divider over the substrate I, we investigated the effect of the glue on the circuit performance. Figure 6.41 shows the S-parameters before gluing the PCB to the LTCC part. For port one, S11 is not good but for the other it shows 0.58GHz from 10.8GHz to 11.38GHz. In fact any air gap between the PCB and LTCC part can really disturb the circuit function. Furthermore becuse the components are not so flat it is better to put glue to avoid airgaps.

Figure 6.41 S-parameters of two dual polarized patch antennas connected with a divider on the substrate 591 Green Tape before cutting the pins and sticking with glue

Figure 6.42 shows the S-parameters after gluing. This figure shows a shift in the frequency. It shows a 0.6GHz bandwidth at 13GHz. The S11 is a little low but not so much at frequencies 9.6 GHz and 11GHz.

Figure 6.43 shows the S-parameters after cutting the connector pins. The results are substantially better. It shows a 1.4GHz bandwidth from 10.75GHz to 12.15GHz in one port. It also shows a 1.1GHz bandwidth at 16GHz.

Note3:

Using glue can help eliminate air gaps but has its own problems.
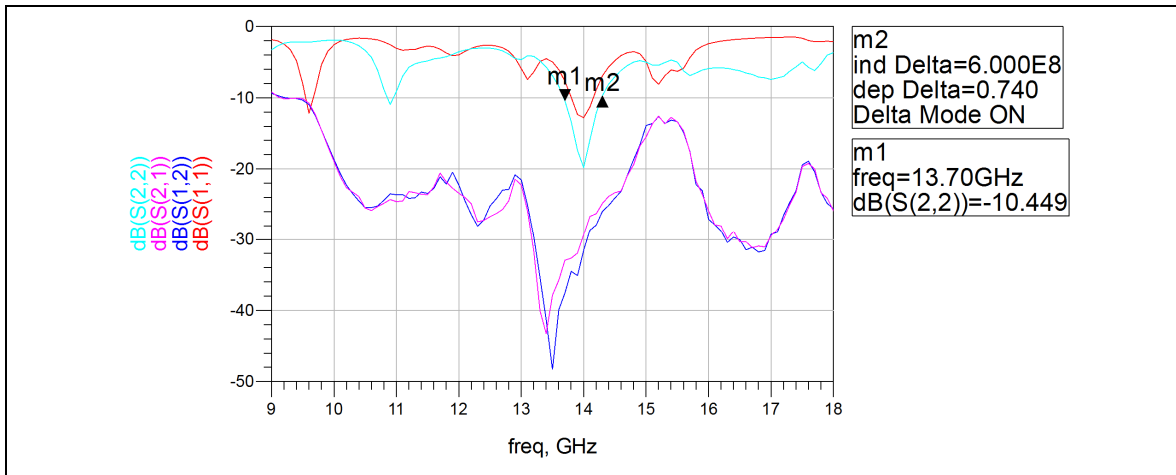
Figure 6.42 S-parameters of two dual polarized patch antennas connected with a divider on the substrate 591 Green Tape before cutting the pins but after sticking with glue
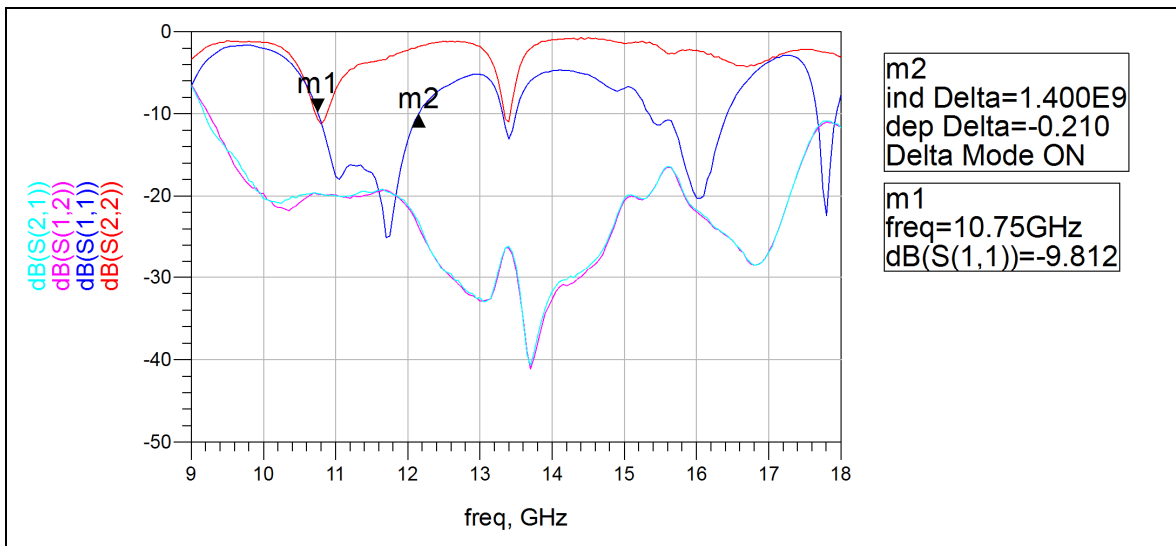
Figure 6.43 Measured S-parameters of two dual polarized patch antennas connected with a divider on the substrate 591 Green Tape after cutting the pins and after sticking with glue

6.7.5.2 Radiation Pattern

Figure 6.44 and 6.46 show the patterns for the two patches C connected by the divider on substrate I before cutting the connector pins and figure 6.45 and 6.47 show the patterns after cutting the pins. As we expected according to the S-parameters, the shape of the patterns for this component is really good. In addition the duality of polarization is shown in these patterns well. Like before, the first pattern is for the frequency which the gain is the most and the second pattern is for the frequency 11.7GHz. The gain at 11.4GHz is 9.8dB and at 11.7GHz is 8.2GHz.

(a)

(b)
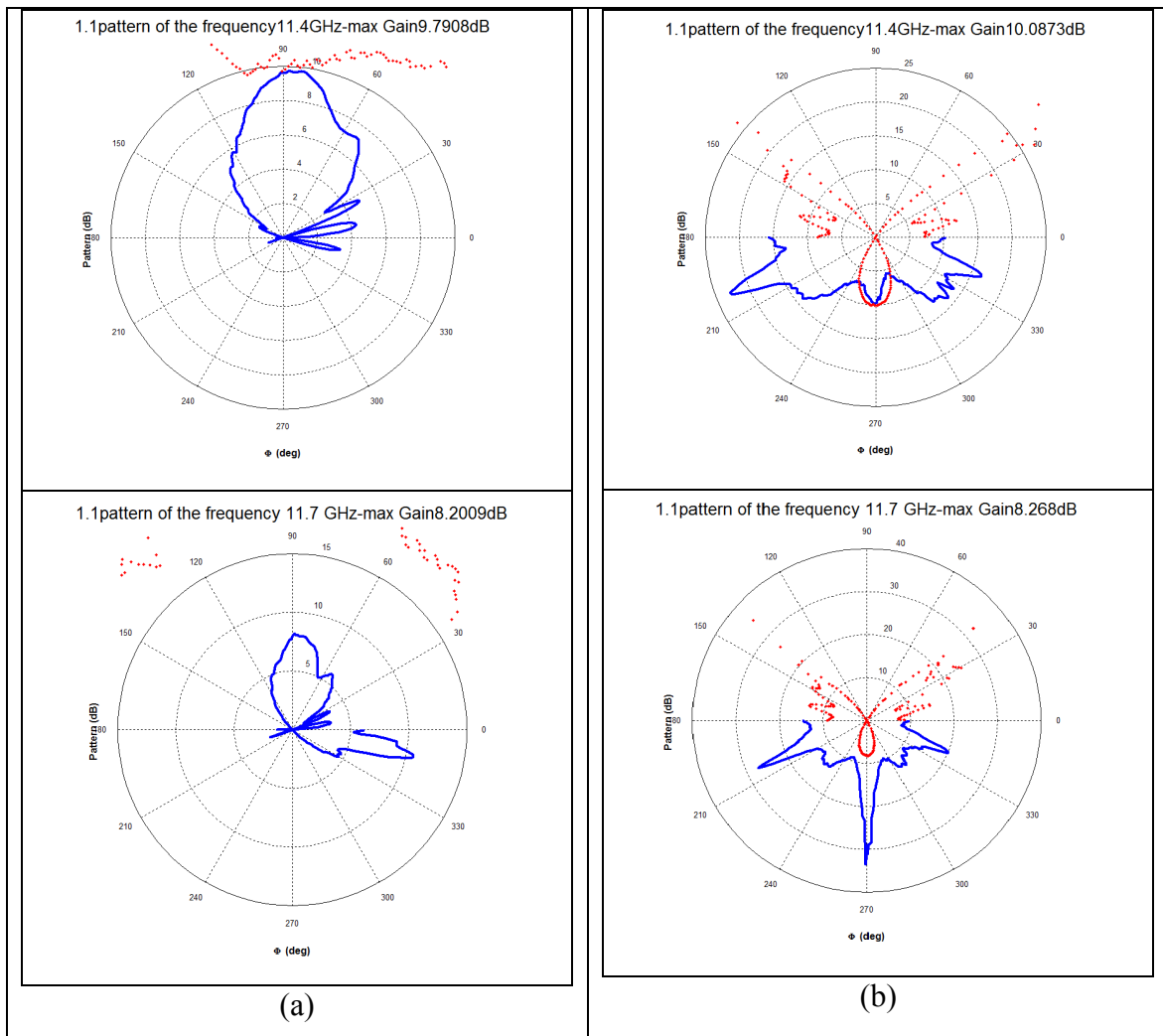
Figure 6.44 (a) Horizontal and (b) vertical pattern of the two patches connected by the divider, port1 before cutting the connector pin (ε_r:7.8) (___co-polar ....cross-polar)

Figure 6.45 (a) Horizontal and (b) vertical pattern of the two patches connected by the divider, port2 before cutting the connector pin (ε_r:7.8) (___co-polar ....cross-polar)

In figure 6.48 the gain at 11GHz is 9dB and at 11.7GHz is 8.2dB for two patches. For the other frequencies for minimum S11, the gain is low.

Figure 6.46 (a) Horizontal and (b) vertical pattern of the two patches connected by the divider, port1 after cutting the connector pin in the minimum S11 points (ε_r:7.8) (___co-polar ....cross-polar)

6.7.6 Two Dual Polarized Antennas D over the Substrate 9K7 GreenTape

6.7.6.1 S-parameters

As it was mentioned in section 6.2 patch D was totally not flat. For this we had to use glue. Figure 6.47 shows the S-parameters after using glue and cutting the pins. It shows for one port 0.9 GHz bandwidth from 11.15GHz to 12.05 GHz and for the other port shows 0.45 GHz bandwidth from 10.35GHz to 10.8 GHz.
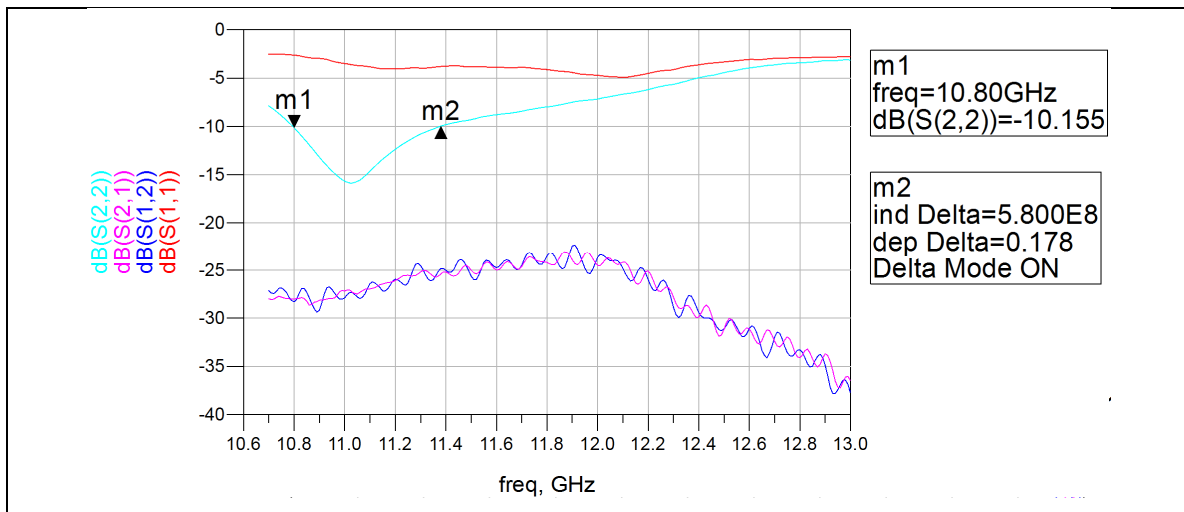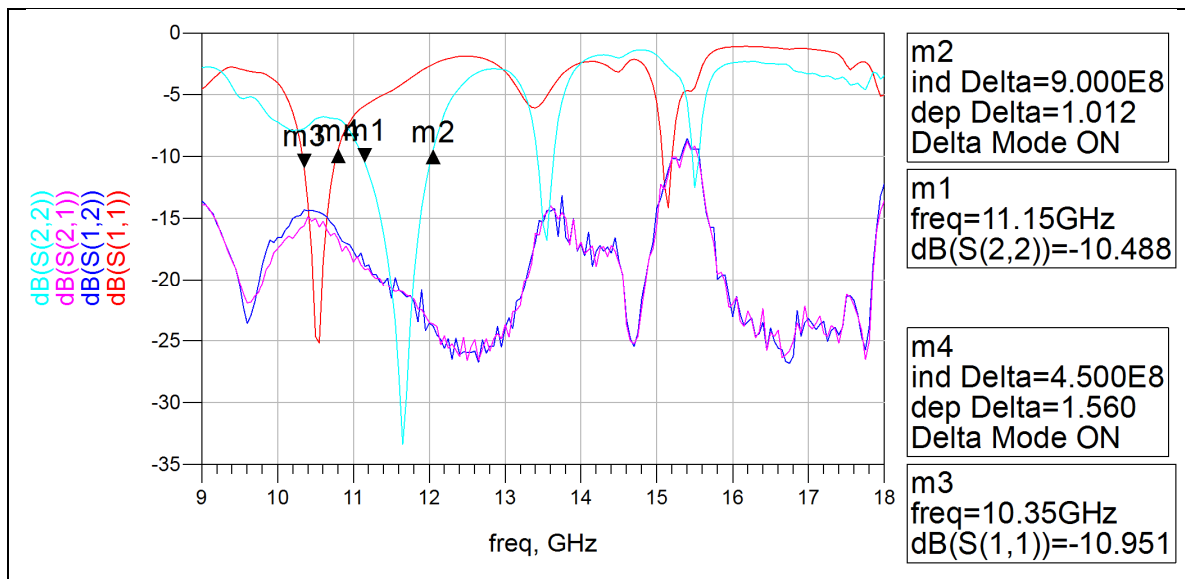

Figure 6.47 Measured S-parameters of two dual polarized patch antennas connected with a divider on the substrate 9K7 Green Tape after cutting the pins and after sticking with glue

Note4:

Another item that can distub the performance of the circuit is the vias put to acces the ground over the LTCC. We think it made a serious effect on the circuit function. It was better to put these vias below the LTCC not on the LTCC near the place of pin. About the last two divider designed over the substrate II, because the ground was below the LTCC and not in the middle of the layers, the sparameters in spite of many problems like not being flat and probability of entering the glue inside the slot, it works better than the other componnents.

6.7.6.2 Radiation Pattern

Figure 6.48 and 6.49 shows the radiation pattern of two patch D connected to each other by a divider. The gain at 11.4GHz, which is the maximum gain for two patches, is 10.5dB and at 11.7GHz that is 9.5dB.
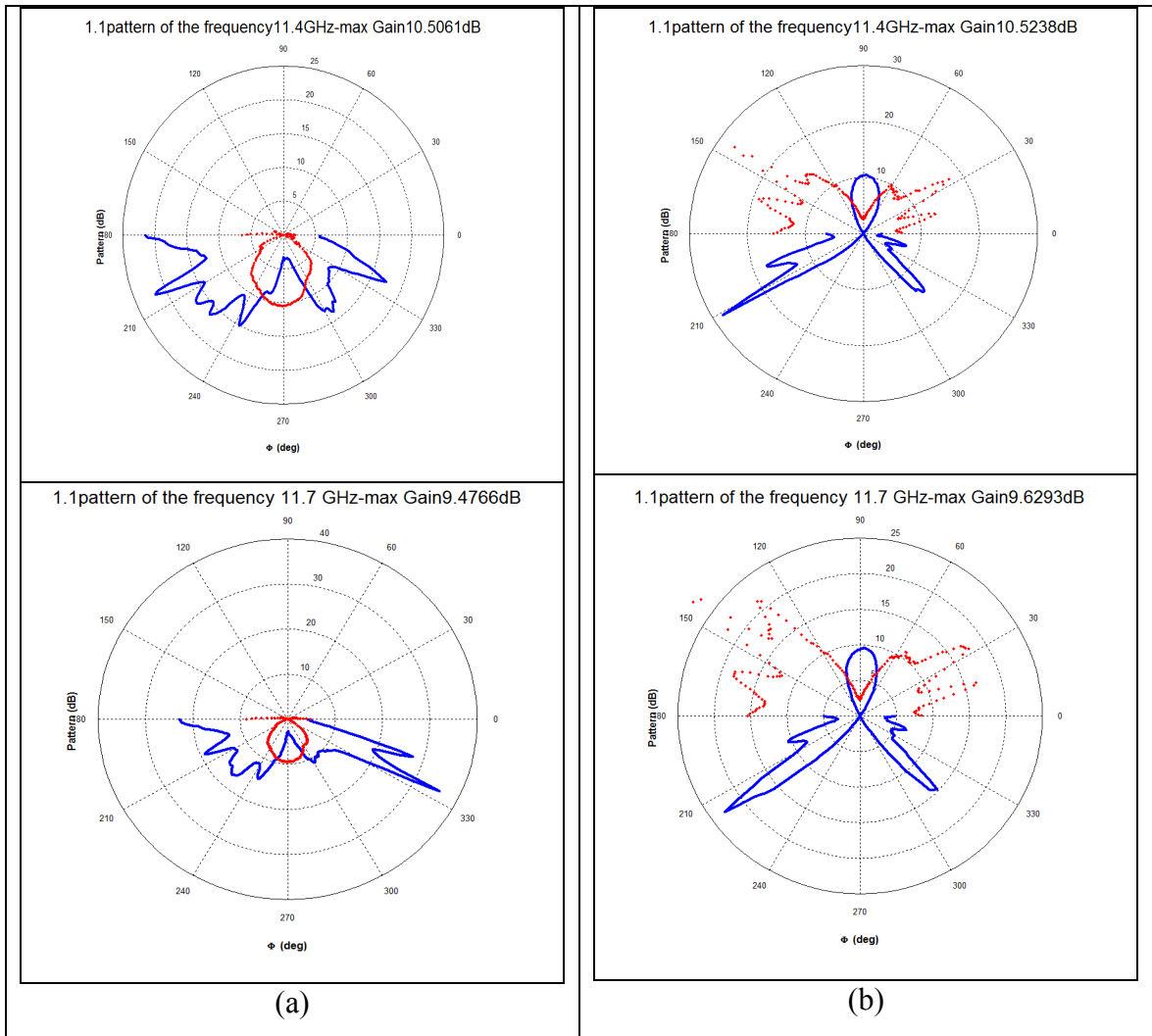
Figure 6.48 (a) Horizontal and (b) vertical pattern of the two patches connected by the divider, port1 after cutting the connector pin (ε_r:7.1)
(___co-polar ....cross-polar)
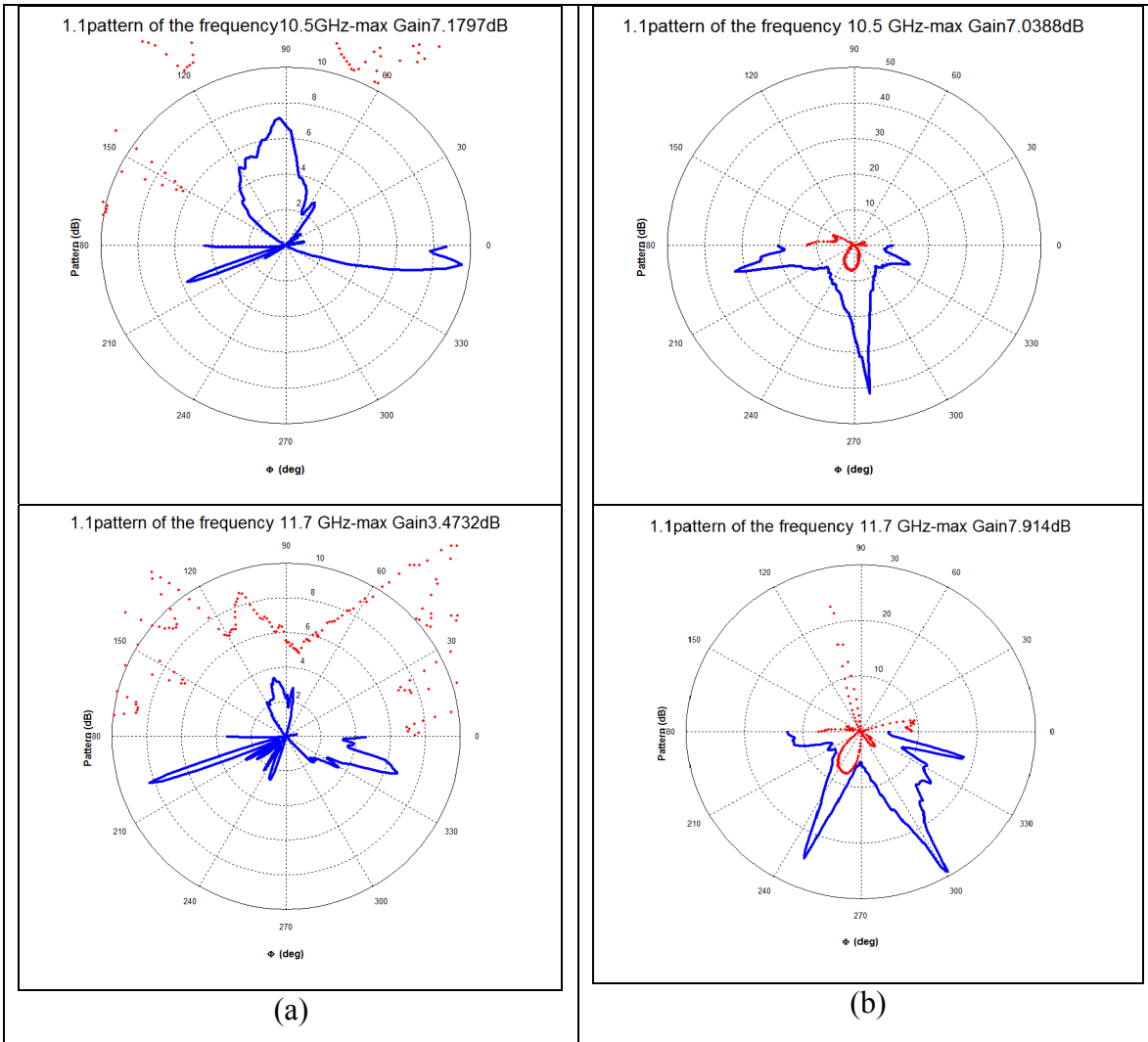
Figure 6.49 (a) Horizontal and (b) vertical pattern of the two patches connected by the divider, port2 after cutting the connector pin (ε_r:7.1)
(___co-polar ....cross-polar)

Figure 6.50 shows the radiation patterns for minimum S11. From them the best gain is at 10.6GHz which is 7dB.
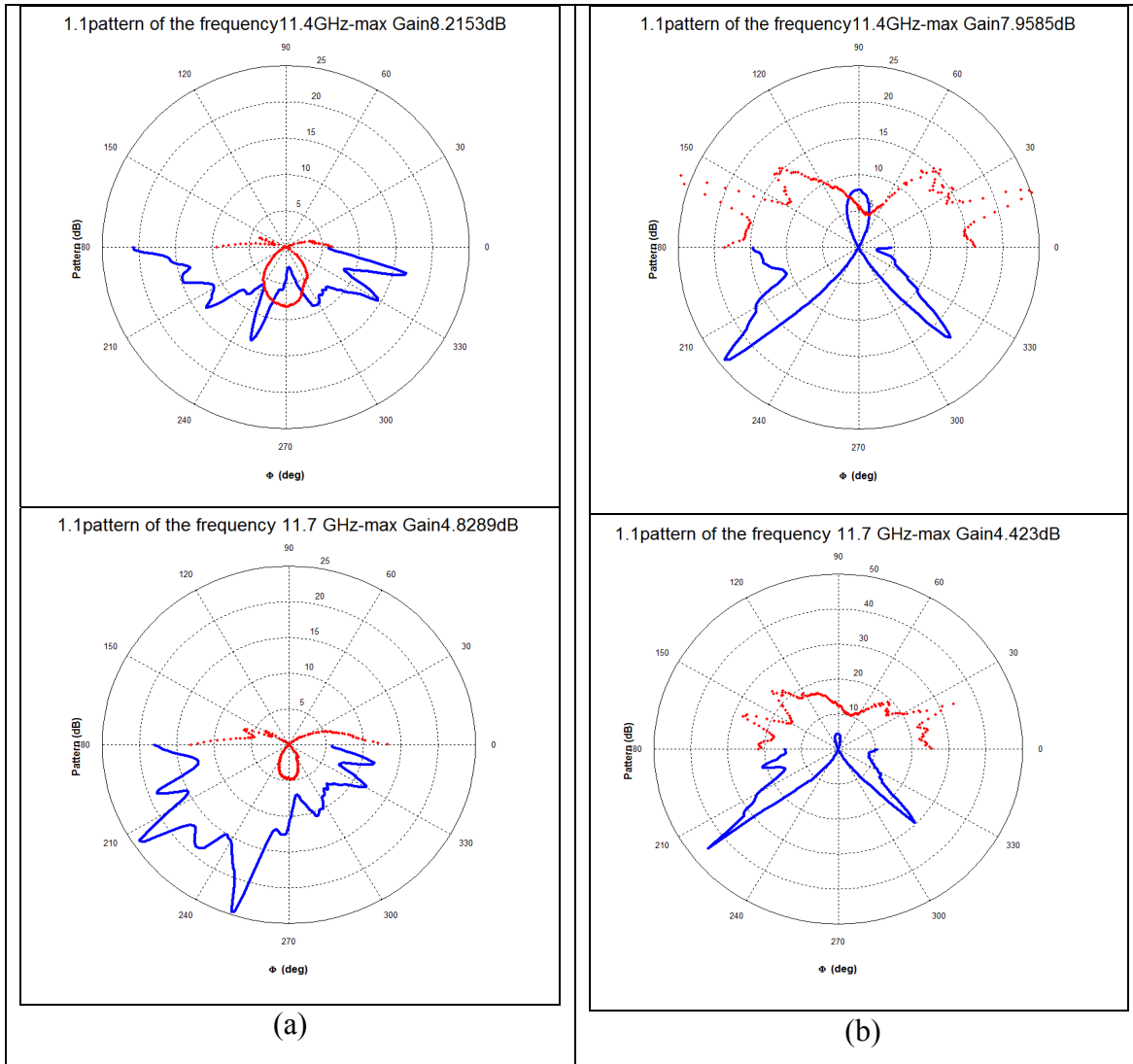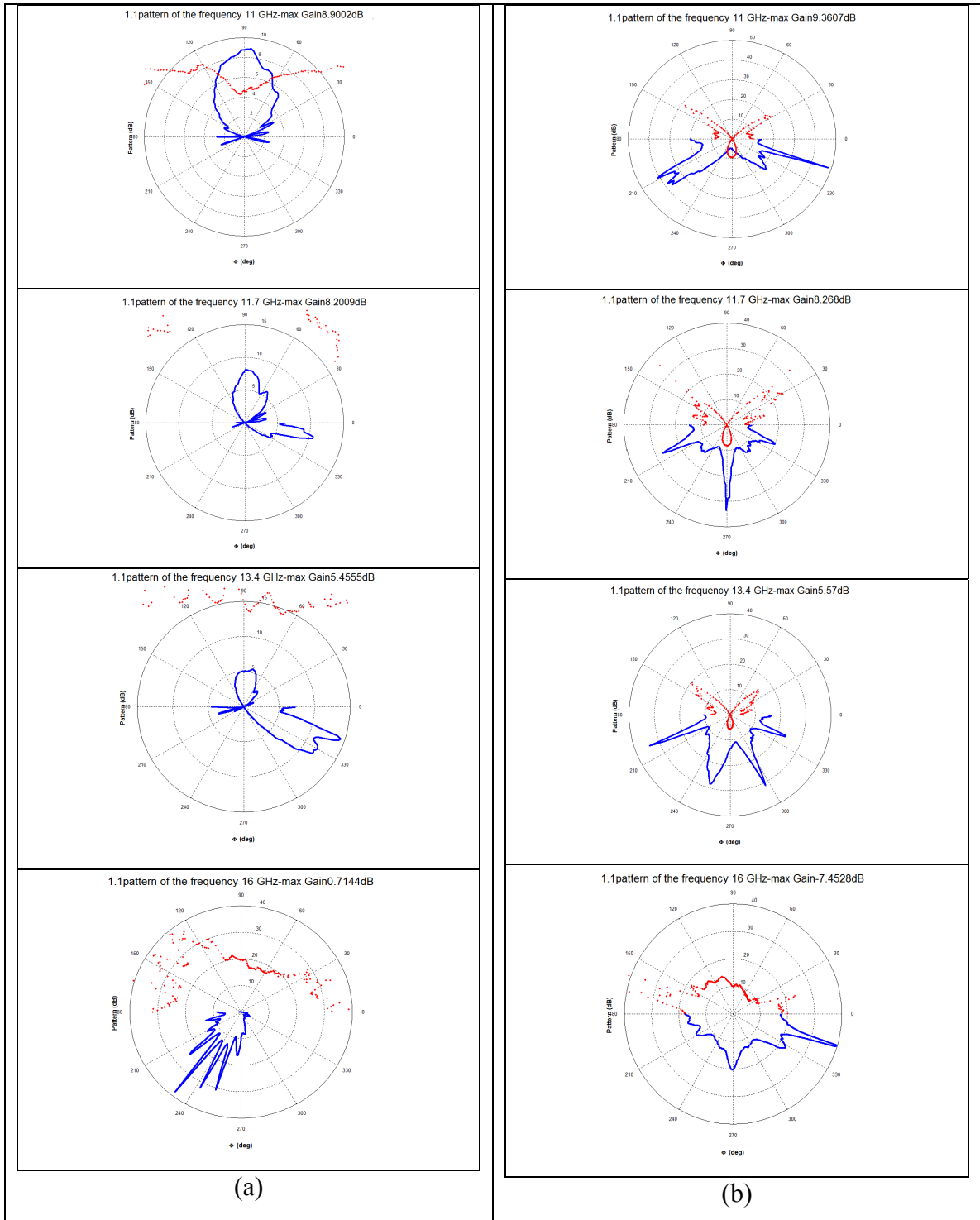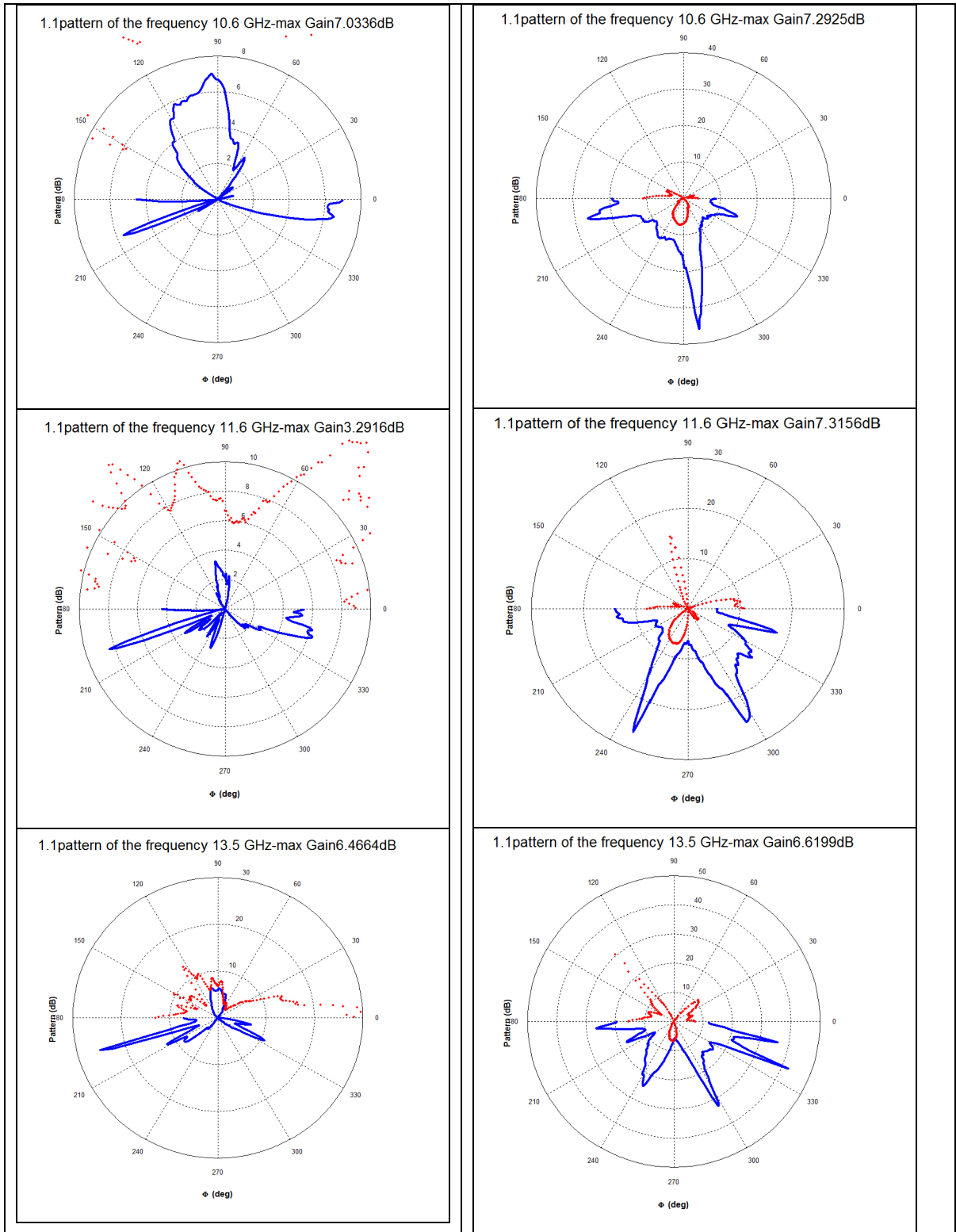
Figure 6.50 (a) Horizontal and (b) vertical pattern of the two patches connected by the divider, port2 after cutting the connector pin in the minimum S11 points (ε_r:7.1) (___co-polar ....cross-polar)

CONCLUSION

In this work we have designed and fabricated several new patch antennas working in the frequency range from 10.7 GHz to 12.7 GHz to be used in planar phased array antenna for satellite communication applications. Planar array antennas are proposed in order to replace dish antennas because of the many advantages that they offer, such as higher reliability, near-instantaneous beam switching and steering capability. To have a planar array equivalent to a dish antenna, the choice of the individual radiating element and its radiation pattern are crucial since they have a direct impact on the directivity and gain of the overall array. We have shown that such equivalence is feasible using printed patch antenna elements and we focused on the design of such elements first as single element, with linear and dual linear polarization, and later as an array of two elements. All designs were carried out using the planar electromagnetic field simulator Momentum, which is a part of the Advanced Design System (ADS) of Agilent technologies.

The most commonly used technology for planar array antennas is microstrip technology. This is because microstrip has low cost, low weight, and can be printed easily over a dielectric substrate with photolithography techniques. However, microstrip patch antennas have some important drawbacks, like low efficiency and narrow bandwidth. Given that our design requires the coverage of a relatively wideband, 17.1%, we had to consider different techniques for increasing the patch bandwidth. One of those techniques is increasing the thickness of the substrate and decreasing the dielectric constant. For this reason we chose to realize the patch element in Rogers RT5870 which has a low dielectric constant of 2.33. The second is using stacked elements with various parasitic elements. This technique was considered but was found not to give significant improvements for our application. The third bandwidth enhancement technique consists of using a suitable feeding technique. In this work we used aperture feeding, since it is one of the most efficient techniques for broadband antennas because it has many adjustable geometrical parameters, i.e., shape and dimensions. Optimization of the feed line and the use of insets were also considered in this work to further improve bandwidth.

In addition to bandwidth, one key challenge is the integration of the beam forming network in a low loss circuit technology that ensures high efficiency and allows miniaturization. In this work, we chose to use LTCC technology to realize the feeding structures, including the feed lines, the dividers/combiners and the coupling slots. Therefore, our resulting microstrip patch antenna design consisted of a hybrid stack of LTCC and standard PCB (Rogers RT5870) technologies. Our simulation results for the designed hybrid patch antenna elements showed that we could achieve a bandwidth of 19% and an efficiency of about 60% for a single patch with a gain of 5.8dB. It was the first time that a hybrid LTCC-PCB integration was attempted at ÉTS. One of the proposed patches was made on the 9K7 LTCC Green Tape and Rogers RT5870 while the others were made on the 591 LTCC Green Tape and Rogers RT5870.

Several antennas were fabricated, integrated (LTCC and RT5870) and tested both for input impedance, i.e., S11, and radiation patterns. The experimental radiation pattern measurements showed a maximum gain of around 5dB for the antennas, which is close to the simulation results. The experimental S-parameters measurements on the other hand, showed a bandwidth of only 8.6% for the patch over 9K7 Green Tape and of 12% for the patch over 591 Green Tape, which are less than the values obtained in simulation. Several reasons can cause this difference such as: the placement of via holes near the connector pins, imperfection in the soldering process, the finite ground of the real circuit that were assumed as infinite ground by the simulator, sensitivity to the transition line lengths, and the type of connectors used. Still, this work can be considered, overall, as a successful first step in using hybrid LTCC-PCB technologies to realize planar antennas at Ku band frequencies.

In light of the obtained results and the potential sources of problems that were identified, we can formulate the following set of recommendations for future work:

- use HFSS software simulate finite ground;
- design longer feed line to decrease the sensitivity of the circuit performance to the line length;

- use a type of connector which is proper for thin substrates in the Ku-band frequency range;

- cut the center pin and ground pins of the connector to have less effects on the circuit performance;

- change the place of the LTCC ground vias to the reverse side of the LTCC stack that contains no feed lines.

BROADBANDING USING STACKED ELEMENTS
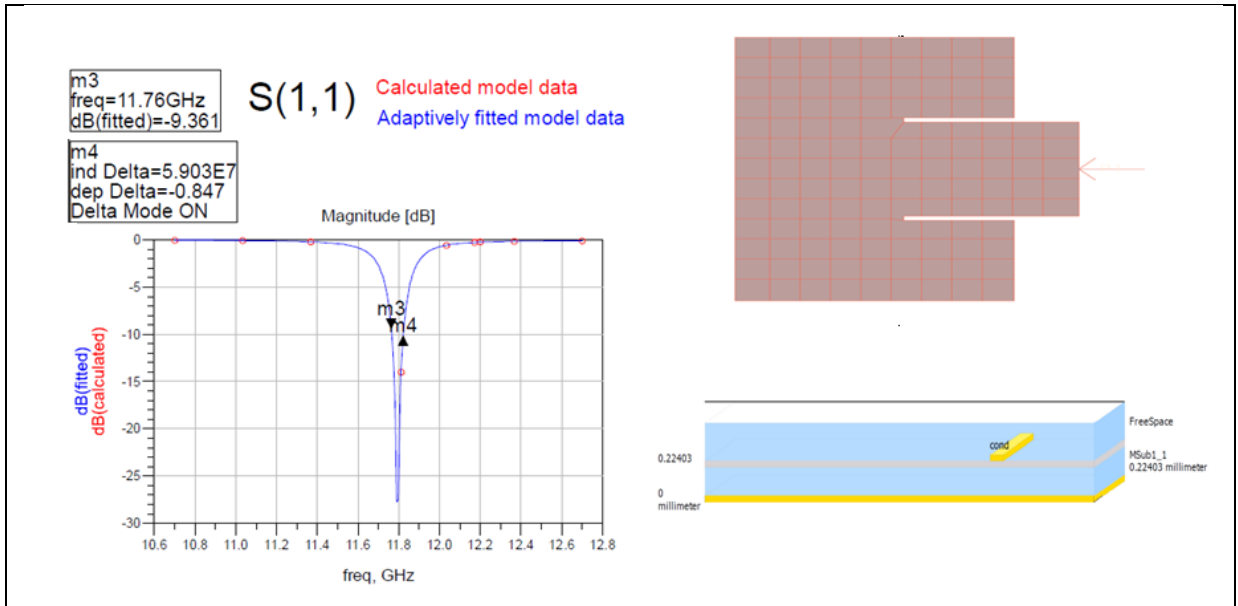
Figure-A I-1 Patch Antenna with One Layer, ε_r=7.8, efficiency=69.329%
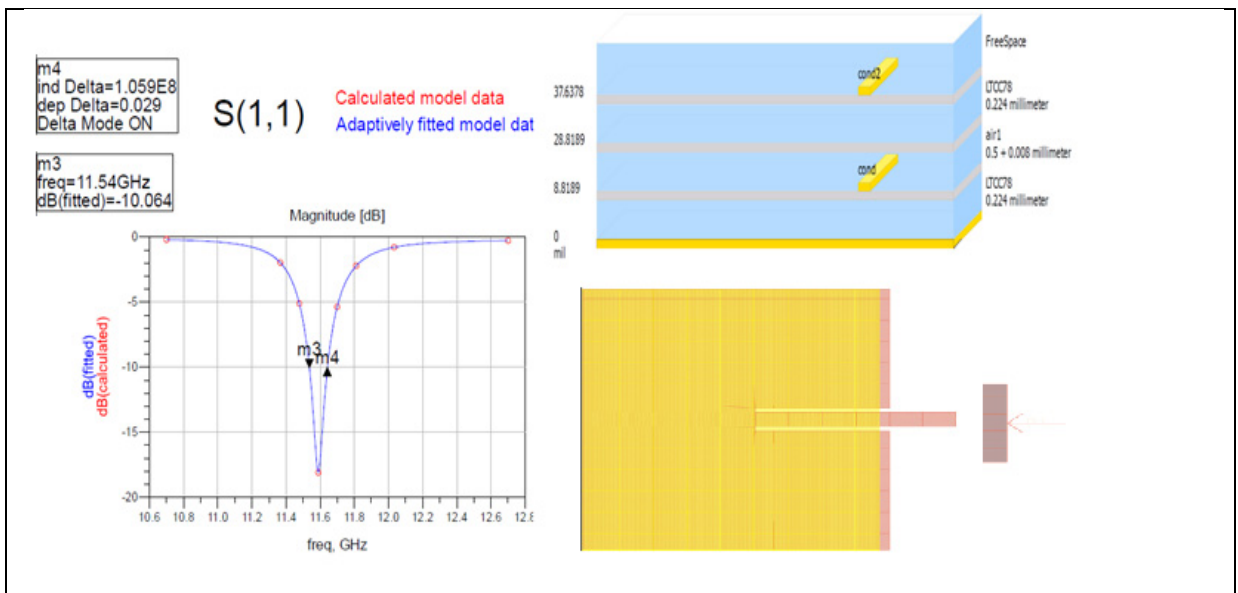
Figure-A I-2 Patch Antenna with Two Layers, ε_r=7.8, efficiency=46.751%
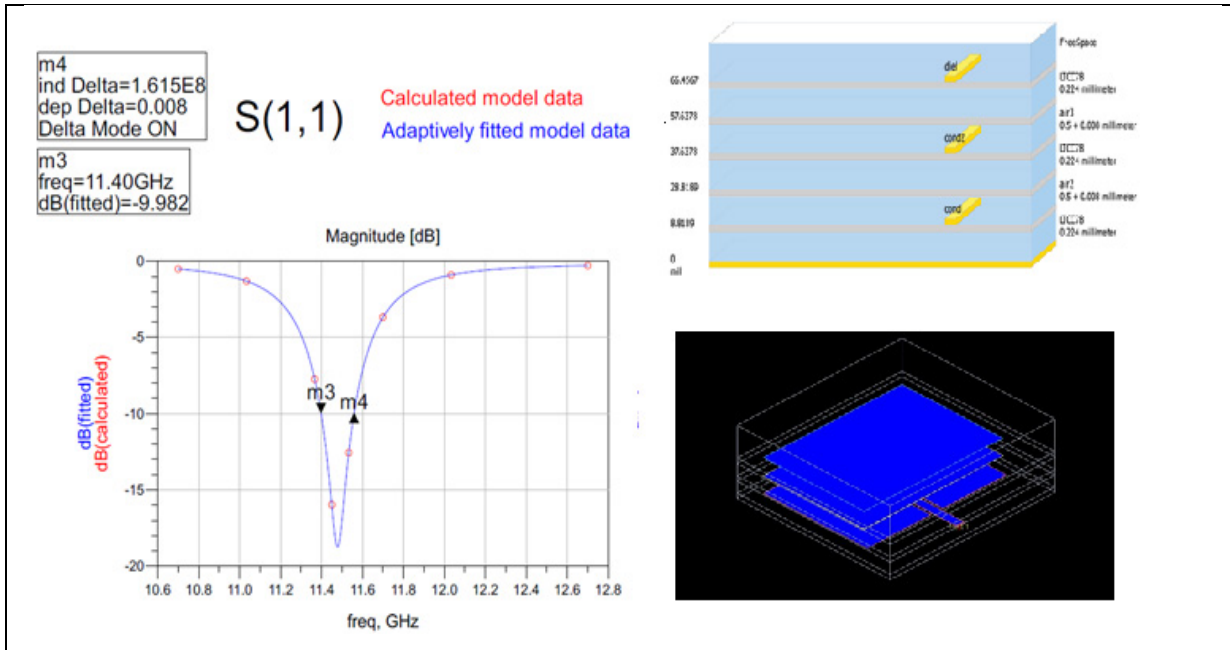
Figure-A I-3 Patch Antenna with Three Layers, ε_r=7.8, efficiency=55.483%
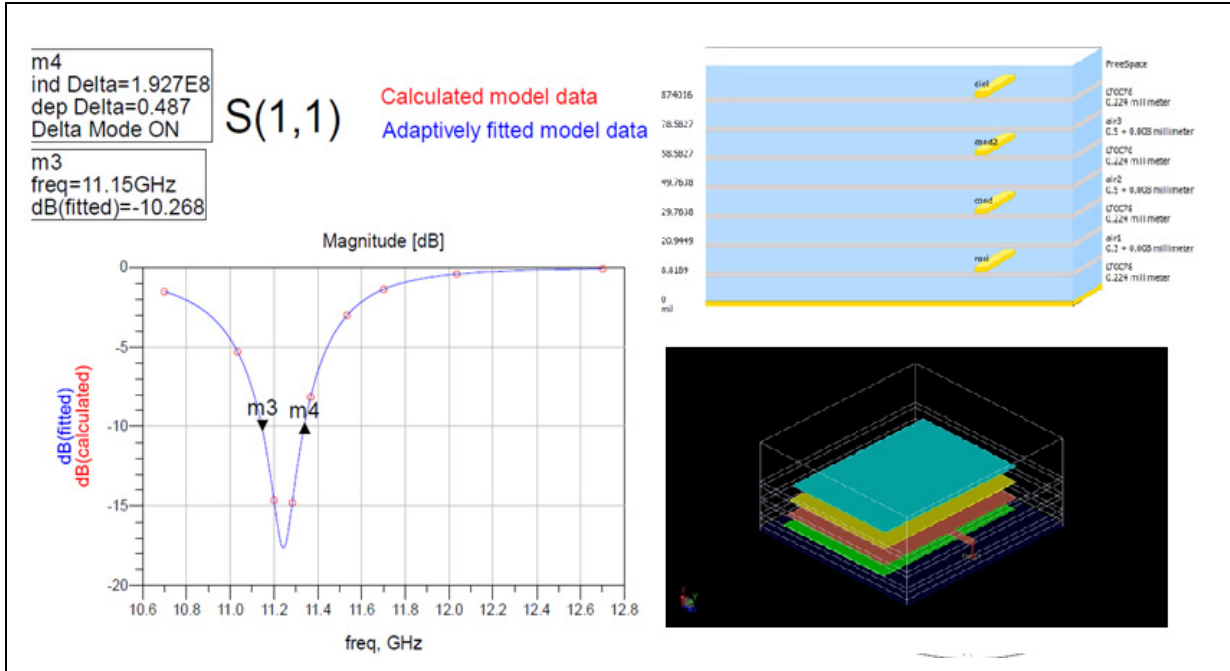
Figure-A I-4 Patch Antenna with Four Layers, ε_r=7.8, efficiency=61.953%
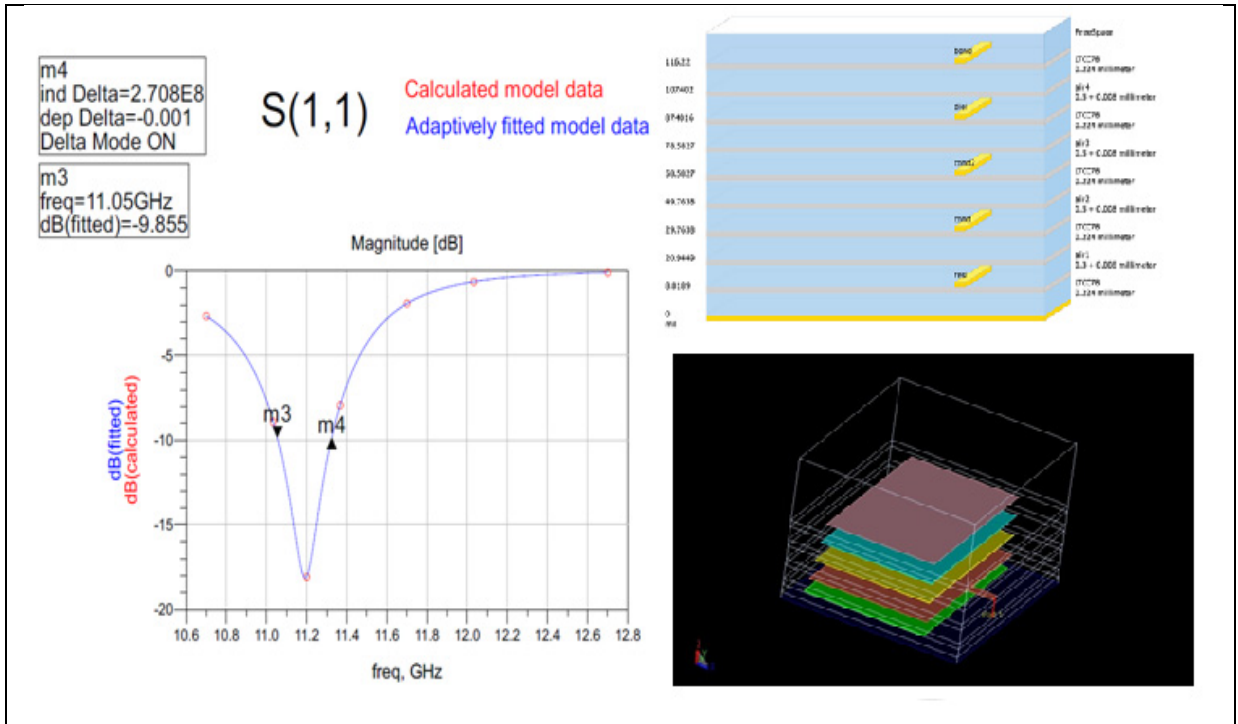
Figure-A I-5 Patch Antenna with Five Layers, ε_r=7.8, efficiency=67.410%

BROADBANDING USING DIFFERENT APERTURE FEED LINES
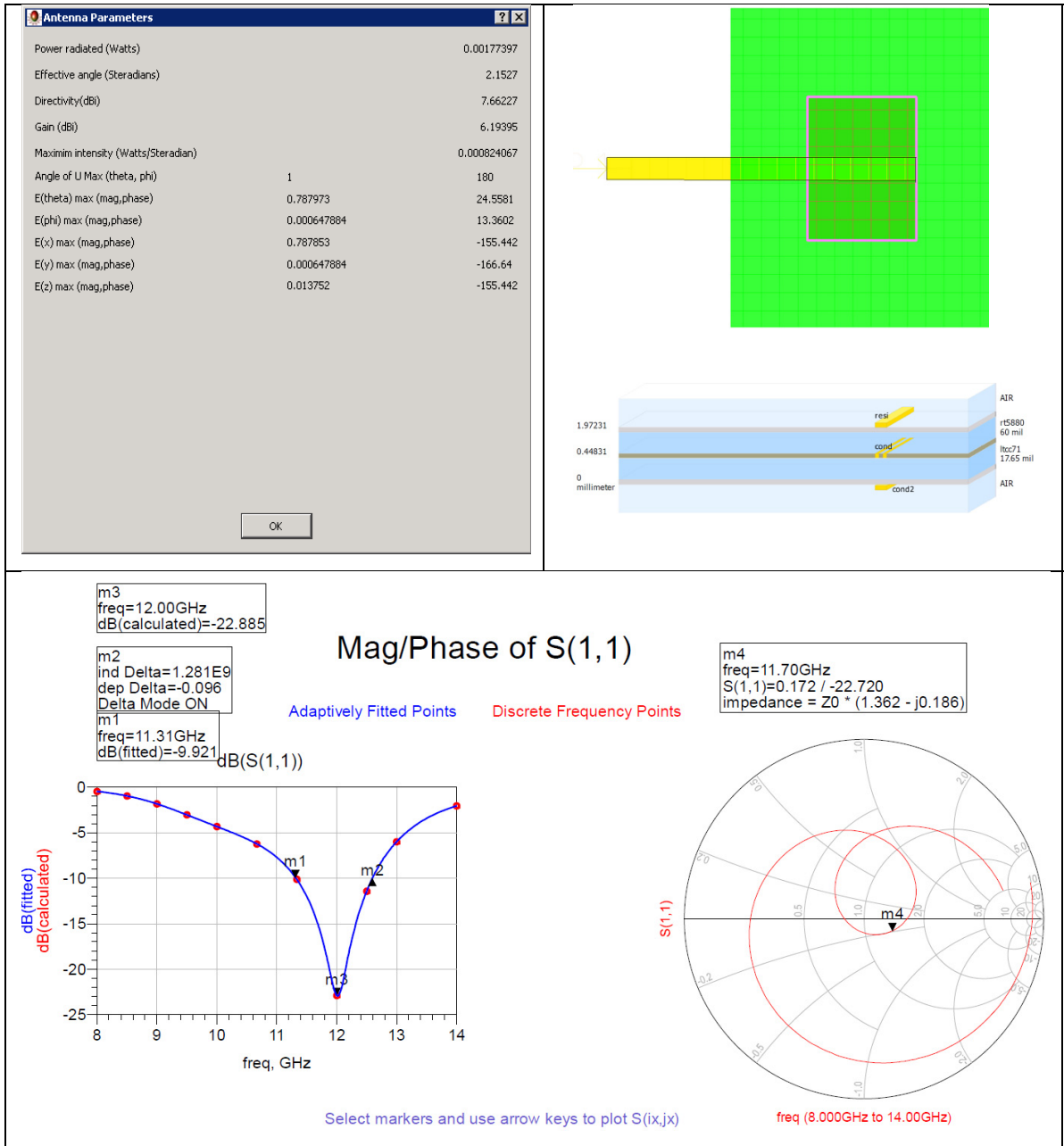
Figure-A II-1 Patch Antenna with Line Feed, ε_r(patch)=2.2(60mils), ε_r(feed)=7.1(17.65mils), efficiency=71.313%

130
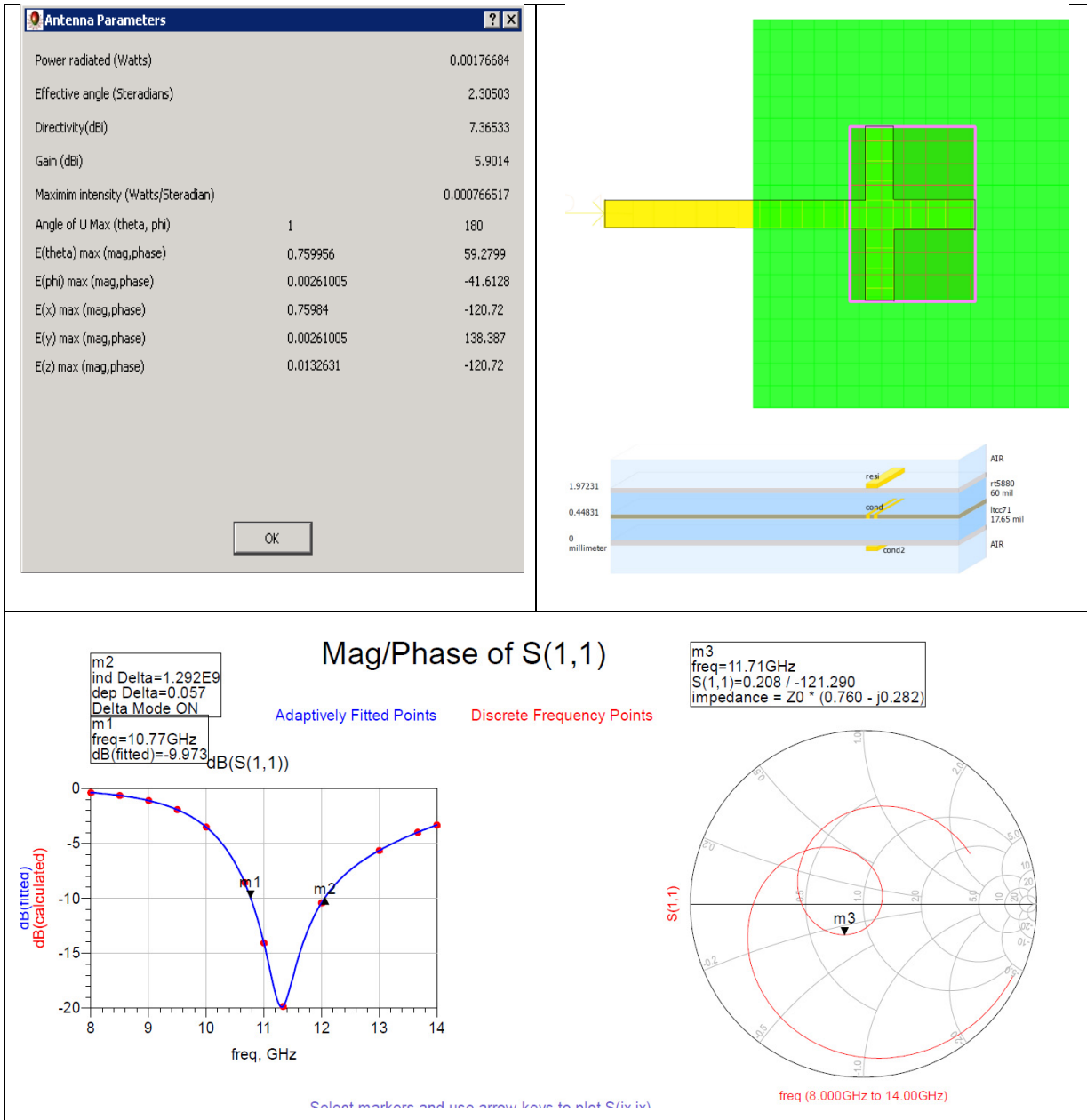
Figure-A II-2 Patch Antenna with Cross Feed, ε_r(patch)=2.2(60mils),
ε_r(feed)=7.1(17.65mils), efficiency=71.385%

Antenna Parameters

Power radiated (Watts)		0.00164852
Effective angle (Steradians)		2.42921
Directivity(dBi)		7.13744
Gain (dBi)		5.80561
Maximim intensity (Watts/Steradian)		0.000678621
Angle of U Max (theta, phi)	0	0
E(theta) max (mag,phase)	0.505469	-145.549
E(phi) max (mag,phase)	0.505782	34.2626
E(x) max (mag,phase)	0.715061	-145.643
E(y) max (mag,phase)	0.00119558	-44.9657
E(z) max (mag,phase)	0	0

OK

Mag/Phase of S(1,1)

m4
freq=12.40GHz
dB(fitted)=-52.272

m3
freq=12.91GHz
dB(fitted)=-9.944

m2
freq=11.33GHz
dB(calculated)=-9.832

m1
freq=11.70GHz
S(1,1)=0.263 / -92.273
impedance = Z0 * (0.854 - j0.483)

Adaptively Fitted Points   Discrete Frequency Points

dB(S(1,1))

Select markers and use arrow keys to plot S(ix ix)

Figure-A II-3 Patch Antenna with Patch Feed, ε_r(patch)=2.2(60mils), ε_r(feed)=7.1(17.65mils), efficiency=73.590%
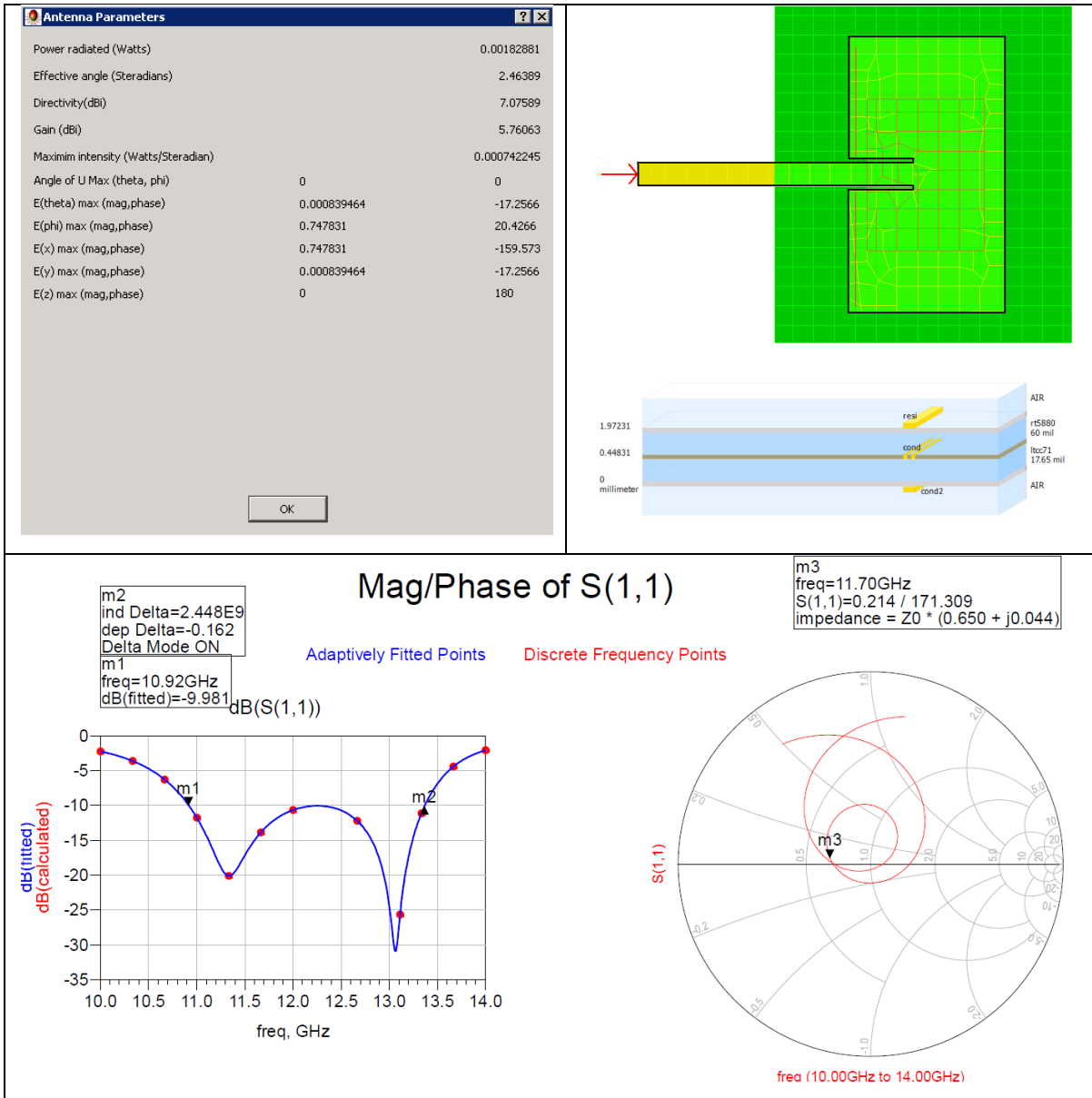
Figure-A II-4 Patch Antenna with Patch-Inset Feed, ε_r(patch)=2.2(60mils), ε_r(feed)=7.1(17.65mils), efficiency=73.871%
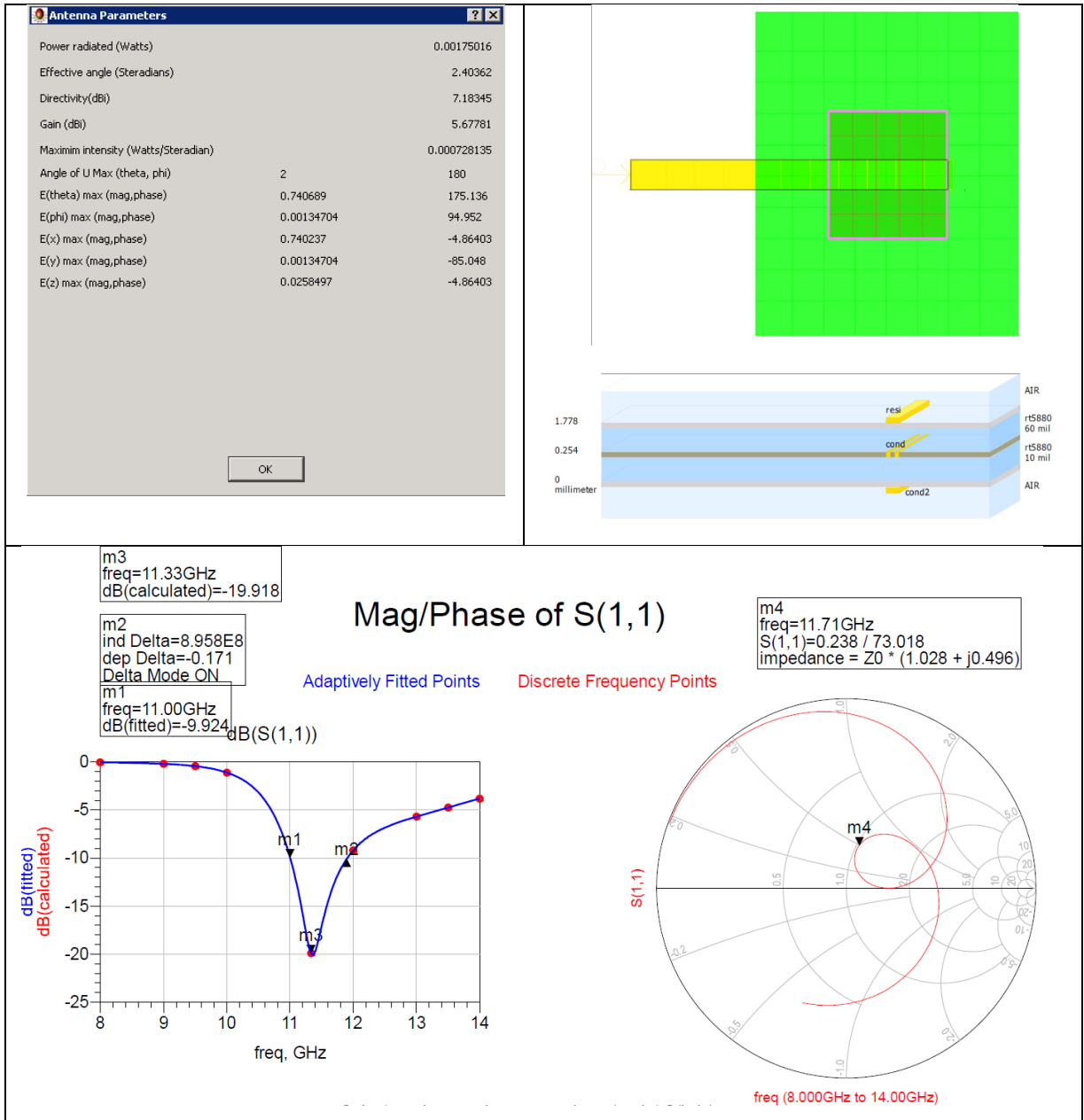
Figure-A II-5 Patch Antenna with Line Feed, ε_r(patch)=2.2(60mils), ε_r(feed)=2.2(10mils), efficiency=70.703%

134
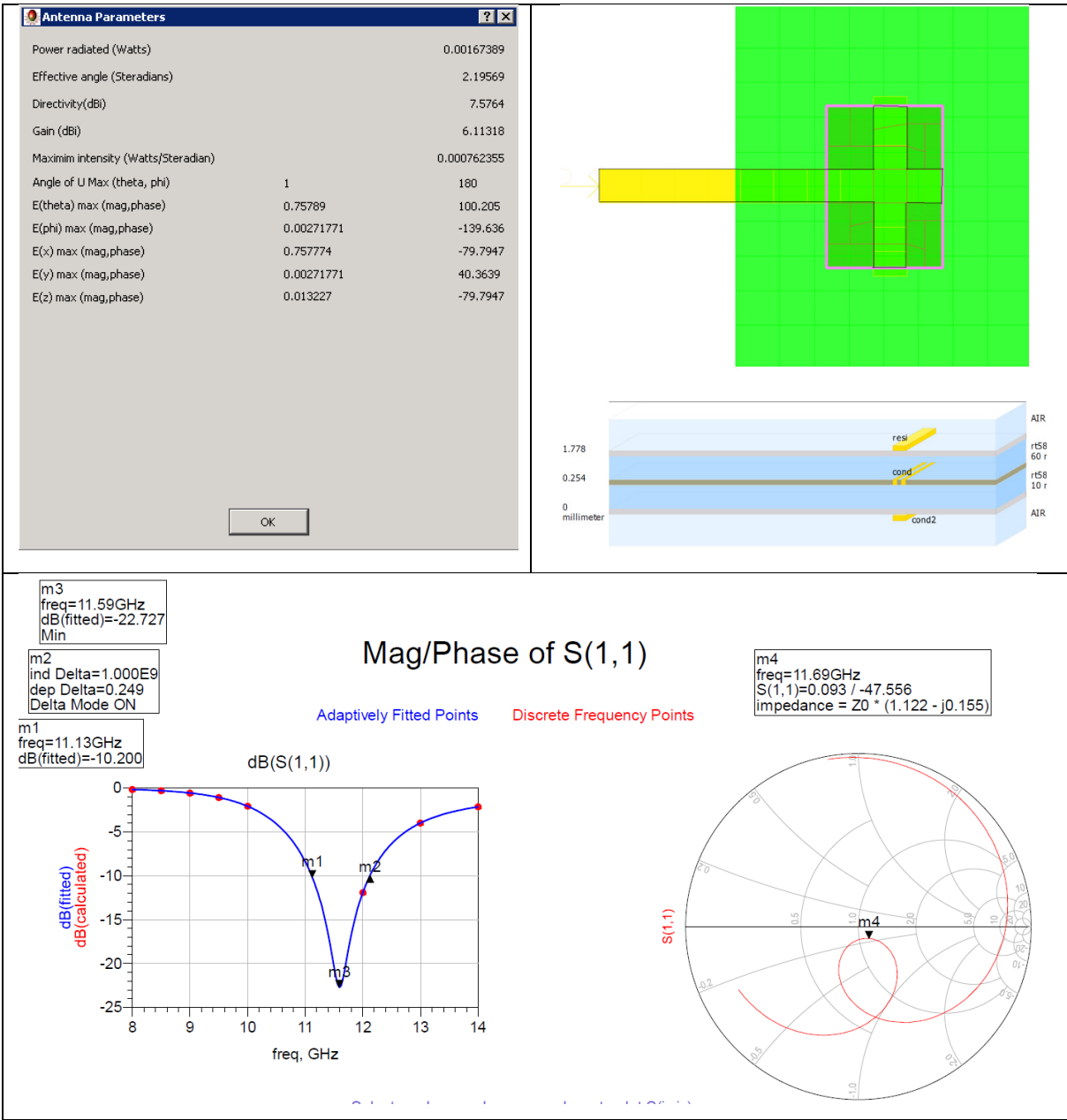
Figure-A II-6 Patch Antenna with Cross Feed, ε_r(patch)=2.2(60mils), ε_r(feed)=2.2(10mils), efficiency=71.397%
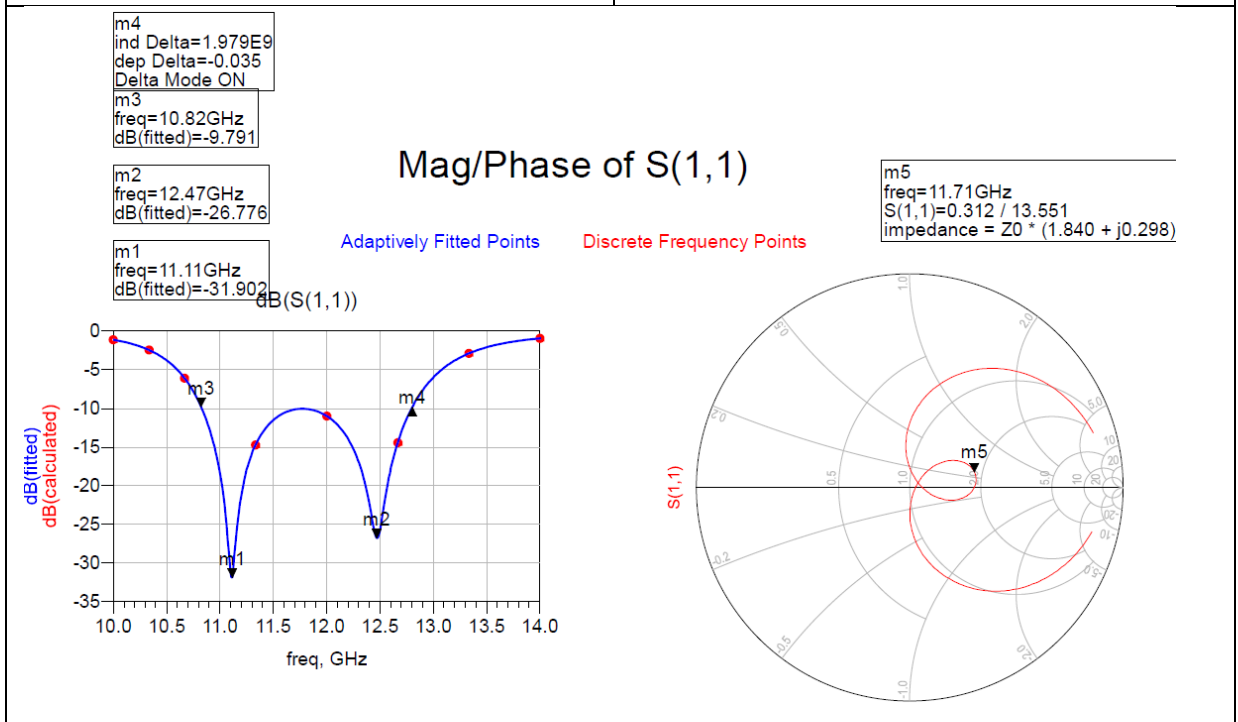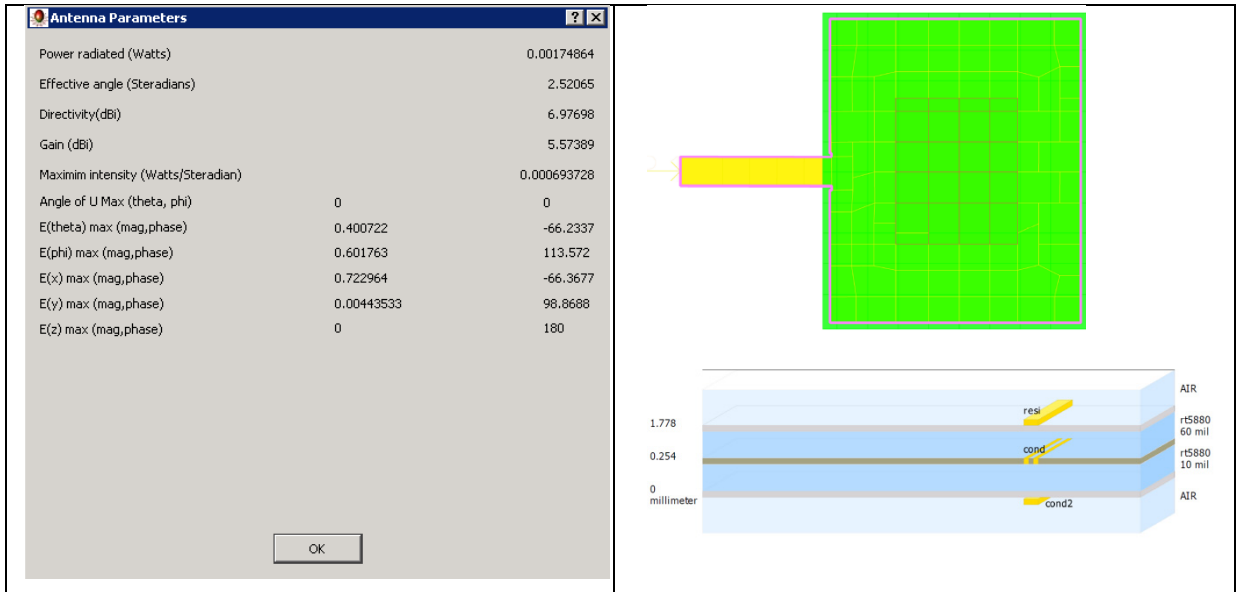
Figure-A II-7 Patch Antenna with Patch Feed, ε_r(patch)=2.2(60mils), ε_r(feed)=2.2(10mils), efficiency=72.392%

Figure-A 0-I
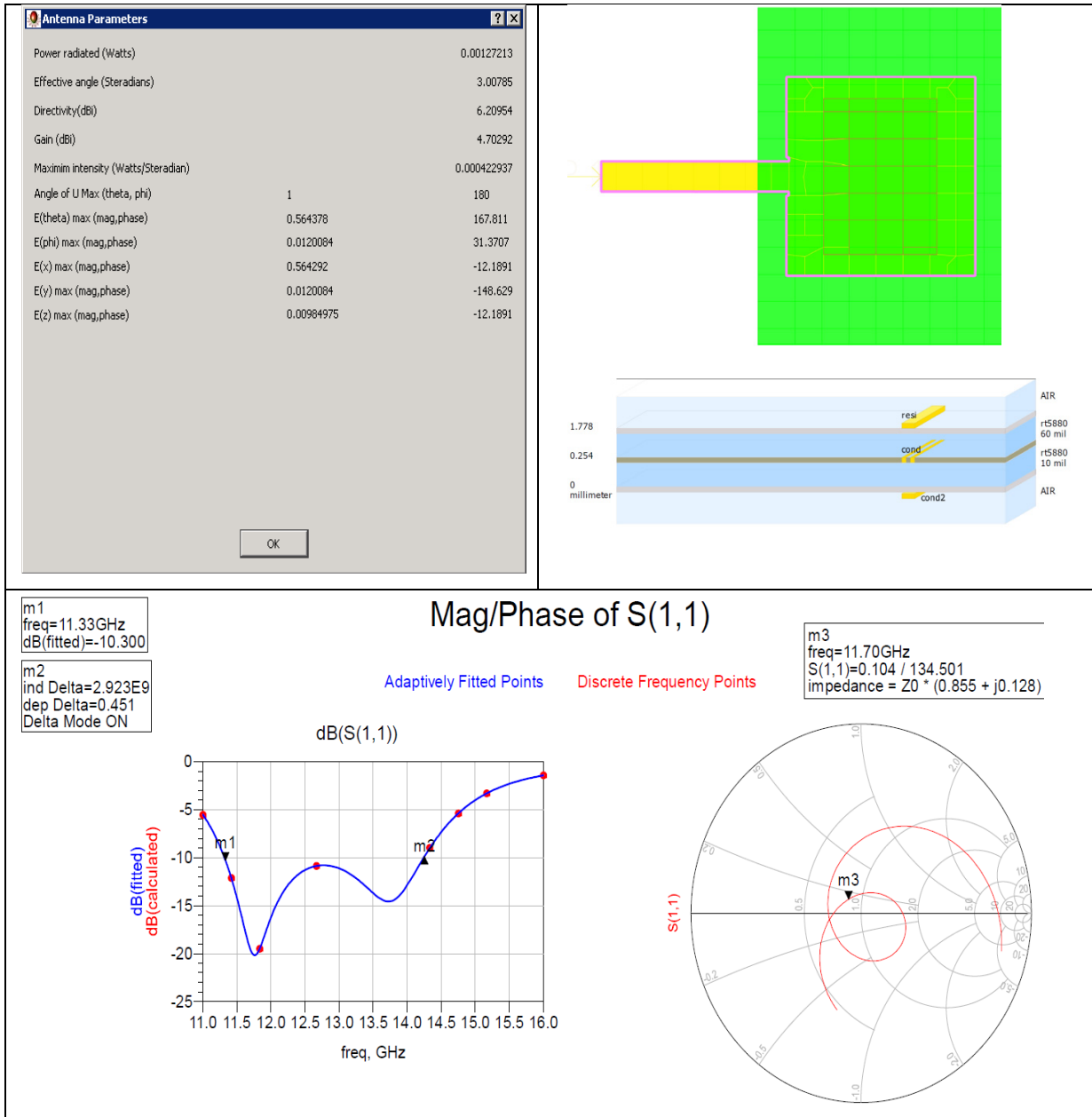
Figure-A II-8 Patch Antenna with Patch-Inset Feed, ε_r(patch)=2.2(60mils), ε_r(feed)=2.2(10mils), efficiency=70.687%

PATCH FEDD LINE
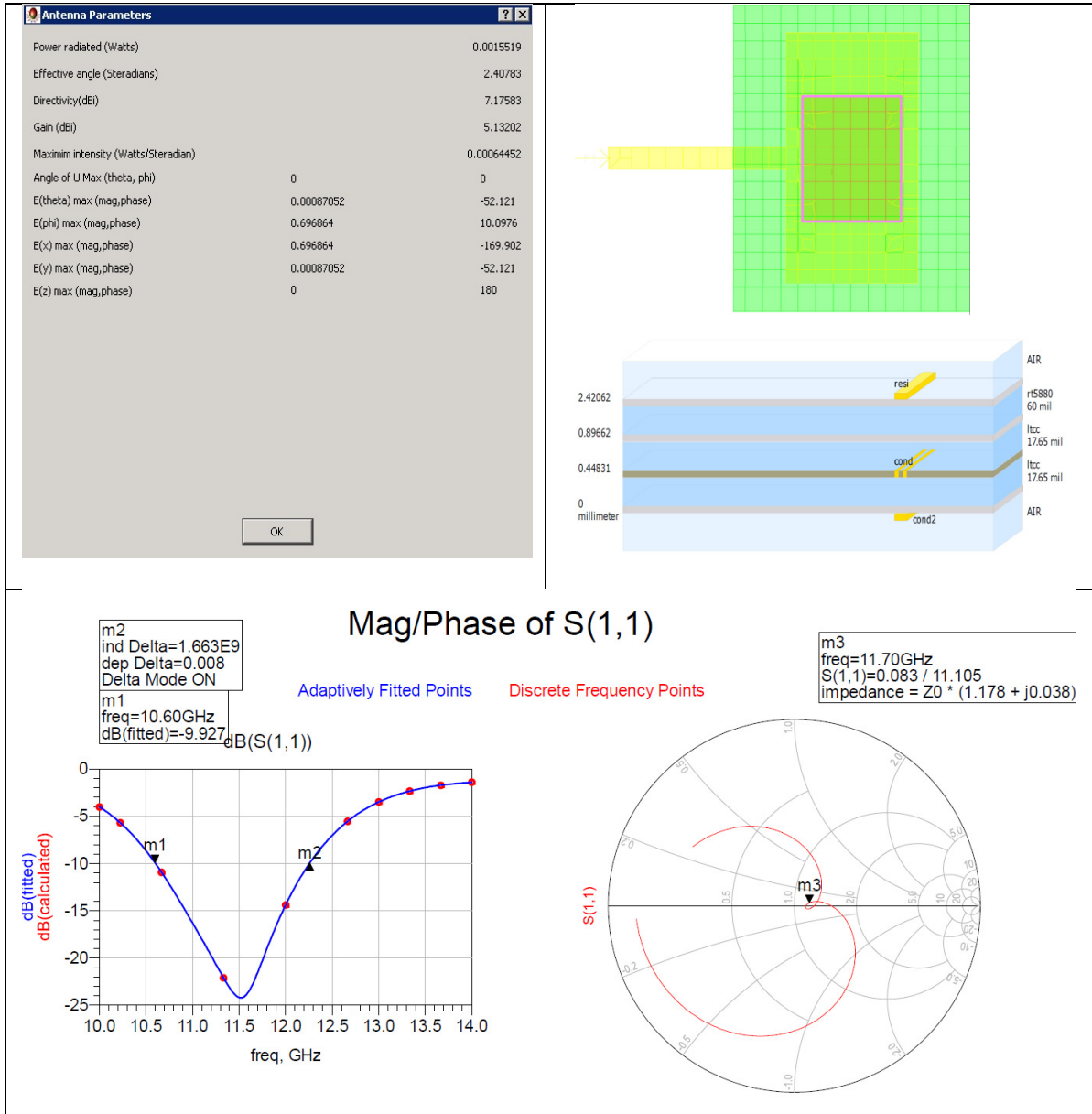
Figure-A III-1 Patch Antenna with Patch Shape Feed and Rectangular Slot,
ε_r(patch)=2.2(60mils)+7.1(17.56mils), efficiency=62.462%

Figure-A 0-I

Antenna Parameters

Power radiated (Watts)		0.00156628
Effective angle (Steradians)		2.40356
Directivity(dBi)		7.18356
Gain (dBi)		5.25697
Maximim intensity (Watts/Steradian)		0.000651649
Angle of U Max (theta, phi)	0	0
E(theta) max (mag,phase)	0.00127873	-105.445
E(phi) max (mag,phase)	0.700707	-15.8166
E(x) max (mag,phase)	0.700707	164.183
E(y) max (mag,phase)	0.00127873	-105.445
E(z) max (mag,phase)	0	0
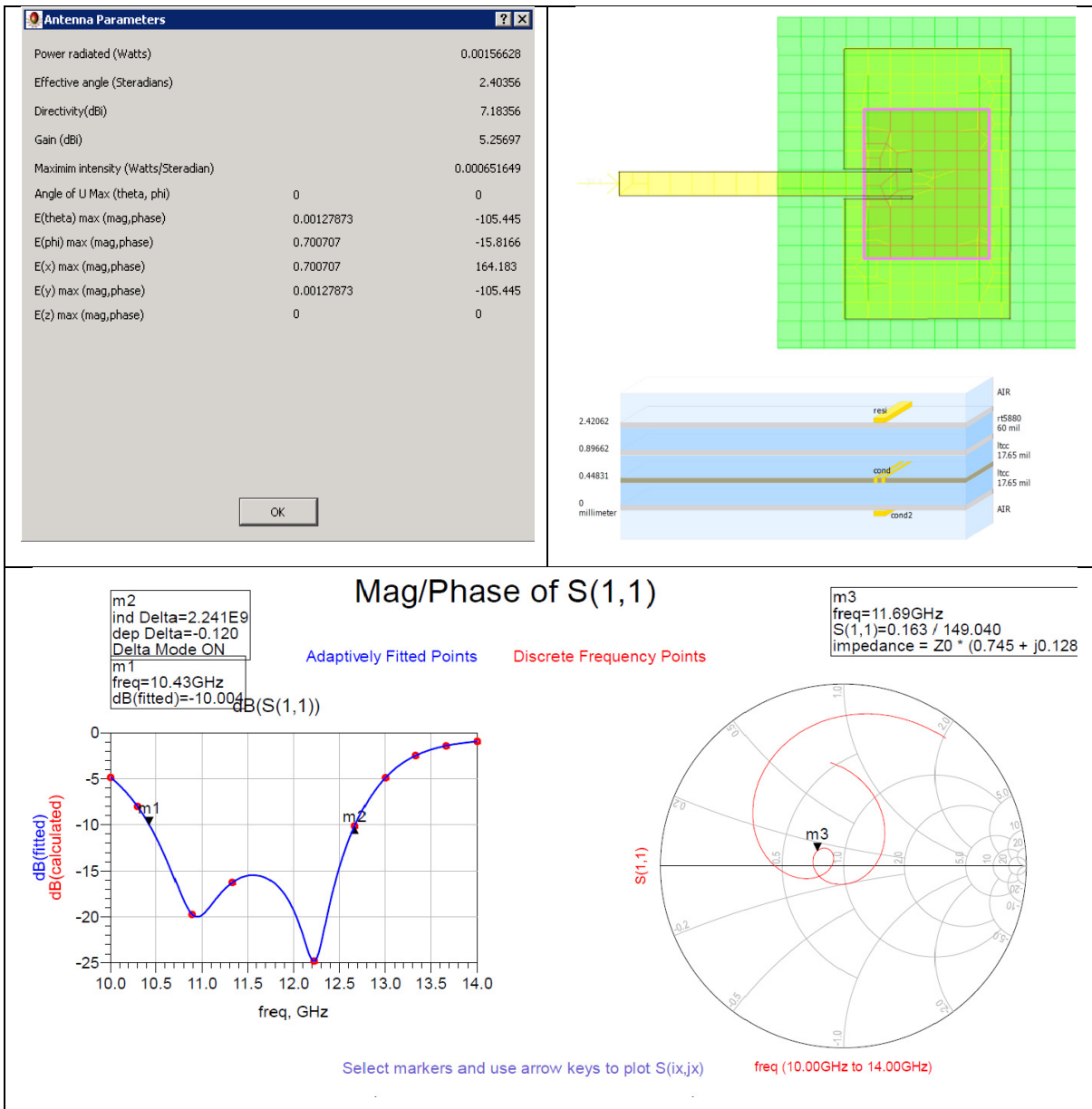
Figure-A III-2 Patch Antenna with Patch-Inset Shape Feed and Rectangular Slot, ε_r(patch)=2.2(60mils)+7.1(17.56mils), ε_r(feed)=7.1, efficiency=64.171%
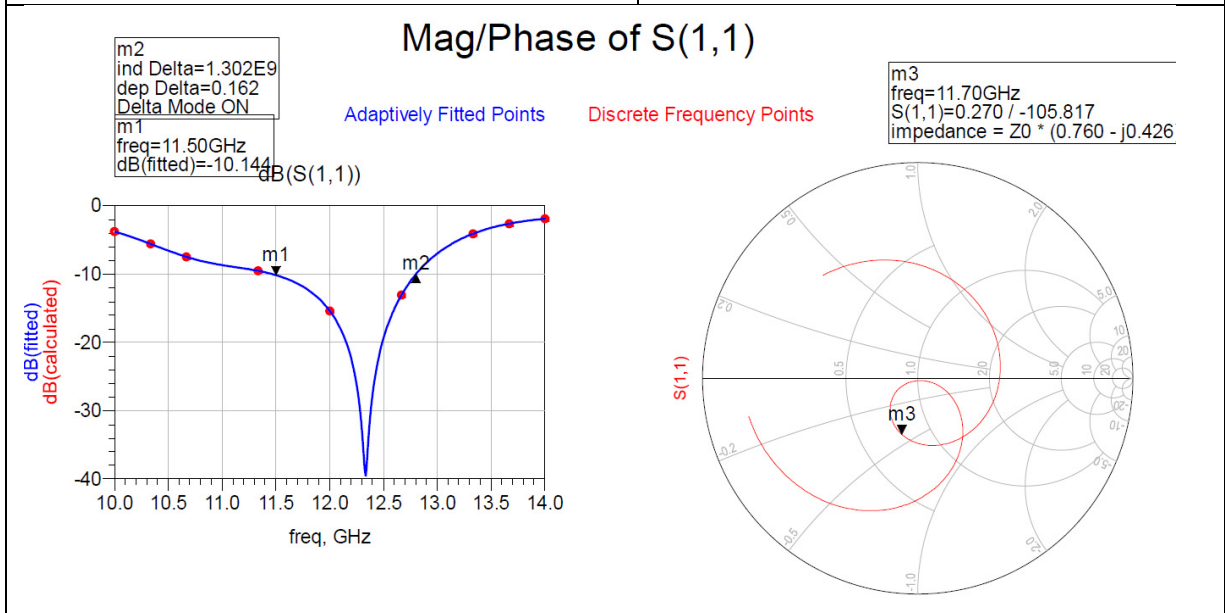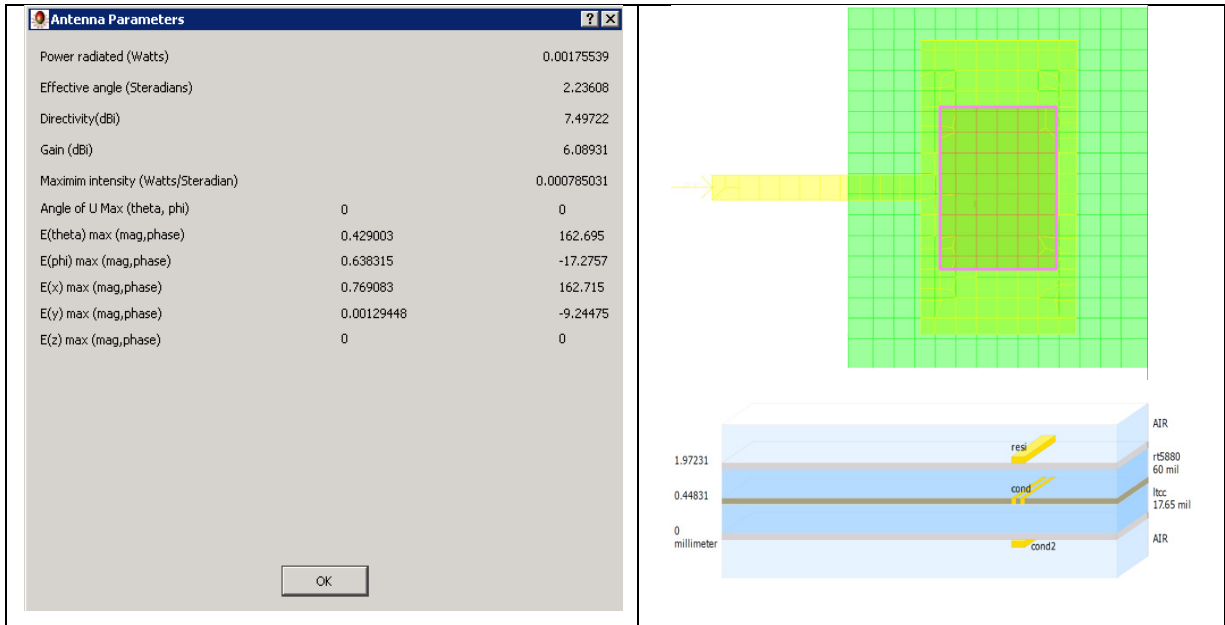
Figure-A III-3 Patch Antenna with Patch Shape Feed and Rectangular Slot,
ε_r(patch)=2.2(60mils), ε_r(feed)=7.1, efficiency=72.312%
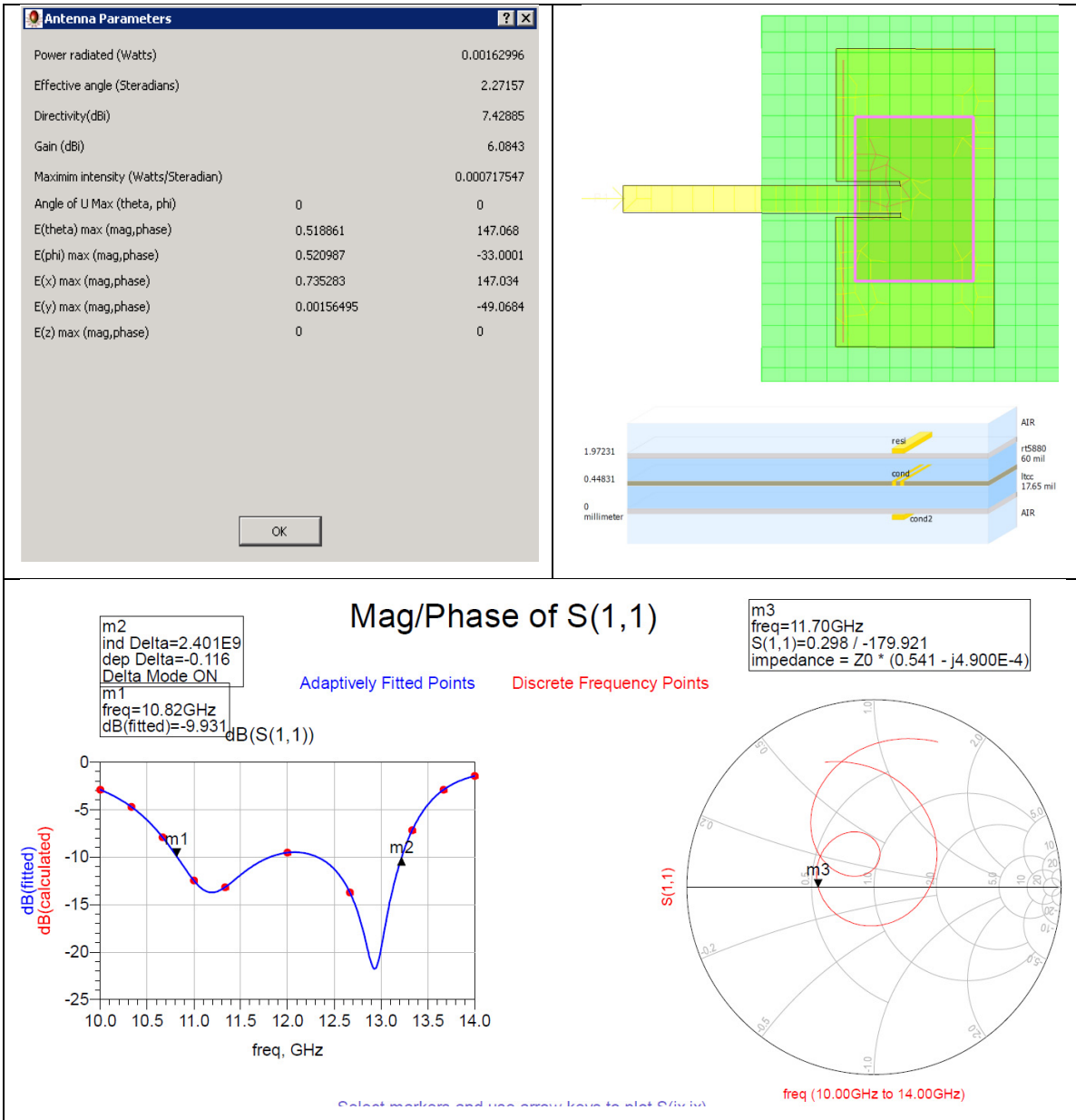
Figure-A III-4 Patch Antenna with Patch-Inset Shape Feed and Rectangular Slot,
ε_r(patch)=2.2(60mils), ε_r(feed)=7.1, efficiency=73.375%

SRUARE PATCH FEED LINE AND SQUARE FRAME PATCH FEED LINE
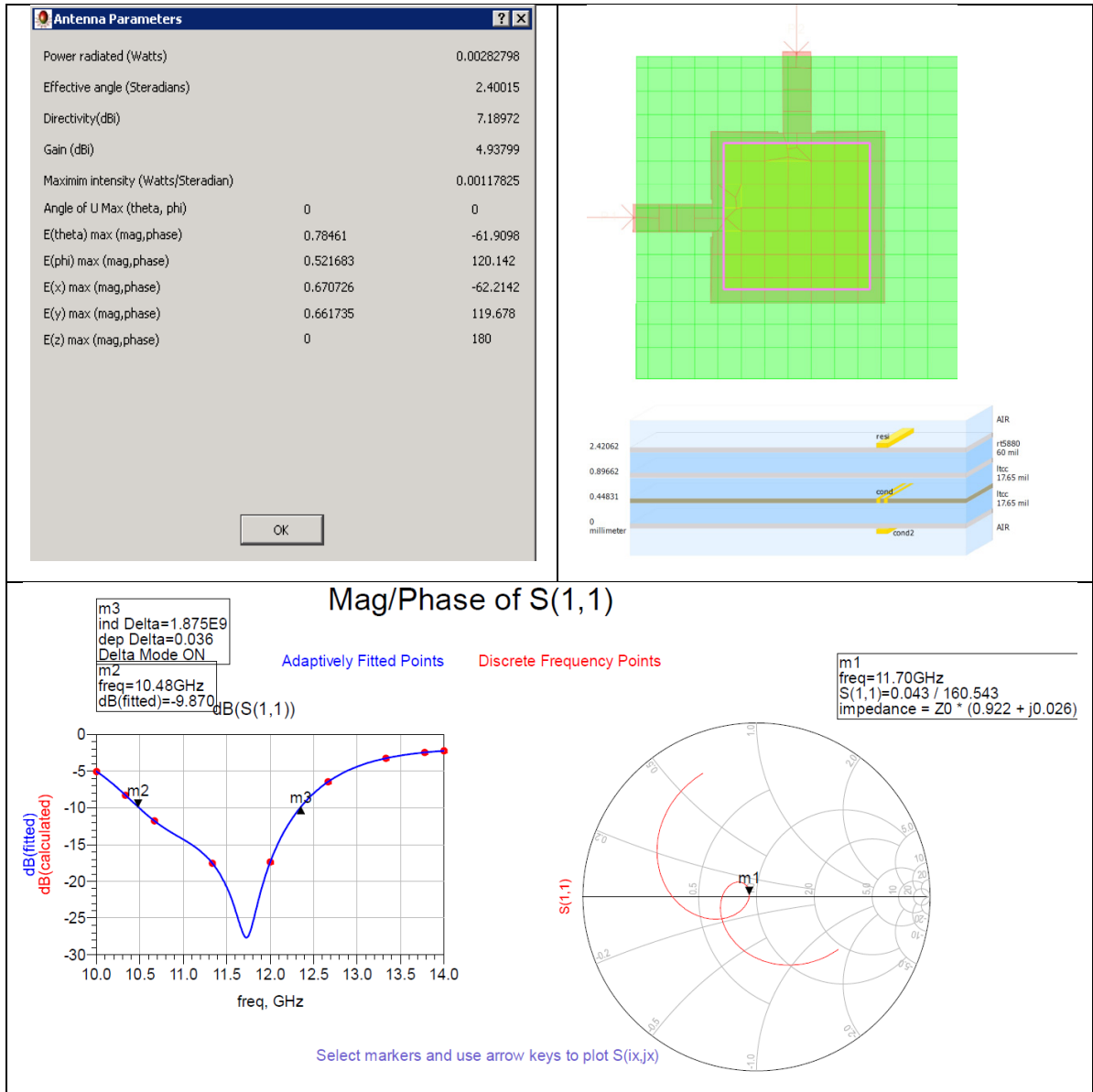
Figure-A IV- 1 Dual Polarization Patch antenna with Square Feed,
ε_r(patch)=2.2(60mils)+7.1(17.65), efficiency=59.543%

Antenna Parameters		
Power radiated (Watts)		0.00305432
Effective angle (Steradians)		2.36312
Directivity(dBi)		7.25724
Gain (dBi)		5.34183
Maximim intensity (Watts/Steradian)		0.00129249
Angle of U Max (theta, phi)	0	0
E(theta) max (mag,phase)	0.181586	132.399
E(phi) max (mag,phase)	0.969985	132.282
E(x) max (mag,phase)	0.702613	-47.7354
E(y) max (mag,phase)	0.69295	132.307
E(z) max (mag,phase)	0	0
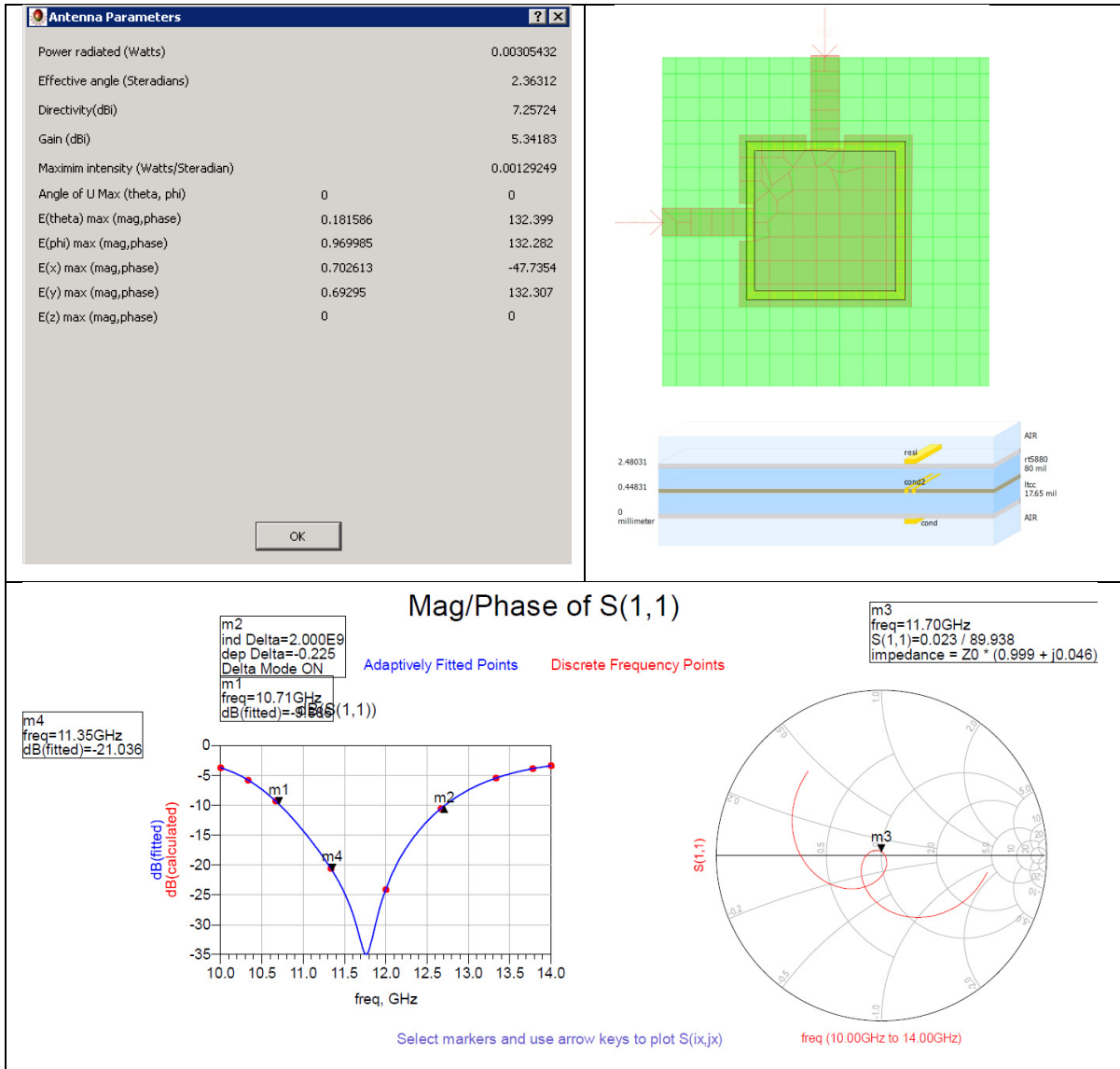
Figure-A IV- 2 Dual Polarization Patch Antenna with Square-Frame Feed, ε_r(patch)=2.2(80mils), efficiency=64.337%

APPENDIX V

MATLAB CODE TO FIND NUMBER OF ELEMENTS OF THE ARRAY

```
Main function:
%this program campute the number of elements of the array in x and y
direction to
%give 36dB gain in (theta,phi)direction.alpha is the ratio of the
%x_dimention to the y_dimention.
%%%%%%%%%%%%%%%%%%%%%%%%%%%%%%%%%%%%%%%%%%%%%%%%%%%%%%%%%%%%%%%%%%%%%%%%%
%%%%
%
%         z
%          |-theta    (theta 0-180 measured from z-axis)
%          |/
%          |_____ Y
%         /\
%       /-phi        (phi 0-360 measured from x-axis)
%     x
%%%%%%%%%%%%%%%%%%%%%%%%%%%%%%%%%%%%%%%%%%%%%%%%%%%%%%%%%%%%%%%%%%%%%%%%%
%%%%
% The azimuth is the horizontal pointing angle of the earth station
antenna.
% The elevation is the angle we look up into the sky to see the satellite
% distance between the elements=0.75*lambda. (d=0.75)
% the gain of the patch is soppused to be 0.58

clear
clc

fprintf('\n please enter this amounts: \n')
theta_R= input('\n Please enter the latitude of the Receiver(positive =
north, negative = south)):');
phi_R= input('\n Please enter the longitude of the Receiver(positive =
east, negative = west):');
phi_S= input('\n Please enter the longitude of the satellite:(positive =
east, negative = west):');
efficiency= input('\n Please enter the efficiency of patch element:');

% CALCULATE THETA AND PHI
G=phi_R-phi_S;
L=theta_R;
theta=atand([cosd(G)*cosd(L)-0.1512]/sqrt(1-[cosd(G)*cosd(L)]^2));
phi=180+atand(tand(G)/sind(L));

%////////////////////////////////////////////////////////////////////////
patch_gain=0.58;
Dx=10^1.35;                      % this amount is fixed
theta_h1=2;                    %theta_h=2 degree
phi_h1=2;                      %phi_h= 2 degree
```

```matlab
d=0.75;                              %distance between the elements=d*lambda;d
is a constant to refuse fromthe coupling effect(0.72<d<0.8)
Gain=10^(3.6-patch_gain);                    %Gain is 36 dB for satellite
D0=Gain/efficiency;              %diewctivity=Gain/efficiency
Gama=32400/D0;                   %Gama is space angle. this is an
estimated formula=theta_h*phi_h;
A=sind(phi);
B=cosd(phi);
C=cosd(theta);

%CALCULATE DIRECTIVITY AND NUMBER OF ELEMENTS///////////////////////////////

x0 = [1; 1];                         % Make a starting guess at the solution
options=optimset('Display','iter'); % Option to display output
Fun = @(x)( mainfun(x, d, A, B, C, Gama, theta_h1, phi_h1) );
[x,fval] = fsolve(Fun,x0,options);  % Call solver


Gx=Dx*efficiency;
Dy=D0/(pi*C*Dx);
Gy=Dy*efficiency;
N=Dy/(2*d);
M=Dx/(2*d);
N=round(N);
M=round(M);
phi_h=sqrt(1/(x(1,1)^(-2)*A^(2)+x(2,1)^(-2)*B^(2)));

%CALCULATE PHASE OF EACH ELEMENTS IN UNIFORM ARRAY
[PHASE]=weigth(M,N,d,theta,phi);


[X1,Y1] = meshgrid([0:d:(M-1)*d],[0:d:(N-1)*d]);


hold on;
for m = 1:M

        for n = 1:N
                phase=PHASE-min(min(PHASE));
                color = (phase(n,m)/max(max(phase)))*[1 1 1];
                plot(X1(n,m),Y1(n,m),'*','Color',color);
        end

end
 hold off;
 axis([0 (M-1)*d 0 (N-1)*d]);

%   ----------------.....M
%   ----------------.....
%   ----------------.....
%   .
%   .
%   N----------------.....NM
```

```matlab
%OUTPOTS//////////////////////////////////////////////////////////////////////
fprintf('\n      phase of each elements in uniform array: \n');
PHASE
fprintf('\n\b   ANTENNA CHARACTERS:\n' );
fprintf('\n       theta=%8.3f degree (0° = north, 90° = east, 180° = south,
270° = west)\n',theta );
fprintf('\n       phi=%8.3f degree (0° = horizontal, 90° = vertical)\n',phi
);
fprintf('\n       number of elemens in X direction= %d \n', M );
fprintf('\n       number of elemens in Y direction= %d \n', N );
fprintf('\n       Dx=%8.3f , %8.3f dB \n',Dx,10*log10(Dx) );
fprintf('\n       Dy=%8.3f , %8.3f dB \n',Dy,10*log10(Dy) );
fprintf('\n       Gx=%8.3f , %8.3f dB \n',Gx,10*log10(Gx) );
fprintf('\n       Gy=%8.3f , %8.3f dB \n',Gy,10*log10(Gy) );
fprintf('\n       theta_x=%8.3f \n',x(1,1));
fprintf('\n       theta_y=%8.3f \n',x(2,1));
fprintf('\n       theta_h=%8.3f \n',theta_h1 );
fprintf('\n       phi_h=%8.3f \n',phi_h );


  -------------------------------------------------------------------------


Mainfun function :
function F = mainfun(x, d, A, B, C, Gama, theta_h1, phi_h1)

%UNTITLED3 Summary of this function goes here

%%%%%%%%%%%%%%%%%%%%%%%%%%%%%%%%%%%%%%%%%%%%%%%%%%%%%%%%%%%%%%%%%%%%%%%%%%%%%
%%%%%%%%%%%%%%%%%%%%%%%%%%%%
%   Detailed explanation goes here
%   theta_x=x1
%   theta_y=x2


% % % ratio1^(-1)-M*d-d=0; %ratio1=1/[(M+1)*d];
% % % ratio2^(-1)-M*alpha*d-d=0; %ratio2=1/[(M*alpha+1)*d];
% % %
% % % theta_x=cosh(c-0.443*ratio1)-cosh(c+0.443 ratio1);
% % % theta_y=cosh(c-0.443*ratio2)-cosh(c+0.443 ratio2);
% % %
% % % Gama^2=1/[(theta_x^(-2)*A^2+theta_Y^(-2)*B^2)*(theta_x^(-
2)*B^2+theta_Y^(-2)*A^2)];

% theta_h=sqrt(1/(x(1,1)^(-2)*B^(2)+x(1,2)^(-2)*A^(2)));
% phi_h=sqrt(1/(x(1,1)^(-2)*B^(2)+x(1,2)^(-2)*A^(2)));
%%%%%%%%%%%%%%%%%%%%%%%%%%%%%%%%%%%%%%%%%%%%%%%%%%%%%%%%%%%%%%%%%%%%%%%%%%%%%
%%%%%%%%%%%%%%%%%%%%%%%%%%%%
F = [
        theta_h1-sqrt(1/(x(1)^(-2)*B^(2)+x(2)^(-2)*A^(2)));
        phi_h1-sqrt(1/(x(1)^(-2)*B^(2)+x(2)^(-2)*A^(2)))

% % %      -x(1)*d+x(2)^(-1)-d;
% % %      -x(1)*alpha*d+ x(3)^(-1)-d;
```

```
% % %     -x(4)+acosd(C-0.443*x(2))-acosd(C+0.443*x(2));
% % %     -x(5)+acosd(C-0.443*x(3))-acosd(C+0.443*x(3));
% % %      x(4)^(-4)*A^2*B^2+x(4)^(-2)*x(5)^(-2)*(B^2+A^2)+x(5)^(-
4)*B^2*A^2-Gama^(-2)
     ];


end


-------------------------------------------------------------
weight function :

function [ PHASE ] = weigth( M,N,d,theta, phi )
%UNTITLED Summary of this function goes here
%    Detailed explanation goes here


x=linspace(0,(M-1), M);
y=linspace(0,(N-1), N);
[X,Y] = meshgrid(x,y);
k0 = 2*180;
phase=[];
phase= -k0*d*sind(theta)*cosd(phi)*X - k0*d*sind(theta)*sind(phi)*Y;
PHASE=rem(phase,360);


end
```

MATLAB CODE TO DRAW ANTENNA PATTERN

```matlab
% This program traces the normalized pattern of antennas.
% % Parisa Moslemi. 1/11/2012
clear all
clc
close all
gain1=load('C:.......\gain.mat');
gain2 = struct2cell(gain1);
gain= cell2mat(gain2);

number=1.10;
ant1=load('C:......\*.mat');
ant2 = struct2cell(ant1);
ant= cell2mat(ant2);

funpattern(gain,ant,number)




function funpattern( gain,ant,number)
%UNTITLED Summary of this function goes here
%   Detailed explanation goes here

[V_ant,I_ant]=max(ant);
xdeg1=0:(2*pi/361):pi;
xdeg2=(pi+pi/361):(2*pi/361):2*pi;

%first plot
[V_an,I_an]=max(V_ant);
pat1=ant(:,I_an)+gain(1,I_an);
pattern1=pat1';
p1=polar(xdeg1,pattern1(1,1:181));
set(p1,'linewidth',3)
hold
p2=polar(xdeg2,pattern1(1,182:362),'.r');
set(p2,'linewidth',3)
xlabel('\Phi  (deg)','FontName','Arial','FontSize',12,'FontWeight','Bold')
ylabel('Pattern                                    (dB)
','FontName','Arial','FontSize',12,'FontWeight','Bold')
title([num2str(number),'pattern    of    the    frequency',num2str(9+(I_an-
1)/10),'GHz-max Gain',num2str(V_an),'dB'],'fontsize',20)

hold on
figure
%second plot
V_ant(1,I_an)=V_ant(1,I_an)-100;
[V_an,I_an]=max(V_ant);
pat2=ant(:,I_an)+gain(1,I_an);
pattern2=pat2';
p3=polar(xdeg1,pattern2(1,1:181));
set(p3,'linewidth',3)
hold
```

```matlab
p4=polar(xdeg2,pattern2(1,182:362),'.r');
set(p4,'linewidth',3)
xlabel('\Phi  (deg)','FontName','Arial','FontSize',12,'FontWeight','Bold')
ylabel('Pattern                                              (dB)
','FontName','Arial','FontSize',12,'FontWeight','Bold')
title([num2str(number),'pattern of the frequency',num2str(9+(I_an-
1)/10),'GHz-max Gain',num2str(V_an+gain(1,I_an)),'dB'],'fontsize',20)

hold on
figure
nomm=28;
%third plot 11.7GHz
pat3=ant(:,nomm)+gain(1,nomm);
pattern3=pat3';
p5=polar(xdeg1,pattern3(1,1:181));
set(p5,'linewidth',3)
hold
p6=polar(xdeg2,pattern3(1,182:362),'.r');
set(p6,'linewidth',3)
xlabel('\Phi  (deg)','FontName','Arial','FontSize',12,'FontWeight','Bold')
ylabel('Pattern                                              (dB)
','FontName','Arial','FontSize',12,'FontWeight','Bold')
title([num2str(number),'pattern of the frequency 11.7 GHz-max
Gain',num2str(V_ant(1,nomm)+gain(1,nomm)),'dB'],'fontsize',20)
end
```

APPENDIX VI

DATASHEETS OF 9K7 GREEN TYAE, 951 GREEN TAPE, AND ROGERS

9K7 Green Tape:

DuPont™ GreenTape™ 9K7
LOW TEMPERATURE CO-FIRED CERAMIC SYSTEM

Technical Data Sheet

Product Description
The DuPont™ GreenTape™ 9K7 low temperature co-fired ceramic (LTCC) system is comprised of a low loss, co-fireable glass-ceramic dielectric tape and compatible gold and silver conductors. The dielectric tape is both cadmium and lead free* and ideally suited for applications requiring low loss at frequencies in the high GHz range:
- Advanced high frequency applications
- Wireless and mobile communications
- High density multilayer interconnect for high speed digital applications

Product Benefits
The GreenTape™ 9K7 system provides a complete co-fireable system of gold, silver and resistive components having excellent low loss properties at frequencies in excess of 100 GHz:
- Co-fire processing and refire stability
- Cadmium and lead free* tape
- Low temperature brazing
- External cavities
- Buried component integration

*Cadmium and lead "free" as used herein means that cadmium and lead are not an intentional ingredients in and are not intentionally added to the referenced product. Trace amounts however may be present.

Processing
For detailed recommendations on the use of the GreenTape™ 9K7 low temperature co-fired ceramic (LTCC) system, consult the DuPont™ GreenTape™ LTCC Design Guide. For compatible post fired and co-fired conductor compositions, consult the DuPont™ GreenTape 9K7 Product Selector Guide.

Printing
Compatible co-fireable thick film compositions are printed directly on preconditioned GreenTape™ 9K7 green sheets using appropriate thick film screen printing methods.

Typical Properties

Physical Property	Value
Unfired thickness, (um)	127, +/- 9 (9K7)
	254, +/- 14 (9K7X)
X, Y, shrinkage, (%) [1]	9.1, +/- 0.3
Z shrinkage, (%) [1]	11.8, +/- 0.5
TCE, (23° - 300° C)	4.4
Density, (g/cm³)	3.1
Camber, (um / 25 mm)	25
Surface roughness, (um)	0.52
Thermal conductivity, (W / m-K)	4.6
Flexural strength, (MPa)	230
Young's modulus, (GPa)	145
Poisson's ratio	0.25

Electrical Property	Value
Dielectric constant, (10 GHz) [2]	7.1, +/- 0.2
Loss tangent, (10 GHz) [2]	0.0010
Insulation resistance, (Ohms)	> 10^{12}
Breakdown voltage, (kV / 25 um)	>/= 1100

[1]: Isostatic lamination, 3000 psi, 70° C, 10 minutes
[2]: split cavity measurement method

The above tables show the anticipated typical physical and electrical properties for GreenTape™ 9K7 based on specific controlled experiments in our labs and are not intended to represent the product specifications, details of which are available upon request.

A vacuum stone or other support structure which distributes a uniform vacuum is recommended to secure the green sheet to the printer's stage plate. Printing should be performed in a clean, well ventilated area. Optimum printing characteristics are generally achieved when the room and paste container temperatures are in the 20° to 23°C range.

150

Drying

Allow conductor prints to level for 5 to 10 minutes at room temperature and then dry in a well ventilated oven or conveyor dryer for 5 minutes at 100°C. Do not over-dry.

Lamination

Collate, stack and laminate multiple sheets of the printed circuit patterns according to the recommended processing parameters detailed in the DuPont™ GreenTape™ LTCC Design Guide.

Typical lamination parameters are 3000 psi at 70°C for 10 minutes. Lamination pressures may vary slightly based upon part design and the individual tape lot shrinkage factors.

Firing

Fire in a well ventilated conveyor or static furnace. Air flows and extraction rates should be optimized to ensure that oxidizing conditions exist within the muffle and that no exhaust gases enter the room.

GreenTape™ 9K7 requires the use of dedicated, specially coated setters in order to prevent parts from sticking during firing.

The initial fire/co-fire should use the recommended 26.5 hr. profile. For further information regarding firing profiles, furnace recommendations and setter tile choices, please contact your local DuPont Technical Service Representative.

Post Fire Processing

Compatible post fired materials are printed directly on the co-fired GreenTape™ 9K7 laminate surface and fired at the recommended post fire profile.

Storage and Shelf Life

Containers should be tightly sealed and stored in a clean, stable environment at room temperature (<25°C). The shelf life of the material, in unopened containers, is six months from the date of shipment. Some settling of solids may occur and compositions should be thoroughly mixed prior to use.

Safety and Handling

For Safety and Handling information pertaining to this product, refer to the Material Safety Data Sheet (MSDS).

DuPont™ GreenTape™ 9K7
Cofire Profile - 850°C / 26.5 Hours
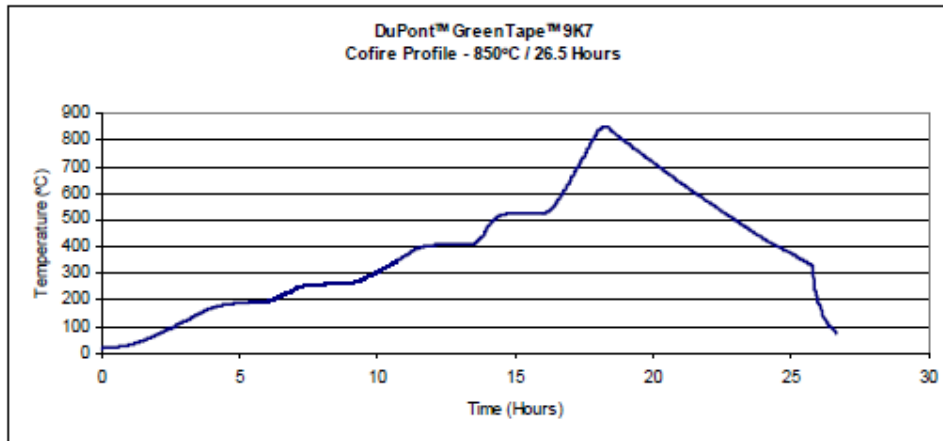
For more information on DuPont™ GreenTape™ 9K7 low temperature co-fired ceramic system or other DuPont Microcircuit Materials products, please contact your local representative:

Americas

DuPont Microcircuit Materials
14 T.W. Alexander Drive
Research Triangle Park, NC 27709
Tel.: 800-284-3382

Europe

Du Pont (U.K.) Limited
Coldharbour Lane
Bristol BS16 1QD
U.K.
Tel.: 44-117-931-3191

Asia

DuPont Kabushiki Kaisha
Sanno Park Tower, 11-1
Nagata-cho 2-chome
Chiyoda-ku, Tokyo 100-611
Japan
Tel.: 81-3-5521-8650

DuPont Taiwan Ltd
45, Hsing-Pont Road,
Taoyuan, Taiwan 330
Tel.: 886-3-377-3616

DuPont China Holding Co. Ltd
Bldg 11, 399 Keyuan Rd., Zhangji Hi-Tech Park,
Pudong New District, Shanghai 201203, China
Tel.: 86-21-6386-6366 ext.2202

DuPont Korea Inc.
3~5th Floor, Asia tower #726,
Yeoksam-dong, Gangnam-gu
Seoul 135-719, Korea
Tel.: 82-10-6385-5399

E. I. DuPont India Private Limited
7th Floor, Tower C, DLF Cyber Greens,
Sector-25A, DLF City, Phase-III,
Gurgaon 122 002 Haryana, India
Tel.: 91-124-4091818

Du Pont Company (Singapore) Pte Ltd
1 HarbourFront Place, #11-01
HarbourFrong Tower One,
Singapore 098633
Tel.: 65-6586-3022

http://mcm.dupont.com

MCM9K7(10/2009)

DUPONT

The miracles of science™

951 Green Tape :

DuPont Microcircuit Materials

951 Green Tape™
Thick Film Composition

All values reported here are results of experiments in our laboratories intended to illustrate product performance potential with a given experimental design. They are not intended to represent the product's specifications.

Product Description
951 Green Tape™ is a low-temperature cofired ceramic tape. The 951 system comprises a complete cofireable family of Au and Ag metallizations, buried passives, and encapsulants. 951 is available in multiple thicknesses and is designed for use as an insulating layer in:
- Multichip modules
- Single chip packages
- Ceramic printed wiring boards
- RF modules

The 951C2, 951PT, 951P2 and 951PX products are provided on a base film with improved punching characteristics. Tape performance properties are not affected by base film type.

Product Benefits
When used with compatible metallizations, 951 offers the following benefits:
- Component integration – buried resistors, capacitors, and inductors
- Hermetic packaging
- Low temperature brazing
- Cavities
- High density interconnections
- Cofire processing and refire stability

Processing
Design
For detailed recommendations on use of 951 Green Tape™, see the 951 Green Tape™ Design Guide. For compatible metallizations and their recommended use see the 951 Product Selector Guide.

System Capability
The 951 Green Tape™ system is designed to deliver line and space resolution of 100 µm, via diameters of 100 µm, and maximum layer counts in excess of 100.

Typical Tape Properties	
Physical	
Unfired Thickness (µm)	50 ± 3 (951C2)
	114 ± 8 (951PT/951AT)
	165 ± 11 (951P2/951A2)
	254 ± 13 (951PX/951AX)
X, Y Shrinkage (%)	12.7 ± 0.3
Z Shrinkage (%)	15 ± 0.5
TCE(25 to 300°C), ppm/°C	5.8
Density (g/cm³)	3.1
Camber, inch/inch	Conforms to setter
Surface Roughness , µm	<0.34
Thermal Conductivity, W/m-K	3.3
Flexural Strength¹, MPa	320
Young's Modulus, GPa	120
Electrical	
Dielectric constant @ 3 GHz	7.8
Loss Tangent @ 3 GHz	0.006
Insulation resistance at 100VDC,Ω	$>10^{12}$
Breakdown voltage, V/µm	>1000/25

¹ Four point bend

Printing
Following blanking and preconditioning of 951 green sheets, print compatible compositions directly onto unfired 951 Green Tape™ using thick film printing methods and a vacuum stone or other support structure that uniformly distributes vacuum. Follow specific printing and drying recommendations described on individual composition product data sheets.

Inspection
Inspect via, conductor and other prints prior to collation and lamination.

Typical Process Flow

Slit & Blank → Precondition → Form Vias, Layer 1 / Form Vias, Layer N → Fill Vias, Layer 1 / Fill Vias, Layer N → Print Conductor, Layer 1 / Print Conductor, Layer N → Collate & Laminate → Cofire → Post-fire Processing → Singulation

Recommended Firing Profile

environment at room temperature (<25°C). Shelf life of material in unopened containers is six months.

Lamination and Firing
Laminate multiple sheets of 951 Green Tape™ according to processing parameters detailed in the DuPont™ 951 Green Tape™ Design Guide. Recommended parameters for lamination are 3000 psi at 70°C for 10 minutes. Cofire laminates of 951 using the recommended firing profile and a belt or box furnace.

Post-fire Processing
Print compatible compositions onto cofired substrate surface and refire.

Singulation
Singulate multi-up substrates either in the green state using a hot-knife or after cofire using either a diamond saw (preferred) or laser scribe.

Storage and Shelf Life
Tape rolls, or boxes of sheeted tape, should be stored tightly sealed in a clean, stable

Safety and Handling
DuPont dielectric tapes are intended for use in an industrial environment by trained personnel. Users should comply with all appropriate health and safety regulations regarding storage, handling, and processing of such materials. 951 contains organic solvent and materials. The following precautions should be taken when handling 951:

- Use with adequate ventilation
- Avoid prolonged breathing of vapor
- If contact with skin occurs, wash affected area immediately with soap and water
- Dangerous if swallowed – DO NOT CONSUME.
- Refer to MSDS for additional details.

United States	Europe	Japan
DuPont Microcircuit Materials	DuPont (UK) Limited	DuPont Kabushiki Kaisha
14 T.W. Alexander Drive	DuPont Microcircuit Materials	ARCO Tower
Research Triangle Park, NC 27709	Coldharbour Lane	8-1, Shimomeguro 1-Chome
Tel.: 800-284-3382	Bristol BS16 1QD	Meguro-ku, Tokyo 153-0064
	England	Japan
	Tel.: 44-117-931-1444	Tel.: 81-35-434-6573

Visit our website at: http://www.dupont.com/mcm

DuPont The miracles of science

ROGERS, RT5870:

RT/duroid 5870/5880 Laminates

PROPERTY	TYPICAL VALUE [2]				DIRECTION	UNITS[3]	CONDITION	TEST METHOD
	RT/duroid 5870		RT/duroid 5880					
[1]Dielectric Constant, ε_r Process	2.33 2.33 ± 0.02 spec.		2.20 2.20 ± 0.02 spec.		Z Z		C24/23/50 C24/23/50	1 MHz IPC-TM-650 2.5.5.3 10 GHz IPC-TM 2.5.5.5
[5] Dielectric Constant, ε_r Design	2.33		2.20		Z		8 GHz - 40 GHz	Differential Phase Length Method
Dissipation Factor, tan δ	0.0005 0.0012		0.0004 0.0009		Z Z		C24/23/50 C24/23/50	1 MHz IPC-TM-650, 2.5.5.3 10 GHz IPC-TM-2.5.5.5
Thermal Coefficient of ε_r	-115		-125			ppm/°C	-50 - 150°C	IPC-TM-650, 2.5.5.5
Volume Resistivity	2 X 10⁷		2 X 10⁷		Z	Mohm cm	C96/35/90	ASTM D257
Surface Resistivity	2 X 10⁷		3 X 10⁷		Z	Mohm	C/96/35/90	ASTM D257
Tensile Modulus	Test at 23°C	Test at 100°C	Test at 23°C	Test at 100°C		MPa (kpsi)	A	ASTM D638
	1300 (189)	490 (71)	1070 (156)	450 (65)	X			
	1280 (185	430 (63)	860 (125)	380 (55)	Y			
ultimate stress	50 (7.3)	34 (4.8)	29 (4.2)	20 (2.9)	X			
	42 (6.1)	34 (4.8)	27 (3.9)	18 (2.6)	Y			
ultimate strain	9.8	8.7	6.0	7.2	X	%		
	9.8	8.6	4.9	5.8	Y			
Compressive Modulus	1210 (176)	680 (99)	710 (103)	500 (73)	X	MPa (kpsi)	A	ASTM D695
	1360 (198)	860 (125)	710 (103)	500 (73)	Y			
	803 (120)	520 (76)	940 (136)	670 (97)	Z			
ultimate stress	30 (4.4)	23 (3.4)	27 (3.9)	22 (3.2)	X			
	37 (5.3)	25 (3.7)	29 (5.3)	21 (3.1)	Y			
	54 (7.8)	37 (5.3)	52 (7.5)	43 (6.3)	Z			
ultimate strain	4.0	4.3	8.5	8.4	X	%		
	3.3	3.3	7.7	7.8	Y			
	8.7	8.5	12.5	17.6	Z			
Deformation Under Load, Test at 150°C			1.0		Z	%	24hr/14 MPa (2 Kpsi)	ASTM D621
Heat Distortion Temperature	>260 (>500)		>260 (>500)		X,Y	°C (°F)	1.82 MPa (264 psi)	ASTM D648
Specific Heat	0.96 (0.23)		0.96 (0.23)			J/g/K (cal/g/C)		Calculated
Moisture Absorption	0.02		0.02			%	.062" (1.6mm) D48/50	ASTM D570
Thermal Conductivity	0.22		0.20		Z	W/m/K	80°C	ASTM C518
Coefficient of Thermal Expansion	22 28 173		31 48 237		X Y Z	ppm/°C	0-100°C	IPC-TM-650, 2.4.41
Td	500		500			°C TGA		ASTM D3850
Density	2.2		2.2			gm/cm³		ASTM D792
Copper Peel	27.2 (4.8)		31.2 (5.5)			pli (N/mm)	1 oz (35µm) EDC foil after solder float	IPC-TM-650 2.4.8
Flammability	V-0		V-0					UL94
Lead-Free Process Compatible	Yes		Yes					

[1] Specification values are measured per IPC-TM-650, method 2.5.5.5 @ ~10GHz, 23°C. Testing based on 1 oz. electrodeposited copper foil. ε_r values and tolerance reported by IPC-TM-650 method 2.5.5.5 are the basis for quality acceptance, but for some products these values may be incorrect for design purposes, especially microstrip designs. We recommend that prototype boards for new designs be verified for desired electrical performance.
[2] Typical values should not be used for specification limits, except where noted.
[3] SI unit given first with other frequently used units in parentheses.
[4] References: Internal TR's 1430, 2224, 2854. Test were at 23°C unless otherwise noted.
[5] The design Dk is an average number from several different tested lots of material and on the most common thickness/s. If more detailed information is required, please contact Rogers Corporation. Refer to Rogers' technical paper "Dielectric Properties of High Frequency Materials" available at http://www.rogerscorp.com/acm.

STANDARD THICKNESS		STANDARD PANEL SIZE	STANDARD COPPER CLADDING
0.005" (0.127mm), 0.010" (0.254mm), 0.015" (0.381mm), 0.020" (0.508mm),	0.031" (0.787mm) 0.062" (1.575mm) 0.125" (3.175mm)	18" X 12" (457 X 305mm) 18" X 24" (457 X 610mm) 18" X 36" (457 X 915mm) 18" X 48" (457 X 1.224m)	¼ oz. (9 µm) electrodeposited copper foil. ½ oz. (17µm), 1 oz. (35µm), 2 oz. (70µm) electrodeposited and rolled copper foil. Thick metal cladding are also available. Contact customer service for available claddings and panel sizes.

The information in this data sheet is intended to assist you in designing with Rogers' circuit material laminates. It is not intended to and does not create any warranties express or implied, including any warranty of merchantability or fitness for a particular purpose or that the results shown on this data sheet will be achieved by a user for a particular purpose. The user should determine the suitability of Rogers' circuit material laminates for each application.

LIST OF BIBLIOGRAPHICAL REFERENCES

Aanandan, CK, P. Mohanan et KG Nair. 1990. « Broad-band gap coupled microstrip antenna». Antennas and Propagation, IEEE Transactions on, vol. 38, no 10, p. 1581-1586.

Balanis, C.A. 1982. Antenna theory: analysis and design. Harper & Row New York.

Chang, BK, et BP Johnson. « Effects of element pattern on the performance of a rectangular array ». In., p. 1254-1257 vol. 3. IEEE.

Cleto Pescia. 2004. «Satellite antenna bearing calculator». <http://www.giangrandi.ch/ electronics/satcalc/satcalc.shtml>. Retrieved 12 September 2012

ES100 Introduction to Engineering Design. 2005. «Parabolic Antennas». <http://www.montgomerycollege.edu/Departments/cadtecgt/es100c/materials/Bern/parabolic%20antennas.pdf>. Retrieved 12 September 2012.

Garg, R. 2001. Microstrip antenna design handbook. Artech house publishers.

Holzwarth, S., J. Kassner, R. Kulke et D. Heberling. 2001. « Planar antenna arrays on LTCC-multilayer technology ». In. Vol. 2, p. 710-714. IET.

Hall, PS, et CM Hall. 1988. « Coplanar corporate feed effects in microstrip patch array design ». In. Vol. 135, p. 180-186. IET.

HIRSCHMANN. «Satellite Components». Type Hit FESAT 65. <http://www.ozelbinaelektronik.com/HirschmannUyduAntenler.pdf>. Retrieved 12 September 2012.

Huang, J., et R.J. Pogorzelski. 1998. « A Ka-band microstrip reflectarray with elements having variable rotation angles ». Antennas and Propagation, IEEE Transactions on, vol. 46, n° 5, p. 650-656.

Joint Information Systems Committee (JISC). «Basics of satellite communications». <http://www.jisc.ac.uk/whatwedo/themes/network/sat/report3.aspx>. Retrieved 12 September 2012.

James, J.R. 1989. Handbook of microstrip antennas, 2. Peregrinus.

Jamnejad, V., J. Huang, B. Levitt, T. Pham et R. Cesarone. 2002. « Array antennas for JPL/NASA deep space network ». In. Vol. 2, p. 2-911-2-921 vol. 2. IEEE.

156

Jang, YW. 2000. « Broadband cross-shaped microstrip-fed slot antenna ». Electronics Letters, vol. 36, no 25, p. 2056-2057.

KEKO EQUIPMENT. «Equipment for Production of Multilayer Based Components in LTCC Production». <http://www.keko-equipment.com/LTCC.php>. Retrieved 8 December 2012.

Kishk, A.A. 2009. « Fundamentals of Antennas ».

Knittel, G. 1965. « Choosing the number of faces of a phased-array antenna for hemisphere scan coverage ». *Antennas and Propagation, IEEE Transactions on,* vol. 13, n° 6, p. 878-882.

Management and Operation of Armed Forces Radio and Television Service (AFRTS). 2010. «Defense Media Center Satellite Handbook». V.3.26

Mano, S., M. Ono et Y. Takeichi. 1974. « Effects of the element pattern on the directive properties of a scanning planar array ». Antennas and Propagation, IEEE Transactions on, vol. 22, no 2, p. 169-172.

Maral, G., M. Bousquet et Z. Sun. 2009. Satellite communications systems: systems, techniques and technology. Wiley.

Moernaut, G.J.K., et D. Orban. 2006. « The Basics of Antenna Arrays ».

Radio-Electronics.com. «Communications Satellites Technology». <http://www.radioelectronics.com/info/satellite/communications_satellite/communications-satellite-technology.php>. Retrieved 12 September 2012

Roddy, D., et Inc ebrary. 2001. Satellite communications. McGraw-hill.

Ryu, K.S., et A.A. Kishk. « A DUAL-POLARIZED SHORTED MICROSTRIP PATCH ANTENNA FOR WIDEBAND APPLICATION ».

Schippers, H., J. Verpoorte, P. Jorna, A. Hulzinga, A. Meijerink, C. Roeloffzen, RG Heideman, A. Leinse et M. Wintels. 2008. « Conformal phased array with beam forming for airborne satellite communication ». In., p. 343-350. IEEE.

Schoebel, J., et P. Herrero. « Planar Antenna Technology for mm-Wave Automotive Radar, Sensing, and Communications ».

Silver, JP. « Satellite Communications Tutorial ». Space Research, vol. 713, p. 798.

Stutzman, W.L., et G.A. Thiele. 1998. Antenna theory and design, 320. J. Wiley.

Visser, H.J., et J. Wiley. 2005. Array and phased array antenna basics. Wiley Online Library.

WIKIPEDIA. 2012. «Patch antenna». <http://en.wikipedia.org/wiki/Patch_antenna>. Retrieved 12 September 2012

WIKIPEDIA. 2008. «List of satellites in geosynchronous orbit». <http://en.wikipedia.org/wiki/List_of_satellites_in_geosynchronous_orbit>. Retrieved 12 September 2012

Wolff, I. 2009. « From antennas to microwave systems-LTCC as an integration technology for space applications ». In., p. 3-8. IEEE.